SALT-WATER APPROXIMATION OF SMOKE LAYER EVOLUTION WITHIN TWO-ZONE MODELS

A thesis submitted in partial fulfilment of the requirements for the Degree

of Master of Engineering in Fire Engineering by

Peter James Marriott

Supervised by

Professor Charles Fleischmann

Professor Roger Nokes

Department of Civil and Natural Resources Engineering

University of Canterbury

Christchurch, New Zealand

2019

Abstract

Smoke evolution and propagation is an important consideration in building design for assessing the risk of death or injury to evacuating occupants during a fire. Fire engineers commonly use two-zone computer models to calculate smoke layer propagation and temperature within a compartment. A two-zone model assumes that smoke from a fire instantaneously creates a homogeneous hot (upper) smoke layer with a homogeneous cool (lower) air zone below it. The smoke layer lowers as the fire produces smoke.

The objective of this research is to investigate the applicability limit of two-zone models when the modelled compartment is much wider than it is tall. A salt-water physical model was used to assess the applicability of two-zone computer models. Applicability of two-zone models was investigated by comparing the height of the layer interface between the salt-water mixture and freshwater to the layer interface between the smoke and air calculated in the two-zone model. Comparison was possible between the different mediums through appropriate non-dimensionalisation of the time and length scales.

The geometric constraints of application for the two-zone computer model are described by a shape factor defined as A_f/H^2, where A_f is floor area (m^2) and H is room height (m). Experimental results suggest that salt-water experiments and two-zone models produce comparable results for shape factors up to fifty. Above a shape factor of fifty, experimental and computational model behaviours diverge.

Acknowledgements

A special thank you to Charley and Roger, without your patience and feedback this research would not have been possible.

I would like to thank the team in the University of Canterbury Fluids Lab for their support throughout the setup and completion of my salt-water experiments.

A big thank you to all of my family and friends. I am incredibly lucky to have such a supportive group of people around me, who all helped tremendously through the difficult times these past few years.

This thesis would not have been possible without financial support from the Building Research Association of New Zealand and Olsson Fire & Risk.

Contents

List of tables

List of figures

Nomenclature

Symbol	Unit	Name
g	$m.s^{-2}$	Acceleration due to gravity
T_0	K	Ambient temperature
C	$-$	Area multiplier
C_p	$-$	Asymptotic value of the plume width
$I^*_{u,av}$	$-$	Average of the depth integrated density values above layer height
$I^*_{l,av}$	$-$	Average of the depth integrated density values below layer height
B	$m^4 s^{-3}$	Buoyancy flux
B_f	$m^4 s^{-3}$	Buoyancy flux of the fire
B_{sw}	$m^4 s^{-3}$	Buoyancy flux of the salt-water
N	$-$	Chosen percentage
A_f	m^2	Cross-sectional area of the fire compartment
A_{sw}	m^2	Cross-sectional area of the salt-water compartment
d	m	Diameter of the discharge source
D_f	m	Diameter of the fire
$\dot{Q}^*$	$-$	Dimensionless heat release rate
γ	$-$	Dimensionless ratio of heat capacities
$y^*_{LH,f}$		Dimensionless two-zone layer height
r_{av}	$-$	Direct averaging integral
ρ	$kg.m^{-3}$	Density of air
ρ_a	$kg.m^{-3}$	Density of ambient fluid
ρ_0	$kg.m^{-3}$	Density of discharge fluid
I^*	$-$	Depth integrated density profile

Symbol	Unit	Name
μ	$kg.m^{-1}s^{-1}$	Dynamic viscosity of ambient air
E_v	J	Energy leaving the vent
E_L	J	Energy stored within the layer
A_f	m^2	Floor area
Fr	$-$	Froude number
Gr_f	$-$	Grashof number
$\dot{Q}$	W	Heat release rate
h_a	m	Height of the lower bound
h_b	m	Height of the upper bound
R	$J.K^{-1}kg^{-1}$	Ideal gas constant
C_{J0}	$g.m^{-3}$	Initial mass concentration in the jet
M_0	m^4s^{-2}	Initial momentum flux
g_0'	$m.s^{-2}$	Initial reduced gravity
u_0	$m.s^{-1}$	Initial velocity of the discharge fluid
Q_0	m^3s^{-1}	Initial volume flux
r	$-$	Integral ratio
l_Q	m	Jet characteristic length scale
v	m^2s^{-1}	Kinematic viscosity of ambient air
v_{sw}	m^2s^{-1}	Kinematic viscosity of salt-water
T_L	K	Layer temperature
l_{jm}	m	Length of transition from jet to mixed buoyant jet behaviour
R_p	$-$	Local Richardson number
r_l	$-$	Lower integral ratio
m	kg	Mass of air
m_L	kg	Mass within the layer

Symbol	Unit	Name
C_m	$g.m^{-3}$	Maximum dye concentration at bottom of the tank
$\dot{q}_l$	kW	Net heat transfer to the lower layer
$\dot{q}_u$	kW	Net heat transfer to the upper layer
t^*	$-$	Non-dimensionalised time
I^*_{sw}	$-$	Normalised salt-water experiment depth integrated density profile
l_M	m	Plume characteristic length scale
Y	$kg.s^{-1}$	Plume mass flux
Pr	$-$	Prandtl number
P	Pa	Pressure
Re	$-$	Reynolds number
Re_f	$-$	Reynolds number for fire
Re_{sw}	$-$	Reynolds number for salt-water
H	m	Room height
D_{sw}	$m^2 s^{-1}$	Salt diffusivity
Sc	$-$	Schmidt number
SF	$-$	Shape factor
C_{PO}	$g.m^{-3}$	Source concentration in a pure axisymmetric plume
c_p	$J.kg^{-1}K^{-1}$	Specific heat of air
T	K	Temperature
T_{LL}	K	Temperature of the lower layer
k	$W.m^{-1}K^{-1}$	Thermal conductivity of ambient air
t	s	Time
δt	s	Time step used in the simulation
r_u	$-$	Upper integral ratio
g^*_{UL}	$-$	Upper layer dimensionless reduced gravity

Symbol	Unit	Name
$\dot{m}_v$	$kg.s^{-1}$	Vent mass flow
V	m^3	Volume
Q	$m^3 s^{-1}$	Volume flux of the source
V_R	m^3	Volume of the room
V_U	m^3	Volume of the upper layer
α	K^{-1}	Volumetric coefficient of thermal expansion
h	m	Water depth

1 Introduction

Commercial buildings must meet an acceptable standard of fire safety to advance from design to construction. The primary objective in establishing building standards is to limit the risk of death or injury to building occupants in the event of a fire. Other intentions are to reduce the potential damage that a fire could incur on and within the building and to reduce the risk of the fire spreading or damaging adjacent property. The most important considerations in design assessments are the quantity and location of smoke and heat produced by a fire.

1.1 Motivation

Understanding smoke movement is an important element of building design for controlling the risk of death or injury to evacuating occupants. When designing for fire incidents, engineers investigate possible smoke activity based on typical fire sizes and locations throughout a building. Predicting the quantity and location of smoke allows engineers to assess potential impact on evacuating occupants. Death of building occupants can occur due to loss of vision, succumbing to heat or inhaling toxic particles from the smoke. The most common cause of occupant death is inhalation of excessive amounts of smoke (Birky & Clarke, 1981). The degree of impact of smoke on occupants is estimated through physical variables such as visibility, thermal effects and species concentration. Because fire evolution and smoke diffusivity are difficult to capture and measure, fire engineers rely on smoke models to design robust buildings.

Fire engineers commonly use two-zone models to predict potential interior conditions when a building is engulfed by a fire. Two-zone models assume that smoke from a fire instantaneously creates a homogeneous hot (upper) smoke layer with a homogeneous cool (lower) air zone below it. High-resolution models produced by computational fluid dynamics (CFD) models may also be used to determine smoke conditions. Detailed CFD models are based on implementing and solving the Navier-Stokes equations. These models are complex and provide detail beyond what is required to design most common buildings. Moreover, even with standard education and training, many fire engineers struggle to solve these equations and interpret model results. Given that the role of fire engineers is to predict formation and evolution of a resultant smoke layer from a fire, the detailed resolution of the smoke layer returned by the Navier-Stokes equations is not required for building design. Although two-zone models are less accurate and less capable of handling complex geometries than CFD models, two-zone models are significantly quicker to run, have been validated against fires in simple geometries, and therefore have been popular for use in designing buildings.

Despite the fact that two-zone models are the popular choice for understanding potential smoke movement in new buildings, few existing studies aim to justify application constraints of two-zone models. Some existing research has provided guidance (Bong, 2011). Fire engineers must be able to trust that two-zone model results are sufficiently accurate for building design. Uncertainty in the limits may unnecessarily confine the ability of the engineer to use this tool in design.

A simpler approach based on cruder physics that still accurately predicts smoke layer evolution has evident advantages for fire engineering. In general, two-zone models give reasonable predictions of how smoke will travel through various building compartments. Two-zone models give the best results for rooms where the room height squared is large relative to the floor area. However, in scenarios where room height squared is small relative to the floor area, two-zone

models return less reliable results. Quantifying the relationship between floor area and room height is the shape factor (SF) (Bong, 2011), which is an areal aspect ratio defined as

$$SF = A_f/H^2 \quad (1)$$

where A_f is the floor area (m^2) and H is the height of the room (m).

1.2 Objectives

The objective of this research is to investigate the applicability and limitations of two-zone smoke movement models. This is achieved by using physical lab-scale models.

The aim of this thesis is to test the applicability and limitations of two-zone models through comparison to a series of physical lab-scale experiments. Experiments involve injecting salt-water into a freshwater tank to simulate the propagation of a smoke layer through air. This study builds upon shape factor limits proposed by Bong (2011). Emphasis is placed on the upper-bound shape factor because as the shape factor increases the fundamental assumptions adopted in the two-zone model are likely to break down and the two-zone model will not be applicable for robust building design.

1.3 Report outline

Chapter 2 provides the pertinent background for the research. Smoke layer formation is described in detail. Modelling of smoke layers by a two-zone model and physical scale salt-water experiments is discussed.

Chapter 3 describes and discusses the methodology used to undertake computer and physical modelling. The experimental setup is described and the procedure used to generate comparable data is discussed, including how the two models are compared.

Chapter 4 compares experimental results with predictions from two-zone models. Results from computer and physical models for different shape factors are examined and directly compared as non-dimensionalised data. A discussion of the underlying assumptions of each method is presented.

Chapter 5 draws conclusions from the research.

2 Background

This chapter describes dynamics of smoke layer formation. Modelled layer formation and evolution are also described through both CFD and two-zone computer models. Assumptions and limitations of two-zone models are explained. A description of the setup and use of a physical scale model to simulate the smoke dynamics is presented. Characteristics and flow dynamics—including transport and mixing—of buoyant jets within fire-induced and salt-water flows are further described. Mathematical equations that describe the dynamics of both flows are stated and a method of comparison between flows is developed. Finally, the limitations of this comparison method are discussed.

2.1 Smoke layer formation

In the event that an object ignites within an enclosed space, a fire may grow. Fire growth is dependent on fuel, enclosure geometry, compartment openings, and the properties of the compartment bounding surfaces (Karlsson & Quintiere, 1999). A burning fire releases heat energy, combustion particulates and gases. Combustion products are emitted when an object or material undergoes burning or pyrolysis. The resultant mixture of these products with air is smoke. The amount of smoke produced by a fire is dependent on the type and amount of fuel available for burning (Cooper, 1984).

Smoke has elevated temperature and therefore has a lower density than ambient air, thus it experiences a positive buoyancy force. As a result, smoke rises towards the ceiling and forms a plume of upward-moving gases above the fire. Turbulence within the plume causes entrainment of ambient air, mixing the air with smoke and causing dilution of the smoke. The time-average steady state temperature along the centreline of the plume reduces with height while the plume spreads laterally with height (Morton, Taylor, & Turner, 1956).

While the fire burns, it contributes hot smoke to the plume. When the smoke plume encounters the ceiling and can no longer continue travelling vertically, it spreads radially and becomes a ceiling jet (Figure 1). Radial expansion of the ceiling jet is driven by horizontal momentum generated by pressure gradients within the vertical plume and buoyancy forces. The ceiling jet experiences friction as it moves through ambient air and along the ceiling, which decreases its momentum. As the smoke moves outwards, additional air is entrained and heat energy is transferred to the ceiling. Both processes cause buoyancy forces within the ceiling jet to

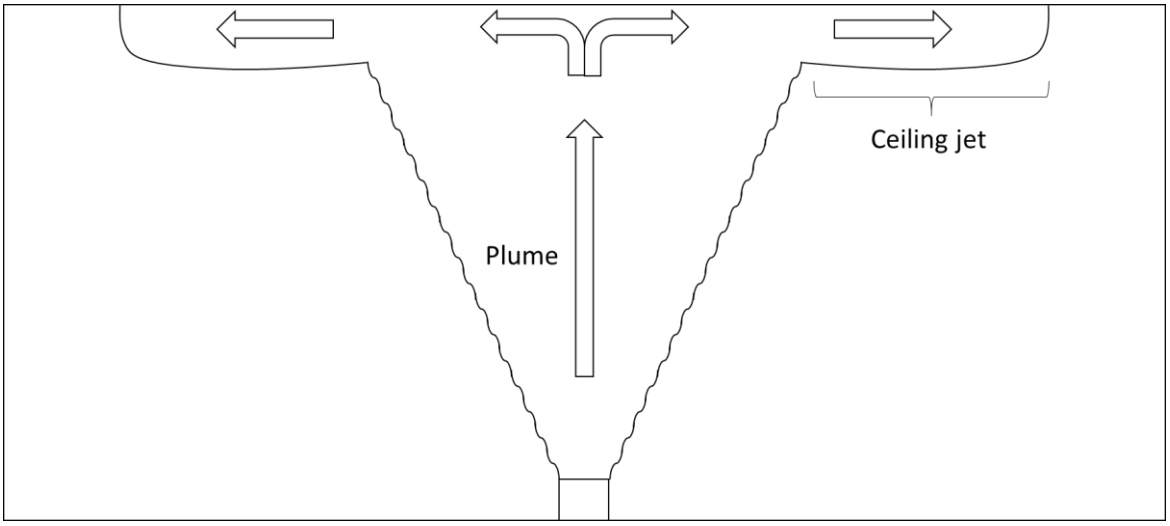

Figure 1. Fire plume impinging on ceiling and travelling radially outwards as a ceiling jet.

decrease. The decrease in buoyancy forces is due to a decrease in average temperature and concentration of the smoke front. The entrained air causes the depth of the smoke front to increase as it travels outwards. Alpert (1975) derived equations of motion that can be applied to describe the smoke front in terms of temperature, concentration and depth.

Smoke will continue to flow radially outward from where the centre of the plume meets the ceiling until it reaches the walls of the enclosure. When smoke encounters walls, horizontal momentum is directed vertically downwards via pressure gradients caused by subsequent smoke travelling along the ceiling (Figure 2). The downward-directed smoke has a higher temperature and lower density than that of the ambient air. The downward momentum of the smoke flow is opposed by internal buoyancy forces; this opposition causes flow momentum to decrease. Moreover, smoke in the flow cools as it descends due to heat transfer to the wall, which causes internal buoyancy forces to decrease. When the buoyancy forces decrease the downward momentum to zero, the smoke flow no longer moves downward, instead moving away from the wall and travelling upward and inward toward the centre of the room (Figure 3).

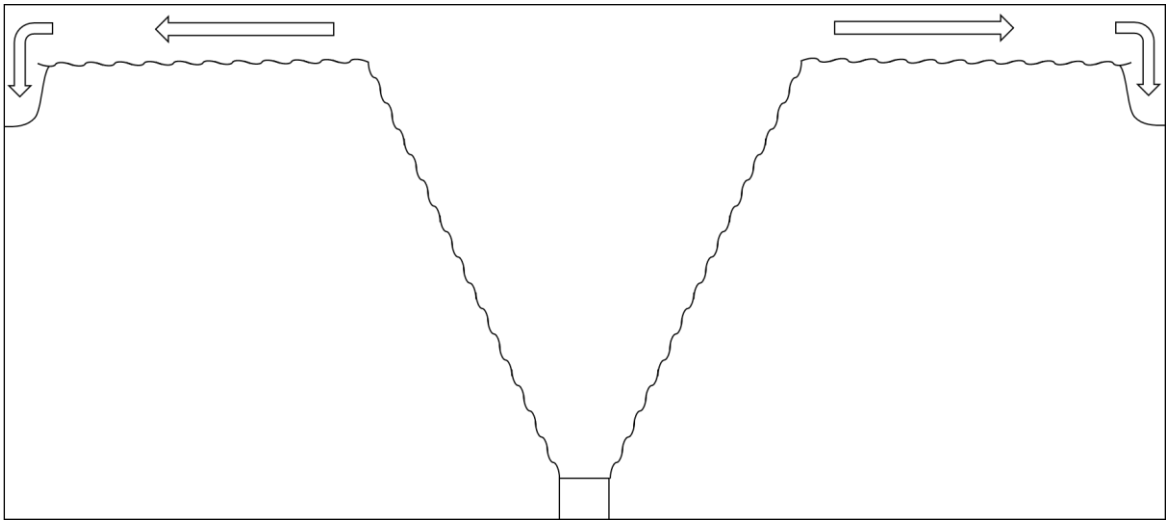

Figure 2. Smoke interacting with walls during smoke layer formation.

The smoke is driven back upwards by buoyancy until it meets the less dense smoke at the ceiling and stops rising. The smoke then travels back towards the plume (Figure 3). Waves form along the interface between the smoke and cool, lower layer. The turbulence causes the smoke in these flows near the ceiling to mix, forming a relatively uniform layer and begin lowering

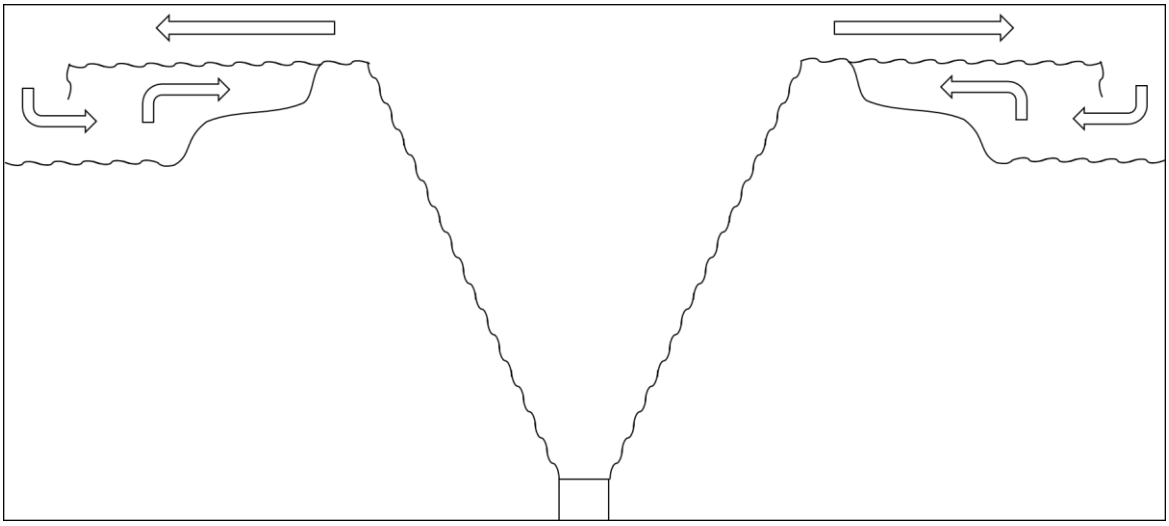

Figure 3. Smoke travelling back inwards as it forms a hot, upper smoke layer

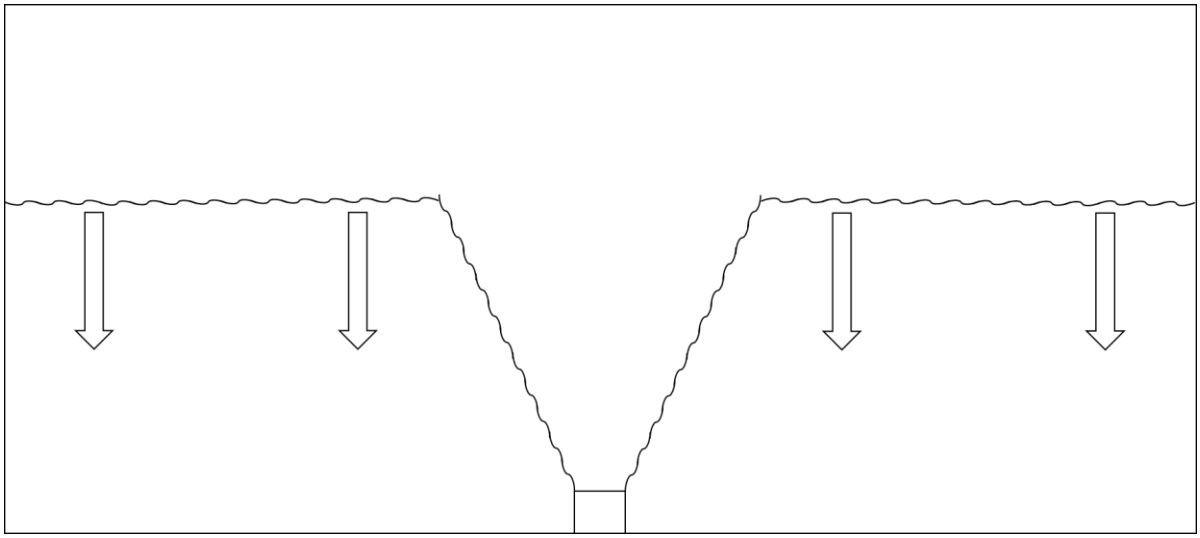

Figure 4. Fully formed smoke layer descending towards the ground.

(Figure 4). With more smoke produced by the fire, the layer will continue to grow and descend. Additional smoke added to the layer will cause average temperature and smoke concentration to increase due to the shorter distance the plume travels through the ambient air.

As the smoke layer thickens, it reaches a level where it will affect evacuating occupants in the room. The effect of the smoke on occupants is called the tenability and depends on several smoke properties which in turn depend on the fire. Gas concentrations and temperature vary depending on fuel-burning characteristics within the fire. The ability to model the effects of the fire through tenability and smoke movement allow fire engineers to determine the risk of death, injury or asset damage associated with a particular building design. Negative effects of smoke on building occupants occur due to increased temperature, smoke concentration, toxic gas concentration, and decreased oxygen concentrations.

2.2 Plumes

Smoke created by fire rises as a pure plume. A pure plume is defined as the generation of a buoyancy flux at a point, such as smoke being produced by a fire (Fischer, List, Koh, Imberger, & Brooks, 1979). The density difference between fluids drives flow through the creation of buoyancy forces. The buoyancy flux is assumed to be constant and therefore the flow of the fluid is dependent on the buoyancy flux at the fire source. Buoyancy flux as a function of a heat source such as a fire is defined as

$$B_{\mathrm{f}} = \frac{g\alpha\dot{Q}}{\rho c_p} \qquad (2)$$

where B_f is the buoyancy flux of the fire ($m^4\ s^{-3}$), g is acceleration due to gravity ($m\ s^{-2}$), α is the volumetric coefficient of thermal expansion (K^{-1}), $\dot{Q}$ is the fire heat release rate (W), ρ is the density of air ($kg\ m^{-3}$), and c_p is the specific heat of air ($J\ kg^{-1}\ K^{-1}$).

2.3 Computer models

Fire engineers model smoke movement for various possible fire scenarios within a building. Fire engineers then provide advice to architects and other engineers working on building design and layout. Computational fluid dynamics and two-zone models are commonly used for modelling smoke and fire phenomena.

2.3.1 Computational fluid dynamics models

A computational fluid dynamics (CFD) model is a multi-dimensional numerical model based on the Navier-Stokes equations of fluid motion with accompanying simplifying assumptions. CFD models typically require significant computing resources.

The Navier-Stokes equations are complex and require large amounts of computational power to solve, even for simple applications. Simplification is useful for application because solving the Navier-Stokes equations can be challenging due to the large disparity of scales seen in turbulent flow. It is not possible to solve models encompassing all physical scales even with a supercomputer. Therefore, significant computational reductions must be applied. An example of these simplifying assumptions is the large-eddy simulation (LES) method. When LES is undertaken, large scale motions of flows are computed numerically while small scale motions are modelled (Smagorinsky, 1963). Another possible simplifying assumption is using the Reynolds-averaged Navier-Stokes (RANS) approach. The RANS equations are time-averaged Navier-Stokes equations and allow calculation of steady-state flow properties (Reynolds, 1895).

Once the governing equations are defined using suitable assumptions, they are discretized throughout the modelled compartment affected by smoke. The three typical discretization methodologies used in CFD models are finite-difference (Chorin, 1969), finite-element (Onate & Idelsohn, 1992) and finite-volume methods (Onate & Idelsohn, 1992). Use of discrete methods throughout the space provides information about the evolution of flow properties throughout three-dimensional space as a function of time.

Within CFD models several sub-models for fire-specific principles may be implemented. The sub-models take into consideration reaction chemistry kinetics, radiation transport, heat conduction through solids and pyrolysis. Inclusion of these considerations renders CFD modelling capable of producing detailed models of fire and smoke behaviour in complex geometries and applications but has high time and computational resource costs.

2.3.2 Two-zone models

Two-zone models assume that a fire within a compartment will form a hot, upper smoke layer with a cool air layer beneath it. The two layers are separated by an interface of uniform height (Figure 5). Formation of the upper layer is assumed to be instantaneous and does not directly allow for a delay in either smoke transport or smoke layer formation. The lower layer is assumed to consist of air which is much cooler than the smoke. Conservation of mass and

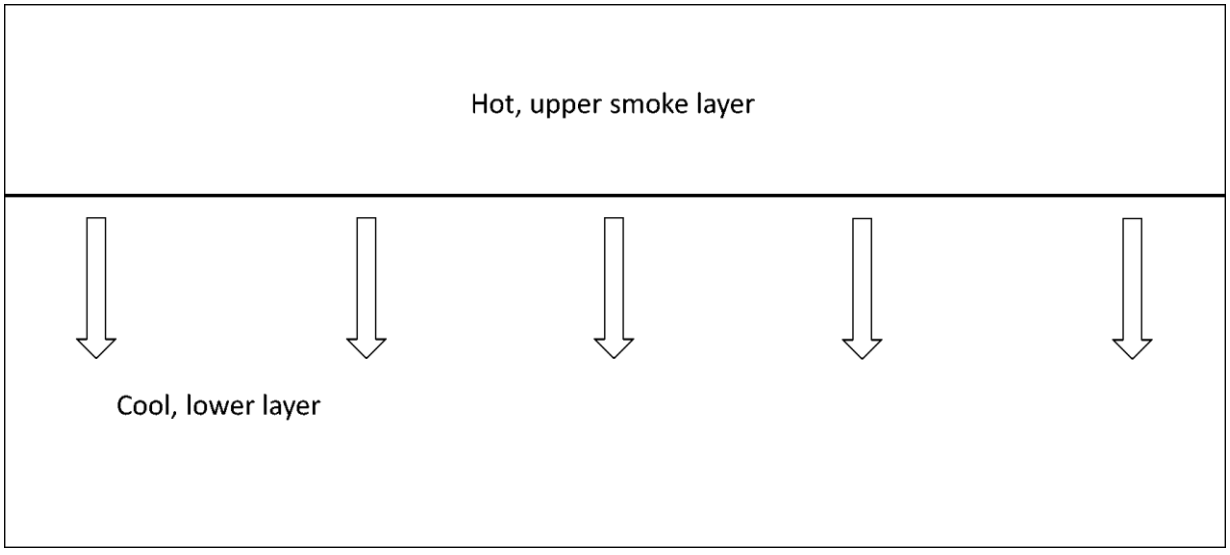

Figure 5. Fundamental two-layer approximation for two-zone model.

energy principles provide a set of differential equations which are solved to find the layer temperatures, layer interface height and internal pressure. Temperatures are assumed to be uniform throughout each respective layer. Conservation of mass within the layers is coupled with the ideal gas law to provide a framework for calculating species concentrations within each layer. Commonly tracked species include soot, carbon monoxide, carbon dioxide, hydrogen cyanide and oxygen gas. Species concentrations are assumed to be uniform throughout each layer.

Conservation of mass and energy lead to mathematical approximations of the properties of the two zones and their interactions (Wade, Baker, Frank, Harrison, & Spearpoint, 2016). Conservation of mass states the rate of change of the mass within the layer is equal to the sum of the mass source terms (R. Peacock, McGratten, Reneke, & Forney, 2015) which include the plume mass entrainment and mass flows into and out of the compartment through ventilation. Conservation of energy states the rate of change of each layers energy is equal to the sum of the heat release rate, convective heat losses to wall and net radiation, minus the energy used in expansion or contraction of the layer (R. Peacock et al., 2015). Pressure change within the room is calculated using the ideal gas law,

$$PV = mRT \tag{3}$$

where P is pressure (Pa), V is volume (m^3), m is mass of air (kg), R is the ideal gas constant with a value of $R = 287.0\ JK^{-1}kg^{-1}$ assuming the use of air properties and ambient temperature and pressure (Mowrer, 2016), and T is temperature (K). Pressure within the room is

$$\frac{dP_R}{dt} = \frac{\gamma-1}{V_R}(\dot{q}_L + \dot{q}_U) \tag{4}$$

where P_R is relative pressure within the room (Pa) and t is time (s). γ is the dimensionless ratio of heat capacities, V_R is the volume of the room (m^3) and $\dot{q}_U$ and $\dot{q}_L$ are the net heat transfer to the upper and lower layers (kW), respectively. The pressure is taken at floor level and is relative to atmospheric pressure. The pressure within the room is used to find the volume of the upper layer

$$\frac{dV_U}{dt} = \frac{1}{\gamma P}\left[(\gamma-1)\dot{q}_U - V_U\frac{dP}{dt}\right] \tag{5}$$

where V_U is the volume of the upper layer (m^3). The lower layer volume is the difference between the volume of the room and the volume of the upper layer. Layer height is calculated by dividing the lower layer volume by the floor area.

2.3.3 Model summary

When designing commercial buildings, the principal aim of fire engineers is to ensure evacuation of as many people as possible. Fire engineers achieve this aim by predicting the timing and evolution of the smoke layer. Both CFD and two-zone models can be used as quantitative tools for this task. Usually, fire engineers do not require the resolution that a CFD model may produce. Two-zone models simulate a simple fire scenario in seconds compared to days for the same situation in CFD models (Tavelli, Rota, & Derudi, 2014). Two-zone modelling allows quick and simple modelling of smoke and fire behaviour within compartments with simple geometry. The validity of underlying assumptions used in the two-zone modelling of high shape factor compartments will be investigated in this research.

2.3.4 Limits of two-zone approximation

The application of a two-zone model is only acceptable within the limits of validation. Validation of two-zone models involves comparing zone temperature, species concentration (typically CO,

CO_2, and O_2), visibility and layer height to real, full-scale fire data (R. D. Peacock, McGrattan, Forney, & Reneke, 2017). A significant number of two-zone models have been validated against full-scale pool fires in enclosures (Steckler, Quintiere, & Rinkinen, 1982). In the absence of full-scale fire tests for validation of a specific phenomenon, two-zone models have been compared with CFD models (Bong, 2011). The specific geometric and size characteristics of validation experiments define model limits. If the two-zone model shape factor upper limit is exceeded by the geometry of a building during design, the fire and smoke may behave differently than predicted. If the amount of smoke or fire is underestimated, there will be a significant negative impact on evacuating occupants and building structure. As such, the limits of the model are important guidelines for design.

To investigate the limits of two-zone model applicability, Bong (2011) compared results from the BRANZFIRE two-zone model to results from the Fire Dynamics Simulator CFD (FDS) model and multiple full-scale experiments. FDS is a CFD model using an LES equation simplification and assuming a low Mach number further simplifies the governing equations. FDS is mainly used for investigating fire-induced flows on a rectilinear three dimensional grid. A dimensionless fire size and shape factor (SF) was used to define the limits of the model. Bong (2011) used the dimensionless fire size defined by Zukoski (1978) as

$$\dot{Q}^* = \frac{\dot{Q}}{\rho_0 c_p T_0 \sqrt{g} H^{\frac{5}{2}}} \tag{6}$$

where $\dot{Q}$ is the heat release rate (HRR) measured in watts (W), $\dot{Q}^*$is the dimensionless heat release rate and T_0 is the ambient temperature (K). The heat release rate was used as a measure of fire size. The recommended limits of the dimensionless heat release rate were $0.002 < \dot{Q}^* < 0.03$ (Bong, 2011). However, Bong (2011) also found that a two-zone model and CFD model gave comparable layer height and upper layer temperature results for an upper fire size limit of up to $\dot{Q}^* < 0.15$ for specific fire characteristics. $\dot{Q}^* = 0.002$ represents a fire that releases a small amount of heat and smoke relative to the large volume of ambient air within the compartment. Below $\dot{Q}^* = 0.002$, the fire has a small heat release rate and there is a negligible rise in temperature smoke and a smoke layer may struggle to form. Two-zone models always assume a layer will form and if a layer does not form, the two-zone model is unlikely to predict accurate smoke behaviour. When $0.002 < \dot{Q}^* < 0.03$ the experiments and models included a period of heat release rate growth before the fire reached a steady state peak heat release rate. The two-zone models provided results comparable to CFD results, which rendered the two-zone approximation appropriate in this $\dot{Q}^*$ range. When $0.03 < \dot{Q}^* < 0.15$, the two-zone and CFD results were comparable for compartments with steady-state fires that immediately reach their peak HRR and stay constant at this HRR. A fire with $\dot{Q}^* = 0.15$ represents a fire producing large amounts of heat and volume of smoke relative to the volume of air within the compartment. Above $\dot{Q}^* = 0.15$ the hot upper smoke layer temperatures were not comparable between the two-zone and CFD models. Despite this discrepancy, layer heights were well predicted up to $\dot{Q}^* = 0.4$. If layer heights agree but upper layer temperatures do not, energy must be being transferred to the lower layer in one of the models. Bong (2011) did not investigate lower layer temperature but due to cooler upper layer temperatures in FDS and the high amount of radiant heat in the vicinity of the fire it is likely that the lower layer temperature is significantly higher in FDS (CFD model) compared to BRANZFIRE (the two-zone model).

Bong's (2011) dimensionless heat release rate limits were restricted to when the compartment geometry adheres to shape factor (SF) limits of $0.4 < SF < 69$ as calculated using Equation (1). The lower limit of $SF = 0.4$ represents the smallest of a number of full-scale atrium fire experiments that were compared to a two-zone model (Bong (2011). A room with a SF of 0.4 is

tall and narrow, such as an atrium or lift shaft. The upper limit of $SF = 69$ is defined by comparisons between fire data modelled in a two-zone model and a CFD model of a series of warehouses of increasing size, which have the largest shape factor of all of Bong's comparisons (2011). A room with a SF of 69 is short and stout, such as a storage warehouse. When the $SF < 0.4$ the room is much taller than it is wide and there will be significant interaction between the smoke plume and the walls. If the SF > 69 the smoke may not have enough buoyancy to effectively form a layer due to dilution of the smoke as it travels the long distance to the walls of the compartment and back to the plume. If the model is used outside the SF limits, the model predictions of fire and smoke behaviour cannot be relied upon.

This study expands upon and refines shape factor limits of applicability for two-zone models. Emphasis is placed on the upper limit of shape factors due to the large number of warehouse-style, short and stout buildings modelled with two-zone models. Shape factor limits are analysed with the B-RISK two-zone model (Wade et al., 2016). B-RISK is a typical two-zone model based on the same governing equations as other commonly used two-zone models (Section 2.3.2). Comparisons of common two-zone models are discussed by Olenick & Carpenter (2003).

2.4 Physical scale model

Comparing two-zone model results to other models that include real fire characteristics refines the limits of the two-zone assumption. Previous modelling of real fires has been conducted using CFD modelling, full-scale fire tests, salt-water modelling and thermal-water modelling.

CFD models have been used to validate two-zone models (Bong, 2011; Wade & Robbins, 2008) because CFD models allow a certain set of conditions to be modelled without the need for a physical lab experiment and both models can be directly compared. Robust validation is necessary for reliable use of two-zone models. CFD models are capable of producing detailed models of fire and smoke behaviour in complex geometries and applications but require large time and computational resources for thorough investigation. Bong (2011) has previously assessed the geometric limitations of a two-zone model using a CFD model and this study is looking to take a different approach to a similar research problem. An alternative to CFD models is to use physical models.

Modelling smoke development using water is common and provides useful experimental results for comparison with two-zone models. To model flows involving buoyancy forces, such as smoke flows, water of altered density is introduced into ambient water. The two typical methods for altering water density are thermal and salinity adjustment. Thermal-water modelling involves injecting heated water into room-temperature water and exploiting the buoyancy forces that arise due to temperature differences to simulate the density difference between smoke and air (Partridge & Linden, 2013). Due to the inability of the heated water to reliably reach a sufficient temperature to provide buoyancy forces of a large enough scale to represent typical smoke flows (Partridge & Linden, 2013), the thermal-water model is not experimentally explored in this study.

Salt-water modelling utilises the interactions between saline water and freshwater to model the density difference between smoke and air. Salinity is typically controlled by addition of pure salt into a solution which is then injected into fresh water. Salt-water physical modelling is well established and has been used extensively in modelling smoke movement in compartments (Clement, 2000; McBryde, 2008; Steckler, Baum, & Quintiere, 1986; Yao, 2006; Yao & Marshall, 2007). Salt-water modelling is a popular fire modelling method because the density difference achieved between salt and freshwater allows creation of buoyancy-driven flows that are sufficiently turbulent for comparison with fire-induced smoke flows. For ease of experimental setup, salt-water represents combustion products and is injected into freshwater. The difference in density creates buoyancy forces which drive the flow of salt-water through the space.

Differences in flow characteristics between fresh- and salt-water interactions and air-smoke interactions introduce errors when comparing flows. When injecting salt-water, it is introduced with an initial velocity. Smoke plumes from fires are purely buoyancy driven. This injection velocity means the salt-water flow is required to travel a distance from the source pipe before being fully buoyancy driven and have fully developed turbulence. For the comparison between the two-zone model and salt-water experiment to be useful the length of this transition of the salt-water to fully developed buoyancy driven flow needs to be small relative to the water depth. Reducing the transition length can be a difficult balancing act of flow velocity, source size, and source fluid properties.

In a real fire, the walls of the room absorb some of the heat. The surfaces of the tank do not absorb salt from the flows due to practical limitations, which presents a major difference between model and reality. The buoyancy forces near the surfaces are therefore relatively

higher than their fire-induced flow equivalents. This discrepancy occurs because the concentration of salt is higher than it would be if salt was removed from the flow through absorption from the walls. Despite this discrepancy, salt-water flows model smoke flow well in regions far from the surfaces of the tank.

As salt-water is introduced into freshwater, there is an increase in fluid volume in the tank. The increase in fluid volume has little effect on the salt-water flows as the free surface of the water only rises a small amount relative to the water depth. When adding smoke and heat to a fire room the compartment volume does not increase and therefore the rising temperature causes the gases in the compartment to expand and pressure increases. To minimise the effect of the increase in pressure, sufficient ventilation must be built into the two-zone model. If over-pressurisation occurs the temperatures in the fire compartment will increase as shown by the ideal gas law (3). The increase in temperature due to over-pressurisation is not captured by the salt-water experiments and is to be avoided through providing adequate ventilation.

Salt-water experiments can be used to investigate fires in compartments due to the assumption of a constant buoyancy flux in each experiment or model. As the fire heats up the compartment, temperature changes which causes small increases in both specific heat capacity and the thermal expansion coefficient, which are normally assumed to be constant in fire-induced flows. The specific heat capacity and thermal expansion coefficient are used to compute the local buoyancy flux (Equation (2)) which is also assumed constant in salt-water experiments and fire induced flows. As temperature increases, the small changes in these air properties will cause a change in the buoyancy flux, meaning it is not constant. These changes are likely to be small for the temperature changes typically seen in the compartment fires that are being investigated and will have a negligible effect on the results.

Once salt-water experiments are finished the data requires scaling to be directly comparable to a fire in a fire compartment due to the differences in buoyancy flux and compartment size. The scaling methods for time and length scales are robust but are not as intuitive to understand as comparing fire compartment to fire compartment at the same scale, as in verification using CFD models or full-scale fire tests.

The most accurate method of measuring the applicability of two-zone models is through using full-scale fire experiments. Full-scale experiments involve igniting a fire within a room typical of a specific building type and function. If correctly designed, conducting a full-scale experiment in a controlled laboratory setting provides results which can accurately reflect physics of fires and smoke transport seen in real fires. The full-scale experiment results can be directly compared to model predictions. Uncertainty in the results of full scale fire tests are due to error in the measurement methods, limited locations of measurement, operator error, environmental conditions, or undetected equipment failures (Lindholm, Brink, & Hupa, 2008). Fire experiments have been used successfully for model validation in the past (Röwekamp et al., 2008) but are not investigated in this study due to time and cost constraints.

Previous research indicates that the salt-water physical model is a promising model for validating two-zone computational models and will be used to validate the use of two-zone models in this research.

2.5 Buoyant-jets

Although the salt-water modelling method is accepted as the most reliable method for validating two-zone computational models, it still has some complications. Modelling smoke plumes with the salt-water method is difficult because the source must have an initial velocity. The flow that exits the vertical salt-water source creates a buoyant jet when leaving the source and converts into a plume far from the source with a transition region between the two limits. Far from the source, results are scalable into properties comparable to smoke plumes. Smoke plumes and the plume portion of the salt-induced flow are similar. The buoyancy flux (B) within the salt-water buoyant jet is conserved throughout the flow and is defined as

$$B = g'Q_0 = g_0'Q_0 = B_{0,sw} \tag{7}$$

where B is the buoyancy flux at any point in the plume ($m^4\ s^{-3}$). g_0' is the initial reduced gravity at the source ($m\ s^{-2}$) given by

$$g_0' = g\left(\frac{\rho_0 - \rho_a}{\rho_a}\right) \tag{8}$$

where g is acceleration due to gravity ($m\ s^{-2}$), ρ_0 is the initial density of the discharge fluid ($kg\ m^{-3}$), and ρ_a is the density of the ambient fluid ($kg\ m^{-3}$). Reduced gravity quantifies the density excess. Q_0 is the initial volume flux ($m^3\ s^{-1}$) defined by

$$Q_0 = u_0 \frac{\pi D_{source}^2}{4} \tag{9}$$

where u_0 is the initial velocity of the discharge fluid ($m\ s^{-1}$) and d is the diameter of the discharge source (m).

The characteristics of the jet portion are dominated by the initial momentum flux, M_0 ($m^4\ s^{-2}$),

$$M_0 = Q_0 u_0. \tag{10}$$

Momentum flux is not conserved throughout the buoyant jet.

To determine the dominance of jet or plume flow properties, a plume characteristic length scale, l_M (m), defined as

$$l_M = \frac{\mathrm{M}^{\frac{3}{4}}}{\mathrm{B}^{\frac{1}{2}}} \tag{11}$$

is used (Fischer et al., 1979). The characteristic length scale and the vertical distance from the source, z (m), define the distance from the source where the transition section occurs.

Defining the location of flow regime transition is based on non-dimensionalised dilution characteristics changing as a function of dimensionless distance from the source. Through investigating experimental results the change in behaviour from momentum-driven flow to the jet-plume transition region occurs at $\xi = 0.5$ and the transition from the jet-plume transition region to buoyancy-driven flow occurs at $\xi = 1$ (Figure 6) where ξ is defined as

$$\xi = \frac{\mathrm{C_p}}{\mathrm{R_p}} \frac{z}{l_M} = C_p \left(\frac{z}{l_Q}\right)\left(\frac{R_0}{R_p}\right) \tag{12}$$

where C_p is the asymptotic value of the width parameter and is constant at $C_p = 0.254$ for a buoyant jet, l_Q is the characteristic length for jets (m), R_p is the asymptotic value of the local Richardson number and is constant at $R_p = 0.557$ for a buoyant jet, and R_p is the local Richardson number defined as

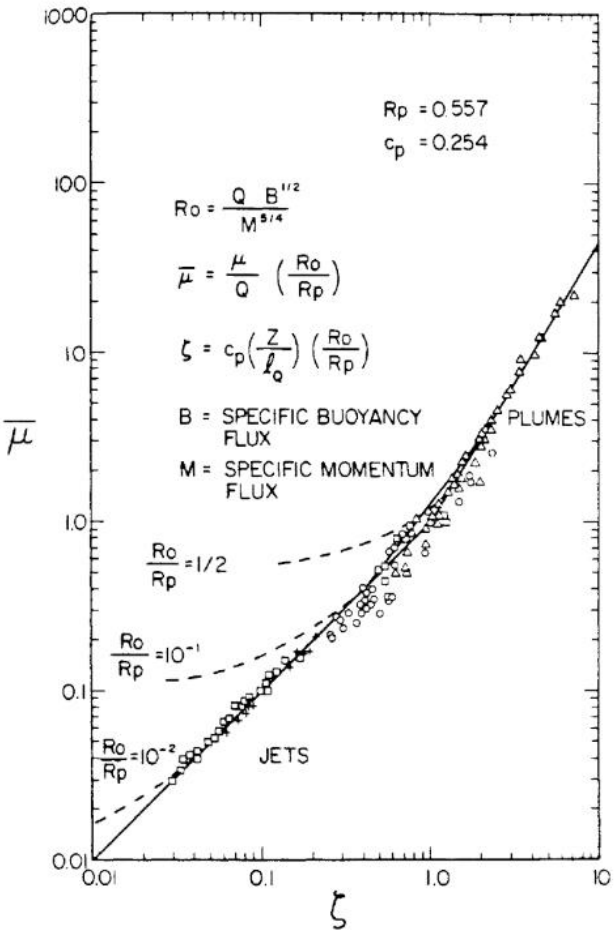

Figure 6. Asymptotic solutions for dilution in a vertical round turbulent buoyant jet compared to experimental data of Ricou and Spalding (1961) (Extracted from Fischer et al (1979))

$$R_0 = \frac{QB^{\frac{1}{2}}}{M^{\frac{5}{4}}} \qquad (13)$$

Through inspection, Fischer et al. (1979) also showed time averaged volume flux ($\bar{\mu}$) grew much more rapidly within the plume-like portion of the flow compared with time averaged volume flux in jet-like flows (Figure 6). However it is noted that all buoyant jets being tested using salt-water modelling exit the source with an approximately uniform velocity and therefore an initial volume flux which will be greater than the plume-flow induced volume flux for a portion of the flow as the plume-flow volume flux grows. A shear layer forms between the two fluids which reduces velocity at the edges of the jet. The shear layer generates eddies along flow edges that cause entrainment of ambient fluid. This entrainment causes the volume and therefore radius of the flow to increase with vertical distance away from the source. The mean velocity profile develops a self-similar Gaussian profile at a distance equivalent to about six source diameters downstream of the source (Fischer et al., 1979). The velocity of the fluid decays as it travels further from the source. The velocity will be dominated by the initial source velocity until it has decayed significantly and the transition to mixed behaviour has occurred. The velocity in the momentum driven part of the flow decays linearly with distance from the source (Fischer et al., 1979). The velocity decay within the buoyancy-driven flow occurs is proportionate to the cube root of the distance from the source, meaning velocity decays much more slowly in buoyancy-driven flows. Once buoyancy-driven flow occurs the velocity is based on the initial source buoyancy flux and distance from the source (Fischer et al., 1979).

The growing volume and radius of the plume with distance from the source lead to an intuitive understanding that density decreases with distance from the source. However, this decrease in density occurs as a function of the distance from the source throughout the flow and also as a function of initial source buoyancy flux within the buoyancy-driven flow region (Fischer et al., 1979). Density decreases linearly with distance from the source while the initial velocity dominates the flow in the momentum-driven flow region. Density then decreases proportionate to $B^{\frac{1}{3}}z^{\frac{5}{3}}$ throughout the buoyancy-driven portion of the flow, which is much more rapid than within the momentum-driven flow region.

2.6 Flow comparison

Salt-water modelling of smoke layer formation and evolution is possible by non-dimensionalising flow properties and geometry through the principles of dynamic similarity (Quintiere, 1989). Buoyancy is the governing driver of flow characteristics and properties within both fire-filled compartments and salt-water experiments. Through non-dimensionalising the key flow variables using the buoyancy flux, these variables scale into quantities that are comparable between two-zone models and salt-water experiments.

Characteristic length and time scales are required to perform the non-dimensionalisation as part of the presentation of the results. Throughout the two-zone model simulation distances are non-dimensionalised using

$$x^* = \frac{x}{H}. \tag{14}$$

The scaling is linearly dependent on the compartment height. Compartment height was used for scaling because the height was the most important length scale for layer interface descent comparisons between two-zone models and salt-water experiments. Throughout the two-zone model simulation time is non-dimensionalised by

$$t^* = t\frac{\sqrt[3]{B_f H}}{A_f}. \tag{15}$$

where t^* is non-dimensionalised time and A_f is the cross-sectional area of the fire compartment (m^2). The scaling is linearly dependent on the compartment cross sectional area and has cube root dependence on the compartment height and buoyancy flux. The scaling is highly dependent on cross-sectional area because for compartments of high shape factor, the time scale of the ceiling jet flows and their impact on the compartment smoke or salt-water layer filling is important. The scaling is also dependent on compartment height as the time scale for smoke to travel to the ceiling were important for comparison of the two-zone models and salt-water experiments. Likewise the buoyancy flux is included in the scaling because of the impact of different buoyancy on the time scale of smoke transport throughout each two-zone model and experiment.

Similarly, salt-water length scaling is non-dimensionalised by

$$x^* = \frac{x}{h} \tag{16}$$

where h is the water depth in the experiment (m). The salt-water scaling for experiment time is non-dimensionalised by

$$t^* = t\frac{\sqrt[3]{B_{0,sw} h}}{A_{sw}} \tag{17}$$

where t^* is non-dimensionalised time and A_{sw} is the cross-sectional area of the experimental tank parallel to the bottom (m^2).

For salt-water experiment comparisons with two-zone models to make sense, the energy of the represented by the salt added in the salt-water experiment must be scaled to be equal to the energy in the two-zone model due to heat added by the fire. The rate of energy added to the two-zone model system is described by HRR and is constant throughout time. The rate of equivalent pseudo-energy added to the salt-water experiments is represented by the mass of salt being injected into the tank. The rate of salt-mass being injected into the talk is constant because flow is constant and the source fluid is well mixed. Because HRR and mass injection rate are constant throughout, energy is added to the two-zone models and salt-mass is added to

the salt-water experiments at constant rates. In each case this causes the rate of change of density deficit to be constant and the area under the density deficit profiles increases linearly with time (Equation (8)). The source buoyancy fluxes, water depth and compartment height are all constant with time and this linear increase can, therefore, be applied to the density deficit profiles. If the areas under the density deficit profiles for the experiment and model are equal, the total energy of both systems will be equal and the systems comparable. To correct the dimensionless density deficit profile for this area, an area multiplier is defined as the two-zone area integral over the experimental profile area integral which is described by

$$C = \frac{\int_0^1 g^*(y^*,t^*)dy^*}{\int_0^1 I_{sw}^*(y^*,t^*)dy^*} \quad (18)$$

which when simplified is

$$C = \frac{g_{UL}^*(t^*)*(1-y_{LH,f}^*)}{\int_0^1 I_{sw}^*(y^*,t^*)dy^*} \quad (19)$$

where g_{UL}^* is the upper layer dimensionless reduced gravity predicted by the two-zone model at t^*, a specific dimensionless time. $y_{LH,f}^*$ is the dimensionless two-zone model layer height and I_{sw}^* is the normalised salt-water experiment depth integrated density profile. The upper layer dimensionless density deficit is calculated by first converting layer temperatures into densities using

$$\frac{\Delta\rho}{\rho} = \alpha\Delta T \quad (20)$$

for small temperature changes estimated by the model. Layer reduced gravities are calculated using Equation (8). The layer reduced gravities are normalised because the reduced gravity of the lower layer is zero.

For the comparisons to work the flows must have the same characteristic properties. These characteristics properties can be defined by Reynolds, Grashof, Schmidt, Prandtl, and Froude numbers. The Reynolds number (Re) is a dimensionless parameter which defines the ratio of the inertial forces to the viscous forces in a flow. When the Reynolds number is high, the flow becomes turbulent and independent of viscous forces. The exact Reynolds number where the flow becomes turbulent is difficult to predict. However, turbulence is assumed when $Re > 2000$ (Fischer et al., 1979). The Reynolds numbers for salt-water flows is defined as

$$Re_{sw} = \frac{u_{sw}D_{source}}{\upsilon_{sw}} \quad (21)$$

where υ_{sw} is the kinematic viscosity of salt-water ($m^2\ s^{-1}$). The Reynolds number for flames in a fire is defined as

$$Re_f = Gr_f^{\frac{1}{3}}. \quad (22)$$

The Reynolds number is wholly dependent on the Grashof number (Gr) because the smoke has no initial velocity (Yao, 2006). The Grashof number is a dimensionless parameter which defines the ratio of the buoyancy forces to the viscous forces in a flow and is related to free convection. The Grashof number for the fire-induced flows is defined as

$$Gr_f = \frac{g\beta_T\dot{Q}_f D_f^2}{\rho_0 c_p \upsilon^2}. \quad (23)$$

Here D_f is the diameter of the fire (m), v is the kinematic viscosity of ambient air ($m^2\ s^{-1}$). When the Reynolds numbers for both flows are above 2000, they are considered turbulent and have independence from viscous forces (Fischer et al., 1979).

The Schmidt (Sc) and Prandtl (Pr) numbers are dimensionless parameters that quantify molecular transport during fluid flows. The Schmidt number is the ratio of the diffusion of the momentum and the diffusion of mass and governs the diffusion of salt during the salt-water flows. The Schmidt number is defined as

$$Sc = \frac{v_{sw}}{D_{sw}} \tag{24}$$

where D_{sw} is the salt diffusivity ($m^2\ s^{-1}$). Salt-water has a typical Schmidt number of around 700 (Haynes, Lide, & Bruno, 2014). The Prandtl number is the ratio of momentum diffusion and the diffusion of heat and governs the diffusion of heat by the smoke during a fire. The Prandtl number is defined as

$$Pr = \frac{c_p \mu}{k} \tag{25}$$

Where μ is the dynamic viscosity of ambient air ($kg\ m^{-1}\ s^{-1}$) and k is the thermal conductivity of ambient air ($W\ m^{-1}\ K^{-1}$). Air has a typical Prandtl number of around 0.7 (Haynes et al., 2014). It is not practical to match the Schmidt and Prandtl numbers for salt-water and fire-induced flows. Fortunately, when flows become fully turbulent (at Reynolds numbers above $Re > 2000$), flows become independent of diffusive effects (Linden, 1999) and molecular transport terms have a negligible effect on flow characteristics (Steckler et al., 1986).

The initial salt-water source flow regime can be defined using

$$Fr = \frac{u_{sw}}{\sqrt{g' D_{source}}} \tag{26}$$

where Fr is the Froude number. The Froude number is a dimensionless parameter which defines the ratio of inertial forces to gravitational forces and is related to the strength of the buoyancy relative to the momentum of the flow at the source or flame. If $Fr \gg 1$ then momentum effects dominate, which results in a long transition length in a salt-water buoyant jet. Alternatively if $Fr \ll 1$, buoyancy effects dominate and transition length is negligible in a salt-water buoyant jet. All fires considered in this research are compartment fires which are considered to cause pure smoke plumes, meaning the buoyancy effects dominate and $Fr \ll 1$.

The Richardson number (R) is a dimensionless parameter related to the Froude number and quantifies the balance between buoyancy and inertial forces. Specifically, R relates to the flow near the source and development of plume-like flow characteristics. If $R \geq 1$ then plume-like characteristics dominate the flow close to the source and the transition lengths are small.

2.7 Summary

Two-zone models, their usefulness and limitations have been discussed and an appropriate experimental representation of fire-induced flow chosen. The physical scale model chosen was salt-water modelling which uses injection of salt-water into fresh-water to simulate smoke movement from a fire within a compartment. The different mediums and geometric sizes produced challenges for comparison. The challenges due to different mediums were unlikely to be significant relative to the scale of the flows. Appropriate scaling of the length and time scales was developed to ensure the behaviour of the two-zone model and the salt-water experiments could be compared directly and easily.

3 Methodology

This chapter describes the experimental setup and methodology used to model smoke flows within a building compartment. This task is accomplished using both computer modelling and physical salt-water modelling. A description of the salt-water experimental setup, discussion of the experimental procedure and analysis of the images is provided in Section 3.1. The setup of the two-zone model and derivation of model variables is provided in Section 0.

3.1 Experimental setup and procedure

3.1.1 Tank

A 0.9-m-deep Perspex experimental tank with a 1.01-m-square cross-section was used for salt-water modelling (Figure 7). An outer tank with a 2-m-by-1.01-m cross-section surrounded the experimental tank, with 0.5 m between the sides of the two tanks. Aluminium box sections formed a platform for the experimental tank. A 50 L pressure tank containing dyed salt-water sat in the space between the outer and experimental tanks. This pressure tank was connected to a compressed air supply and a 20-mm-diameter vertical stainless steel source pipe. The source

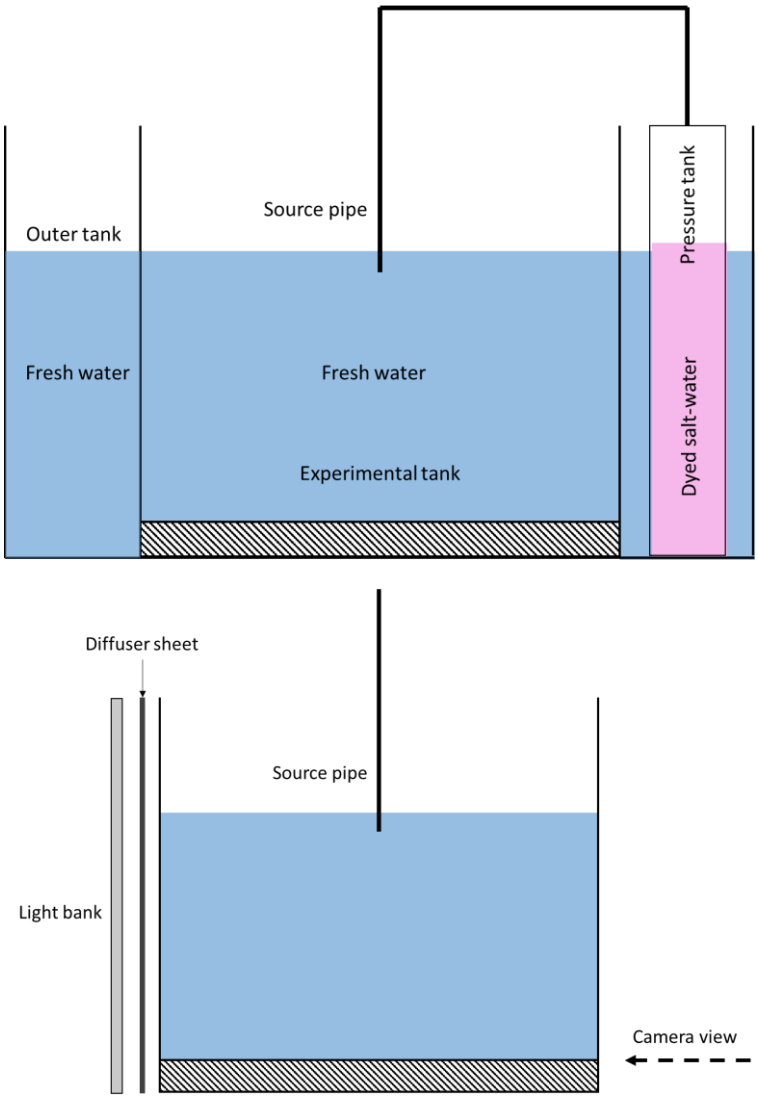

Figure 7. (a) Front view of experimental setup used for salt-water modelling. (b) Side view of experimental setup used for salt-water modelling.

pipe directed the salt-water into the experimental tank. The source pipe was straight for 1000 mm preceding the injection point to ensure the establishment of fully developed pipe flow. Above the straight section was an elbow with a valve to control salt-water flow and another valve connected to a vacuum. The terminus of the source pipe was located in the centre of the experimental tank.

In every experiment, both the experimental and outer tanks were filled simultaneously to ensure that the experimental tank walls remained plumb. Both tanks were first filled with freshwater to a depth corresponding to the shape factor being investigated. The source pipe was adjusted such that the terminus was 2 mm below the free surface of the freshwater. Salt-water containing 0.5% salt by mass was injected into the centre of the experimental tank. Throughout all experiments, salt-water was fed at 0.028 Ls^{-1} from a pressure tank held at 0.1 MPa.

Red Carmoisine powder (colour #25070, food additive code No. 122) was mixed into the salt-water to enable visual differentiation between the salt-water and freshwater by giving the fluids different light absorption properties. Carmoisine was an appropriate dye powder because it does not react with salt (NaCl) and its ability to absorb light does not change significantly over time (Kikkert, 2006).

3.1.2 Image capturing equipment

A JAI GigE Camera captured high-resolution 1392x1040 pixel images of the experiment from a distance of 8 m at 15 images per second. The camera was positioned perpendicular to and at the same height as the centre of the bottom of the tank. The camera lens was centred at the bottom of the tank to reduce the amount of parallax error in measurements of the layer height, which occurred near the tank bottom.

The camera captured colour images of the tank, which was backlit by an array of linear LED strip lights. These lights were spaced evenly and setup behind a white acrylic sheet (Figure 7) to provide backlighting that was uniform.

3.1.3 Calibration

Light attenuation (LA) was a technique used to capture flow phenomena throughout every experiment. LA uses measurements of changes light intensity to quantify concentrations throughout the tank (Cenedese & Dalziel, 1998). The relationship between light intensity variations and source fluid concentrations needed to be determined for each shape factor. LA was able to convert light intensity variation into concentrations through establishing a set of calibration images of the tank for each experiment. These calibration images captured the tank containing fresh-water and fresh-water mixed with dye and salt to make solutions equivalent to 0, 20, 40, 60, 80, and 100% of the maximum expected concentration.

The maximum expected concentration was different for each shape factor due to changes in the amount of dilution. Changing water depth and source height altered the amount of freshwater entrainment within the salt-water plume. The greater the depth, the more entrainment and greater dilution of the dyed salt-water. Differentiation between salt and freshwater is clearest when light absorption is maximised, which occurs when dye concentration is greatest. The relationship between light absorption and dye concentration for Carmoisine powder in salt-water was investigated by McBryde (2008) (Figure 8) and found to be linear below a width integrated dye concentration of 0.12 $g.m^{-3}.m^{-1}$. Therefore the maximum acceptable dye concentration was 0.12 $g.m^{-3}.m^{-1}$. To maximise dye concentration within the salt-water layer, the maximum width-integrated dye concentration was estimated at the bottom of the tank as a function of buoyant jet characteristics. The amount of entrainment and therefore dilution in the

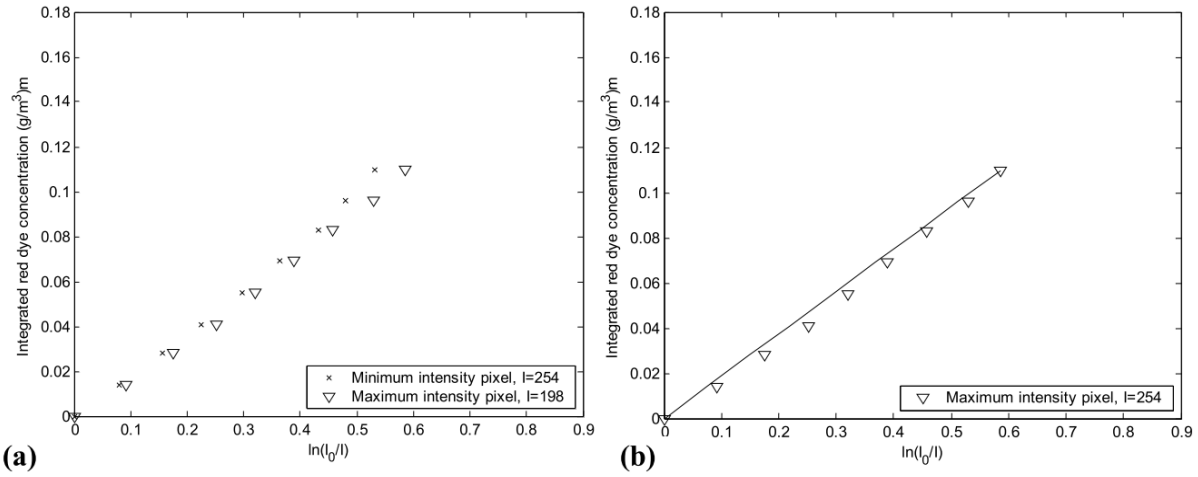

Figure 8. Typical plot of green light optical thickness versus integrated red dye concentration from calibration experiment with red dye and salt: (a) typical experimental dataset, (b) line of best fit from origin to the transitional concentration (McBryde, 2008)

plume was estimated as similar to a jet before the transition to mixed buoyant jet behaviour and similar to a plume after the transition to mixed buoyant jet behaviour. The transition distance between jet and plume was assumed to have plume dilution characteristics because the plume dilution is much greater than the jet or mixed dilution.

The maximum width-integrated dye concentration based on the jet portion of the flow is defined through the ratio of the maximum time-averaged salt-water concentration to the source concentration by

$$\frac{C_m}{C_{J0}} = 5.64\ \left(\frac{l_Q}{h}\right). \tag{27}$$

Here, C_{J0} is the initial mass concentration in the jet (g m^{-3}) and l_Q is the characteristic length of the jet (m). C_m is the maximum dye concentration at the bottom of the tank (g m^{-3}) defined with a practical upper limit of 0.12 g/m^3 m for Carmoisine powder (McBryde, 2008). To include the plume in the estimate of maximum width-integrated concentration, the maximum concentration is calculated using

$$\frac{C_m}{Y} = \frac{9.1}{B^{\frac{1}{3}} h^{\frac{5}{3}}} \tag{28}$$

where B is the initial buoyancy flux (m^4 s^{-3}). Y is the pure plume mass flux (kg s^{-1}) defined by

$$Y = \frac{Q}{C_{P0}} \tag{29}$$

where Q is the volume flux of the source (m^3 s^{-1}) and C_{P0} is the source concentration in a pure axisymmetric plume (g m^{-3}). Initial concentrations required for pure jet and pure plume cases were added proportionally based on the ratio of the transition length and water depth as

$$C_0 = C_{J0} * \left(\frac{l_{jm}}{h}\right) + C_{P0} * \left(1 - \frac{l_{jm}}{h}\right) \tag{30}$$

where l_{jm} was the length of transition from jet to mixed buoyant jet behaviour from the source (m). Equation (30) gave an estimate of the initial source dye concentration required to achieve 0.12 g/m^3 at the impingement point. Maximising source dye concentration allowed the highest accuracy in measuring light intensity changes due to the presence of dye. Concentration was assumed to be homogeneous throughout the width of the tank to ensure maximum dye

concentration was not exceeded. Concentration estimates were acceptable because calibration experiments corrected for the actual salt and dye concentrations in the salt-water.

The calibration tank concentrations were determined at 0, 20, 40, 60, 80, and 100% of the maximum calculated dye and salt concentrations. Once calibration was complete the experimental results were obtained.

3.1.4 Experimental procedure

Every experiment followed an identical procedure. The tank had a constant cross section and therefore different experiment shape factors were represented with different water depths.

Dyed salt-water was pumped through the source pipes, which forced air out of the pipes. Once all air bubbles were removed, the flow was stopped by closing the valve. Air needed to be removed from the pipes because it created turbulence as it exited the end of the source pipe and formed bubbles in the freshwater that ascended through the water. This added turbulence disturbed the buoyant jet flow, which changed flow dynamics and increased uncertainty in the salt-water model results. To minimise the effect of air, a vacuum was attached at the elbow joint of the source pipe. Ambient fluid from the experimental tank was sucked up the tube until all air was removed from the straight section of pipe. The effect of this small volume of freshwater entering the experimental tank before the source fluid was insignificant relative to the volume of fresh-water within the experiment, the total volume of source fluid injected into the tank. The time taken to inject this freshwater was small relative to the total time of the experiment. Moreover, the relative effect of this fluid was small compared with the effect of the turbulence from extra air in the system.

The water used in the experimental and outer tanks, as well as in the source fluid, all used filtered tap water. The temperature of this water was initially significantly colder than the air temperature within the lab. As the water warmed up to room temperature, convection currents formed due to buoyancy forces. Water was allowed to warm to ambient temperature overnight before experiments were conducted to ensure all of the buoyancy forces were due to the addition of salt and dye rather than temperature.

As the water warmed to room temperature, air bubbles formed against the inner surfaces of the tank. Air bubbles refract light and were cleared to ensure consistency in image capturing. Cleaning the Perspex of dust and water droplets immediately prior to commencing experiments ensured a consistent medium through which the light could pass.

After the tanks were prepared for the experiments and air bubbles were removed, image capturing commenced. Experiments began when dyed salt-water was injected into the freshwater tank. The valve was opened slowly to reduce bubble generation within the valve. 15,000 images at 15 frames per second were captured. Each experiment ran for 1000 s to ensure the salt-water layer had fully developed, evolved a significant amount relative to the depth of the water and that the dynamics of the flows were recorded for different stages of the formation and lowering of the layer.

3.1.5 Image processing

Streams is an image processing application developed at the University of Canterbury, New Zealand by Professor Roger Nokes that provides a range of tools for analysing fluid flow experiments involving flow visualisation (Nokes, 2016). For this study, Version 2.06 of the software was used to extract the integrated two-dimensional concentration field from the experimental images as a function of time using Light Attenuation (Cenedese & Dalziel, 1998).

The camera captured colour images of the tank, which was backlit by LED lighting strips behind the tank. To the human eye, the light given off by the LEDs appeared white however the camera showed a green light throughout the image (Figure 9). Correcting the lighting to show a realistic white light is rendered through a process called white balancing. White balancing is a process where the colours at each pixel are scaled such that RGB light intensities are the same number within each pixel (i.e. the red, green and blue colour values are equal at each pixel) (Figure 10). A reference white balanced image of the tank before the experiment began was used to determine the light intensities before dye was injected.

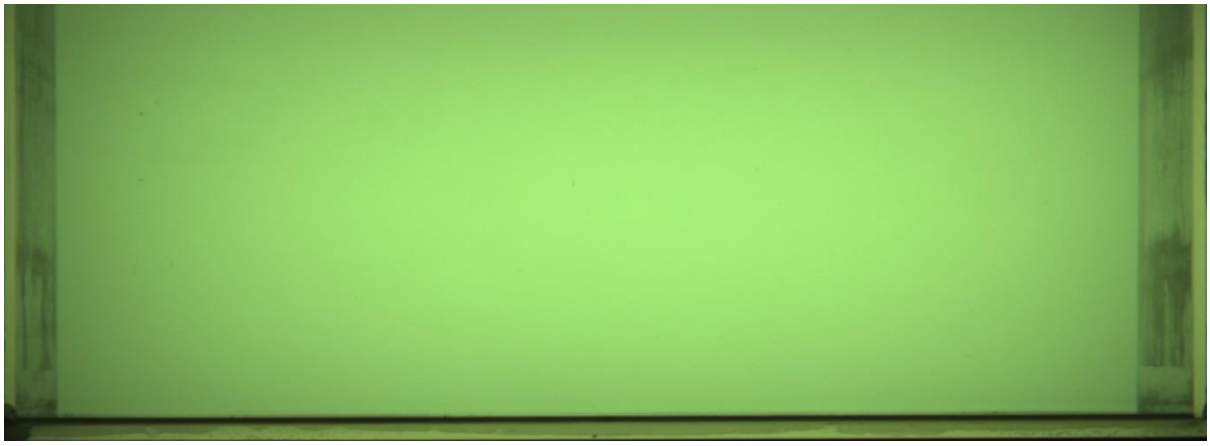

Figure 9. Photo showing the green light given off by the LED backlights and picked up by the camera.

Light intensity at each pixel in the white balanced reference image was compared to each experiment image to quantify absorption of light throughout the experiment. The intensity of each pixel of the white balance reference image was used as a reference intensity for that same pixel in each experimental image. As red dye was added, intensity changed in affected pixels. The amount of change in light intensity was quantified using a 32-bit colour code.

The measured light intensities suffer from noise due to both camera noise and fluctuations in the LED lights. Variations in input voltage fluctuate around an average. The field is time-averaged over one-second intervals to remove the effect of these variations.

Figure 10. White balanced reference image with RGB values constant at each pixel.

3.1.6 Light attenuation

The calibration images were used to convert the 32-bit real value colour fields produced from each image in each experiment to useable depth integrated density fields. The 32-bit real value colour of each pixel in each of the calibration images was used to create a mathematical relationship between depth integrated density added and colour added for each individual pixel. These mathematical relationships were linear. The depth integrated density added was

calculated from these relationships at every pixel and then averaged and computed at a set of uniformly separated nodes on a rectangular grid for each time step. These nodes were distributed throughout the experimental images. As layer height is more important than lateral dispersion of the fluid, there were more nodes in the vertical direction. The number of nodes changed for each experiment based on the extent of the domain. The density field allowed the flow to be analysed both spatially and temporally.

Simplification and development of the depth averaged density deficit field data is necessary in order to ensure the layer height methods provide reliable results. Simplification was achieved through averaging the nodes across the tank allowing a single representative vertical depth averaged density deficit profile to be analysed for each side of the tank. Areas outside the rear wall of the tank and within the plume region were not included in the analysis to reduce the parallax error of measuring through the tank wall and reduce the effect of the higher light intensities found within the plume.

For direct comparison, the model and experiment must represent the same total energy (described in Section 2.6). To create comparable data, the depth integrated density deficit profile must be scaled. To accomplish the conversion, the integral of the depth averaged density deficit profile and the density deficit of the upper layer of the two-zone model were used to calculate the area multiplier through Equation (19). The depth averaged density deficit profile was then multiplied by this area multiplier (C), creating a dimensionless density deficit profile with the same energy as the two-zone model calculation. This profile was determined at each experimental time step which had been non-dimensionalised using Equation (17). Distances were non-dimensionalised using salt-water depth through Equation (16) to allow comparison with non-dimensionalised two-zone layer heights.

3.1.7 Layer height

The depth integrated density fields throughout each experiment were analysed to define experimental layer height for comparison to the two-zone model. Visually, the layer height can be defined with relative ease. However, the layer interface has a non-trivial depth integrated density gradient across it (Figure 11). This meant that it was difficult to define the exact layer height throughout each experiment and a calculation method was employed to provide discrete measurements. Calculation of smoke layer height is well established in the literature for vertical profiles and these can be used to determine the salt-water layer heights in the experiments. Notably, Cooper et al (Cooper, Harkleroad, Quintiere, & Rinkinen, 1982) developed the N-percentage rule and He et al (1998) developed both the integral ratio and least squares

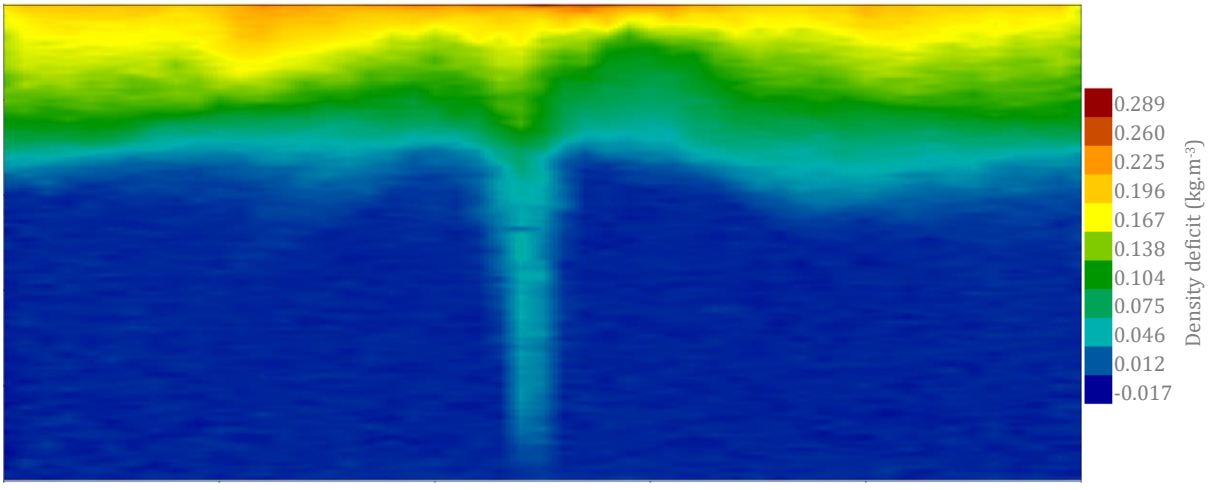

Figure 11. Shape Factor 5 experimental light depth integrated density field at t = 176s, t=0.99.*

methods. These three methods have been explored to determine the most appropriate method for comparison of two-zone model and experimental layer heights.

3.1.7.1 N-percentage method

The N-percentage rule was the first method explored for layer height calculation. This method involved estimating layer height at a certain time through the assumption that the layer interface occurred at a percentage of the maximum dimensionless density deficit within the profile.

In equation form, the N-percentage method was defined as

$$\mathrm{N}[g^*_{UL}] = CI^*_{sw}(y^*_{LH}, t^*) \tag{31}$$

where N was a chosen percentage and C was the area multiplier defined by Equation (19). $N = 1$ represents layer height as the height at which the average two-zone upper layer density deficit occurs for that non-dimensional time. Likewise, $N = 0.1$ represents the layer height occurring at 10% of the average two-zone upper layer density deficit for that non-dimensional time. The location at which Equation (31) was satisfied for each value of N for each timestep gave a corresponding non-dimensional layer height estimate. Different values of N produced different estimates of the non-dimensional layer height (Figure 12). N values of $0 \leq N \leq 0.5$ were used for comparison with two-zone model values.

3.1.7.2 Integral ratio method

The integral ratio method involved finding the layer height that maximised the uniformity of the profile over the height of the tank (He et al., 1998). Physically, this method was determining the layer height based on the layer height value resulting in the least variation of density in each of

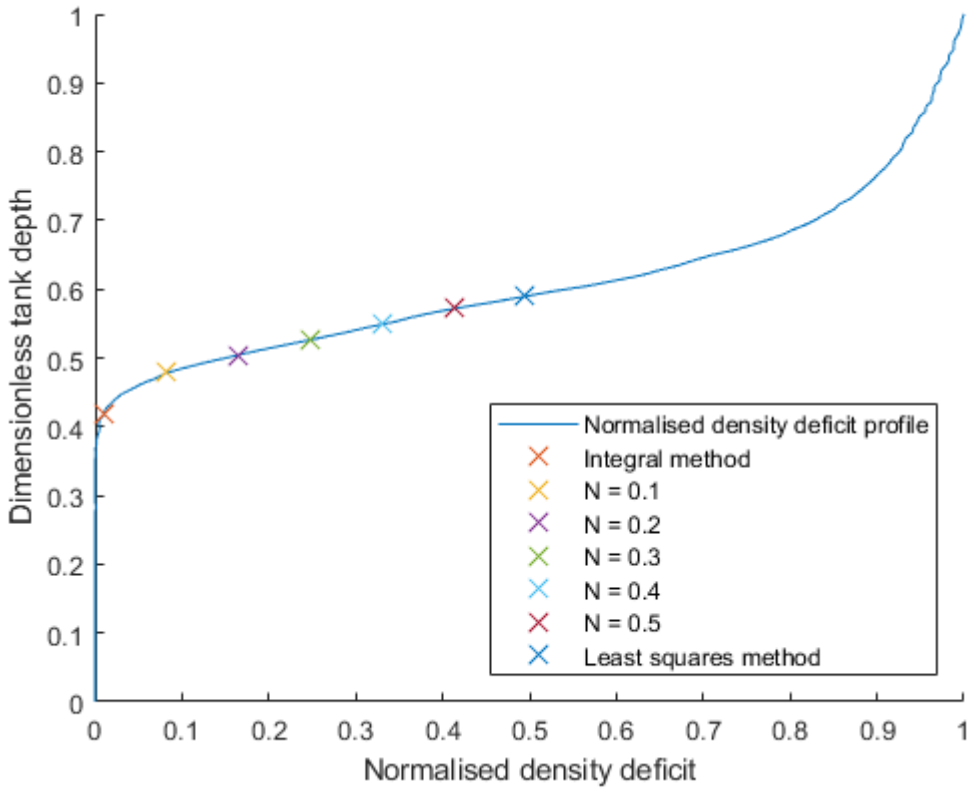

Figure 12. Layer height estimates shown against their corresponding normalised density deficit profile throughout the non-dimensionalised height. SF = 5, t = 534 s, t = 3.*

the layer and upper layers independent of each other. The integral ratio method measures the uniformity and was defined as

$$r = r_{av}\frac{1}{r_{av}} \tag{32}$$

where r was the integral ratio. r_{av} was the direct averaging integral of the non-dimensional density deficit defined by

$$r_{av} = \frac{1}{(h_b - h_a)}\int_{h_a}^{h_b} I^*(y)\,dy \tag{33}$$

where h_b was the height of the upper bound (m) and h_a was the height of the lower bound (m). $I^*(y)$ was the depth integrated density profile as a function of height.

The minimum value of the integral ratio by this definition was one and the closer the integral ratio was to a value of one, the more uniform the density deficit in region $[h_a, h_b]$ (He et al., 1998). The density deficit profile was defined in region $[0, h]$. By estimating layer height as $y = y_{LH}$ where $y_{LH} \in (0, h)$, the integral ratio was calculated for regions $[0, y_{LH}]$ and $[y_{LH}, h]$ by combining Equations (33) and Equation (32) which obtained the following two ratios:

$$r_u = \frac{1}{(h - y_{LH})^2}\int_{y_{LH}}^{h} I^*(y)\,dy \int_{y_{LH}}^{h}\frac{1}{I^*(y)}\,dy \tag{34}$$

$$r_l = \frac{1}{(y_{LH})^2}\int_{0}^{y_{LH}} I^*(y)\,dy \int_{0}^{y_{LH}}\frac{1}{I^*(y)}\,dy \tag{35}$$

where r_u and r_l denote the upper and lower integral ratios respectively. The layer height estimate that minimises the sum of these two integral ratios was defined as the layer height for that particular profile and time.

3.1.7.3 Least squares method

The least squares method is a curve fitting method. The least squares fit of a piecewise function to experimental depth integrated density profile was used to estimate the layer height. The piecewise function was defined as

$$\phi(y) = \begin{cases} I^*_{l,av} = constant, & y < y_{LH} \\ I^*_{u,av} = constant, & y > y_{LH} \end{cases} \tag{36}$$

where $I^*_{l,av}$ is the average of the depth integrated density values below the non-dimensionalised layer height estimate and $I^*_{u,av}$ is the average of the depth integrated density values above it. The variance between the piecewise function and the vertical depth integrated density profile was defined by

$$\sigma^2 = \frac{1}{y_{LH}}\int_0^{y_{LH}}[I^*(y) - I^*_l]^2 dy + \frac{1}{h - y_{LH}}\int_{y_{LH}}^{h}[I^*(y) - I^*_u]^2 dy\,. \tag{37}$$

The layer height estimate that minimises the variance is defined as the layer height for that particular depth integrated density profile and time.

3.2 Two-zone model setup

Use of correct input variables in the two-zone model ensured reliable results that were directly comparable to the salt-water models. Input variables included compartment geometry, compartment lining material, ventilation opening size, fire size, and fire properties. From these, three types of input variables were determined: variables that allow the model to replicate the conditions within the experimental tank, variables that describe the change in shape factor and variables that control the type of behaviour described by the two-zone model.

The two-zone simulation attempted to replicate conditions of the salt-water experiments as closely as possible. The tank surfaces did not absorb salt. To model fire compartment surfaces that provide similar behaviour was difficult because the B-RISK two-zone model did not allow surfaces to be treated as adiabatic. Instead, the surfaces within the modelled room were lined with a highly insulating boundary material that approximated the temperature of the adjacent gas layer throughout the calculations. The boundaries had a thermal conductivity of 0.01 $W.m^{-1}K^{-1}$, specific heat of 2000 $J.kg^{-1}K^{-1}$ and were defined as a blackbody with emissivity of 1. This facilitated convective and radiative heat transfer between the gas layers and the surfaces which led to minimal energy loss out of the system and minimised the amount of heat that would have been lost to the ceiling and walls during smoke layer formation. The fire was also defined as having a radiative energy loss fraction of 0.01 and to produce no soot or CO_2 as these affected radiation emission and absorption by the layers. Soot or CO_2 would have altered the tracking of the layer temperature by the surfaces, causing conduction of energy out of the system. Water vapour in the air would have also affected radiation and absorption however altering the amount of water vapour was difficult and time consuming to do using the B-RISK two-zone model and was not undertaken.

The remainder of modelling inputs were explored to investigate their effect on the two-zone-model output. Changes in these inputs were likely to cause changes in behaviour of the two-zone model results because changes in these inputs would lead to changes in geometry or change the energy in the system, resulting in changes to characteristics of compartment smoke filling.

Compartment geometry components such as height, width and length were explored within the two-zone model because of their direct impact on the smoke filling rate for a given fire. If a compartment is too large in any dimension compared to fire size, the smoke may not have enough buoyancy to form a smoke layer. If the compartment is too small, the hot gases may be too turbulent and violent and not form a layer either. Two-zone models assume the layer always forms and therefore do not take into account the inability of the fire to form a smoke layer within the compartment. The fire length and width were established by scaling the cross-sectional area of the source pipe into an equivalent fire area based on the ratio of the pipe diameter to the length and width of the salt-water tank as described by

$$\frac{W_{fire}L_{fire}}{W_cL_c} = \frac{1}{4}\frac{\pi D_{source}^2}{W_tL_t} \tag{38}$$

where L and W are length and width (m) and subscripts $fire$, c, and t correspond to the fire, compartment and salt-water tank respectively. Fire elevation was scaled from the depth of the source pipe within the freshwater at the beginning of the experiment. The fire geometry and elevation could not be found until the determination of the compartment geometry was complete.

Smoke filling depended on fire size. Using a constant non-dimensional fire size allowed the plume entrainment, smoke production and heat production to be similar between models with

different shape factors. Exploration across the range of Bong's (2011) fire size limits was important to determine an appropriate value for modelling.

Ventilation within the two-zone model refers to providing openings between the fire compartment and the outside to allow free flow of air. Sufficient compartment ventilation was required to avoid a ventilation-limited burning regime and avoid fire compartment over-pressurisation. A ventilation-limited burning regime occurred when fire burning was governed by the amount of oxygen in the fire compartment as opposed to a fuel-limited burning regime which was limited by fuel amounts. The ventilation limit is defined as the time when the fire size first diverges from the specified model input fire size due to insufficient oxygen for complete combustion. Once the ventilation limit was reached in the two-zone model, the fire entered a ventilation-limited burning regime. The ventilation-limited burning regime was best avoided for comparison with salt-water experiments as the fire size, CO_2 yield, H_2O yield, heat of combustion, and radiant loss fraction all change and unburned fuel is produced by the fire (Wade et al., 2016). Each of these alone significantly impacted the results of the two-zone simulation by changing the fundamental characteristics of the simulation. These ventilation limited variables removed the ability to compare the two-zone models to the salt-water experiments.

Fire compartment over-pressurisation happened when the expansion of heated air within a compartment caused the compartment air pressure to increase to a point where it affected the fire characteristics. Over-pressurisation typically occurred when there was very limited or no ventilation. Ventilation required to avoid ventilation-limited burning was also sufficient to avoid over-pressurisation. The amount of ventilation required to avoid ventilation-limited burning was dependent on fire size and compartment volume. Fire size governed how quickly oxygen was burnt for combustion and compartment volume governed the volume of oxygen available to be burnt. Therefore, it was important to investigate different ventilation arrangements to determine the effect they had on the fuel combustion within the two-zone model.

3.2.1 Input derivation

Fire and smoke simulations generated with a two-zone model were used to explore layer height descent in compartments geometrically defined by shape factors 5, 10, 50, 60, and 70. Shape factors 5 and 10 were used to determine expected behaviour at a geometry well within the existing shape factor limits. Shape factors 50 through 70 were used to determine expected behaviour near the limit of existing two-zone model application. Compartments with shape factors between these two geometric extremes were not explored. Characteristics of layer interface descent were used to refine two-zone model input variables using a shape factor 5 compartment. Inputs were scaled for the remaining shape factors to explore the effects of adjusting compartment geometry on the two-zone layer simulation.

To illustrate non-dimensional layer height descent behaviour accurately, the model input variables were chosen to display layer descent behaviour independent of changes in that variable where possible. Model input independence showed that when changing the shape factor, model inputs would not impact results. Independence was achieved when changing variables had no effect on the non-dimensional layer height descent throughout non-dimensional time. Independence was shown through self-similarity of transient non-dimensional layer height descent profiles (layer height profiles). Layer height profile self-similarity proves that for particular ranges of variable values, length and time non-dimensionalisation behave consistently. These non-dimensionalisations consisted of various constants and a few major variables: compartment height, compartment width and length, and fire heat release rate (Equation (15) and Equation (17)). Therefore, when layer height profiles

were not self-similar, basic compartment geometry or heat release rate were dependent on whichever changes occurred between the two or more layer height profiles. By defining input variables that allowed the basic compartment geometry and heat release rate to behave independently, layer height profiles showing reliable behaviour were able to be found for Shape Factor 5. These profiles were then used to explore the remaining shape factors up to Shape Factor 70.

3.2.1.1 Compartment geometry

The first input parameter investigated was the height of the compartment. Compartment height was important because it directly influenced layer height non-dimensionalisation. Moreover, compartment height had a direct effect on the quantity of smoke plume entrainment as the plume rose to the ceiling. Layer height profiles using a fire size of $Q^* = 0.002$ (Figure 13) for compartment heights of 2 m through 16 m ($SF = 70$ through $SF = 1$ respectively) were compared. Only height and dimensional heat release rates changed between simulations. Dimensional fire size was changed to keep the height-dependent dimensionless fire size constant between simulations. Dimensionless fire size was kept constant to ensure that any behavioural changes would be due to geometric height changes rather than caused by changes in entrainment characteristics.

When comparing layer height profiles with different model compartment heights, behaviour independent of compartment height was found for model compartment heights of 4 m and greater. The independent behaviour was proven through layer height profile self-similarity (Figure 13). However, due to only small deviations from self-similarity within the set of layer height profiles, the effect of compartment height on layer descent behaviour was considered small for all heights investigated. A compartment height of 5 m was used in all two-zone simulations with a fire size of $Q^* = 0.002$. It was assumed the 5 m height was applicable to other fire sizes within the limits set by Bong (2011).

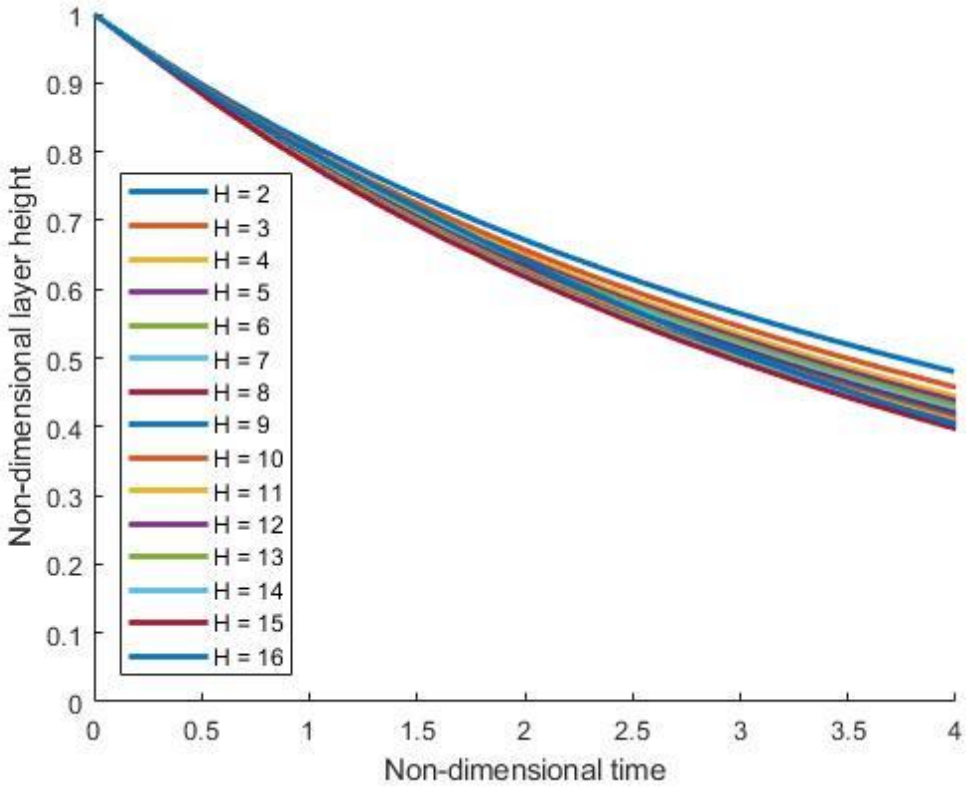

Figure 13. Q = 0.002, L=W=16.7 m, shape factors from 1 to 70, fire width=length=0.294 m, fire elevation=0.033 m.*

Defining compartment width and length was based on compartment height and depended on shape factor. In all two-zone modelling cases, compartment width and length were equal in order to remain consistent with the square tank geometry used in the physical lab model. By definition (Equation (1)) when the shape factor increases, the ratio between compartment height and floor area increases. Two methods of manipulating the geometry and comparing layer height profiles were explored: decreasing the height of the compartment and keeping the cross-sectional area constant (Method 1) (Figure 14), or keeping the height of the compartment constant and increasing compartment width and length to increase cross-sectional area (Method 2) (Figure 15).

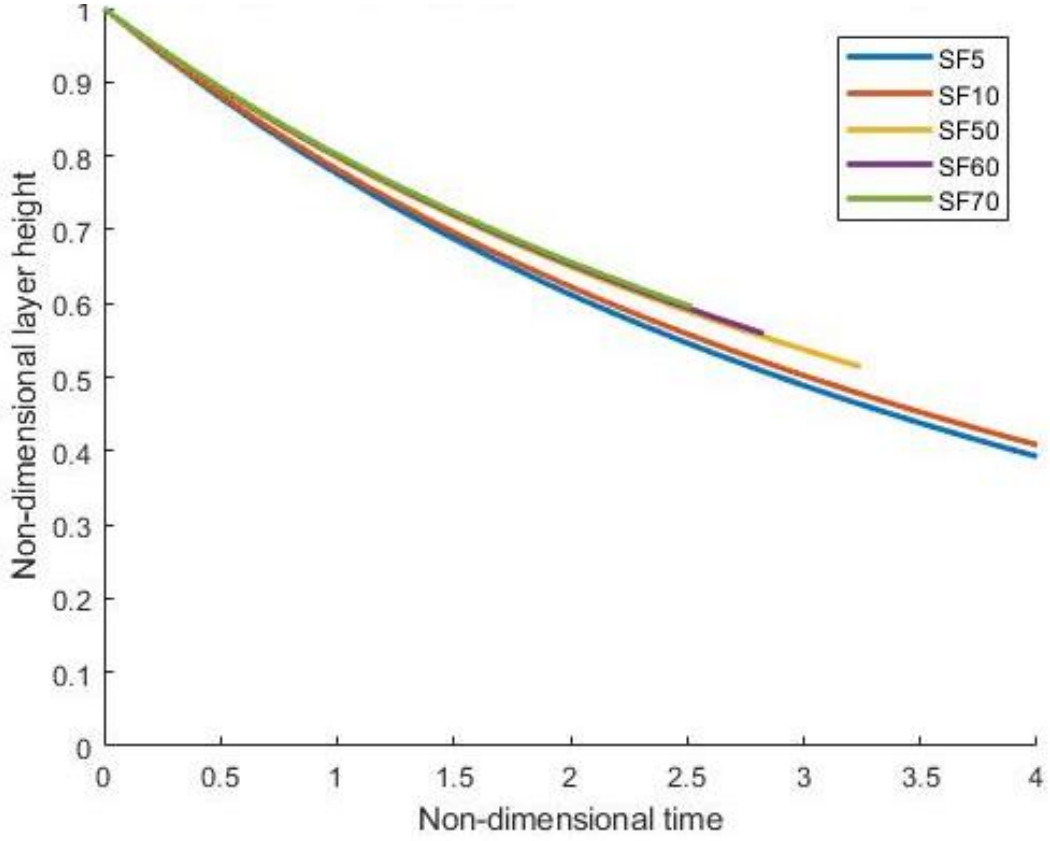

Figure 14. Comparison of two-zone model non-dimensionalised layer height profiles when changing compartment height to change shape factor (Method 1).

As shape factor increased, the non-dimensional layer height profiles diverged less using Method 2 compared to Method 1. Method 2 non-dimensional layer height profiles were closer to achieving self-similarity. Changing shape factor resulted in a negligible change in behaviour of the non-dimensionalisation between simulations when using Method 2. Throughout the final two-zone models, height was maintained at a constant value and cross-sectional area was defined by the shape factor in each two-zone simulation using Method 2.

Changing fire size while changing height, to maintain non-dimensional fire size, was expected to be the cause of the larger divergence in the Method 1 layer height profiles. This was because of the possibility of changes in flame height. Non-dimensional flame height affects the model behaviour because the entrainment of air into the flame region is often significantly different than air entrainment into a smoke plume above flames. The flame heights found in the two-zone simulations using geometry and fire size defined using both Methods were exactly the same for all shape factors. Entrainment was, therefore, the same and the minor layer height profile divergence did not come from the flame height.

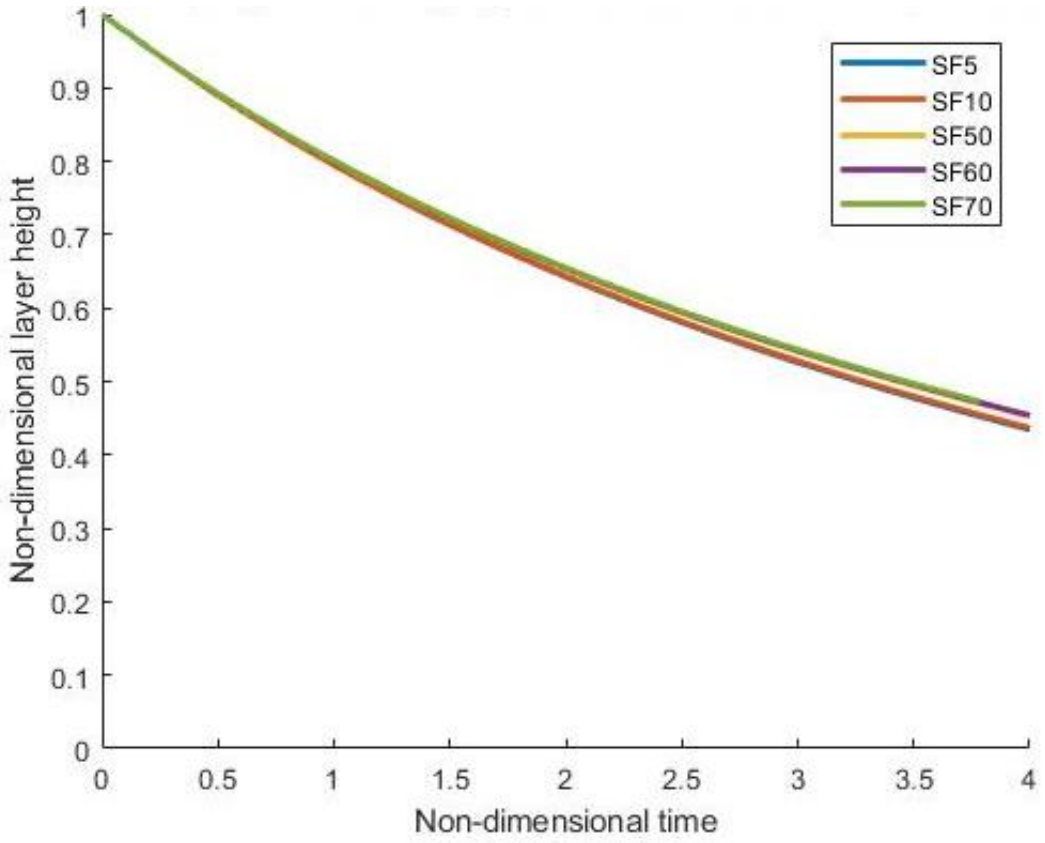

Figure 15. Comparison of two-zone model non-dimensionalised layer height profiles when changing compartment floor area to change shape factor (Method 2).

The difference in behaviour between decreasing the height of the compartment and keeping the cross-sectional area constant (Method 1) and keeping the height of the compartment constant and increasing compartment width and length to increase cross-sectional area (Method 2) exists but is minor and is likely to be due to some small nuance within the calculations methods of the two-zone model.

Compartment and water tank geometries were used together to define the geometric size of the fire within each two-zone simulation. Fire length and width were scaled from the source pipe area using Equation (38). Fire elevation was scaled from the depth of the source pipe within the freshwater at the beginning of the experiment.

3.2.1.2 Fire size

To determine an appropriate non-dimensional fire size, an appropriate non-dimensional heat release was determined using two different methods through investigating the behaviour of the non-dimensional layer height profiles when varying the non-dimensional fire size.

The non-dimensional heat release rates were derived through either maintaining a constant dimensional fire size and changing compartment height (Figure 16) or, changing dimensional fire size and keeping height constant (Figure 17).

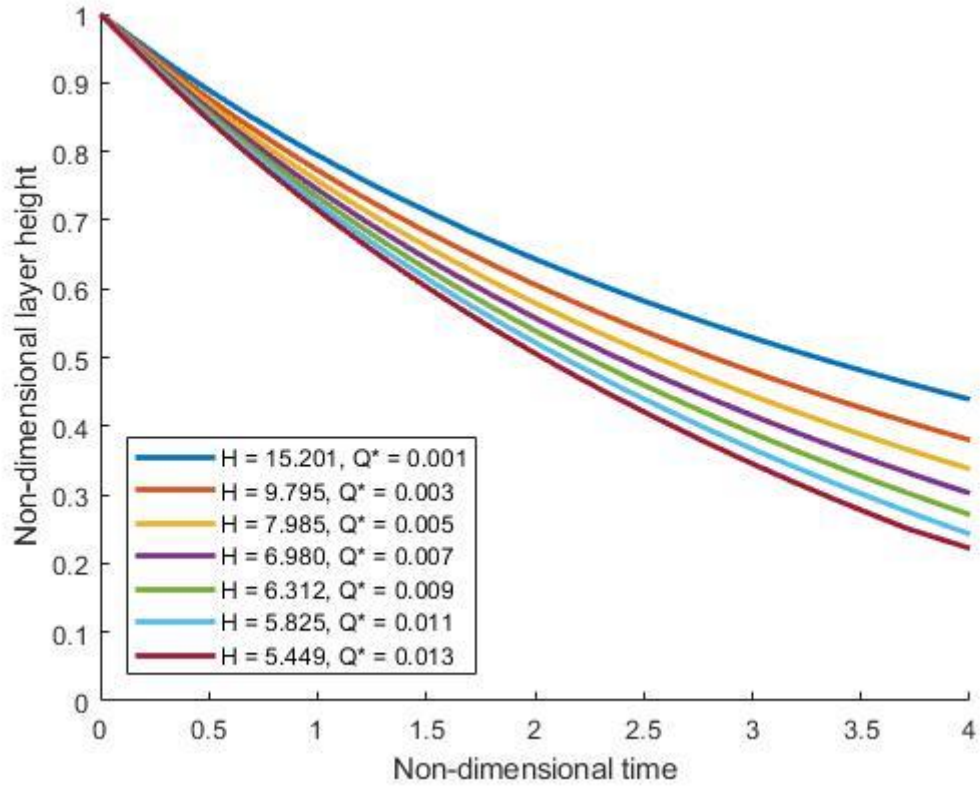

Figure 16. Comparison of two-zone model non-dimensionalised layer height profiles when changing compartment height to change non-dimensional fire size.

Both methods produced results that showed no self-similarity in the layer height profiles between fire sizes. However, minimising fire size led to flaming region height reduction. A small flaming region results in a large smoke plume region with approximate pure plume entrainment characteristics. Minimising the flaming region was important to allow comparison with the salt-water experiments, which did not have a similar flow region. The lower non-dimensional heat release rate limit was found to be $Q^* = 0.002$ (Bong, 2011) and this was used for each two-zone simulation.

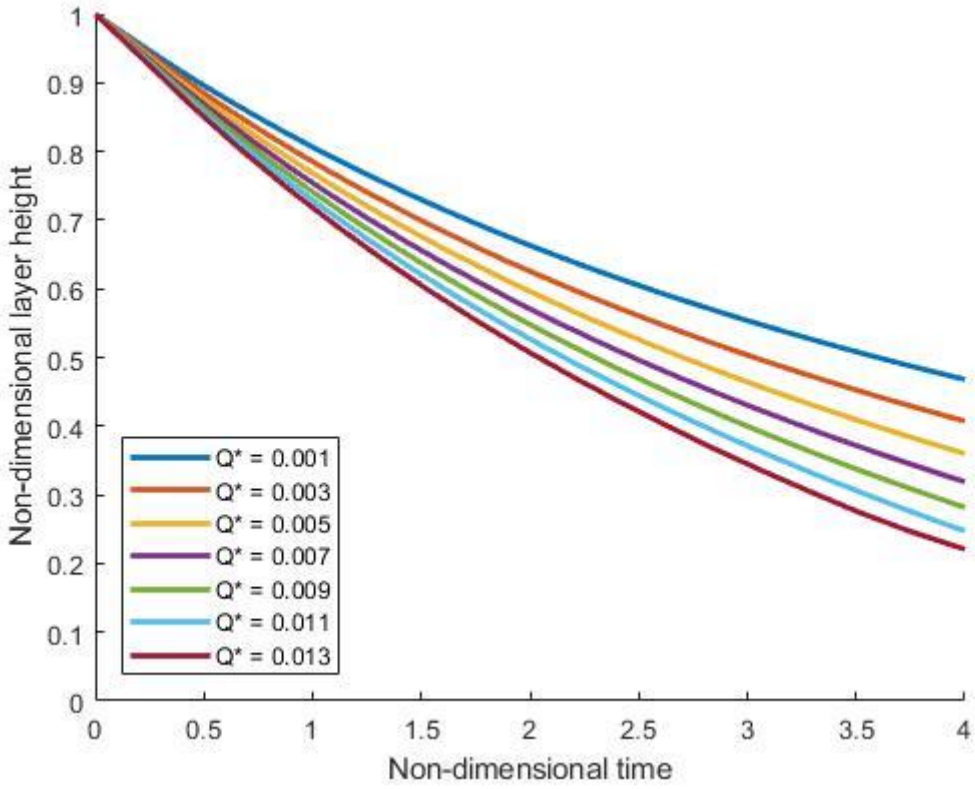

Figure 17. Comparison of two-zone model non-dimensionalised layer height profiles when changing model fire size to change non-dimensional fire size.

3.2.1.3 Ventilation

The amount of ventilation required to avoid ventilation-limited burning is dependent on fire size and compartment volume. Fire size governed how quickly oxygen was burnt for combustion and compartment volume governed the volume of oxygen available for burning. The dimensional fire size was the same in all two-zone simulations because non-dimensional fire size and height were constant throughout. Compartment volume changed dramatically for each shape factor. The smallest compartment volume occurred with a shape factor of 5.

Vents of different sizes were used to explore their effect on ventilation limited-burning and layer height development. Full-width vents with non-dimensional vent heights $H_v^* = 0.0176$ (smallest vent size to keep fire fuel limited) to $H_v^* = 0.5$ showed self-similar layer height behaviour until the layer reached vent height, at which point smoke from the upper layer flowed out of the compartment (Figure 18). Therefore, vents large enough to avoid ventilation-limited burning but shorter than the minimum layer height were used for all shape factor two-zone models.

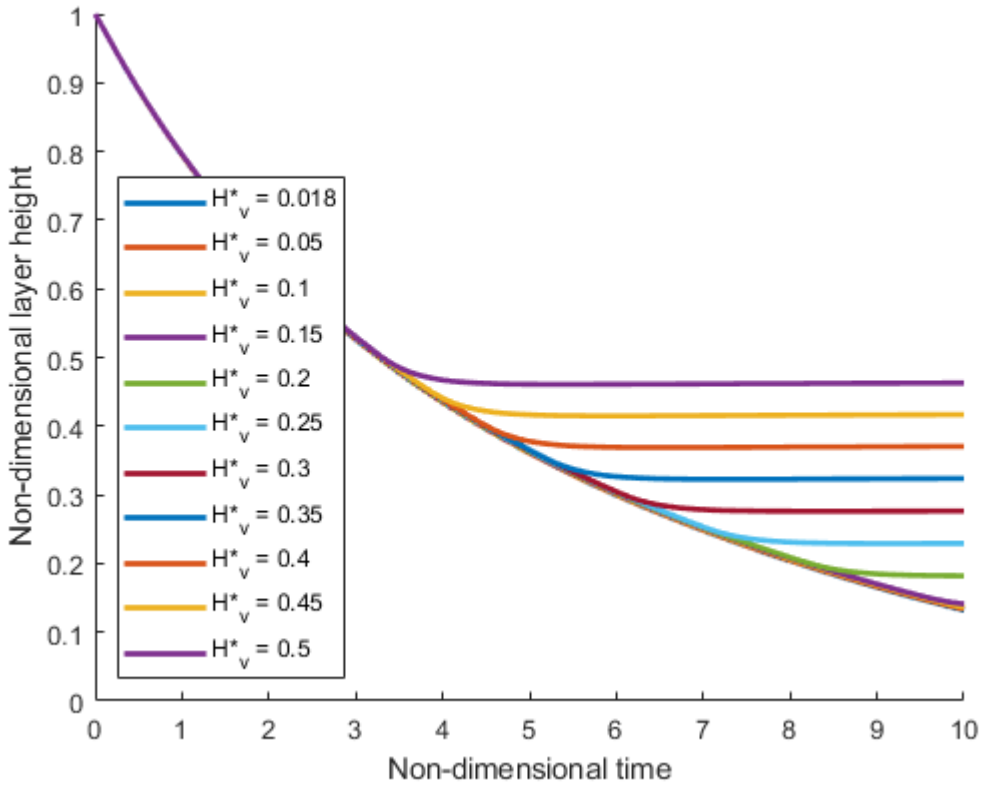

Figure 18. Comparison of two-zone model non-dimensionalised layer height profiles when changing non-dimensionalised compartment ventilation height from $H_v^* = 0.018$ to $H_v^* = 0.5$.

4 Results

This chapter explores the results found using the previously described modelling and experimental setups. Validity and applicability of the two-zone model inputs was discussed. The effect of salt-water experiment source conditions and transient plume effects on experimental measurements are explored. The consistency of salt-water layer height calculation methodologies is discussed. Comparisons between the two-zone model and salt-water experiments are undertaken and discussed.

4.1 Two-zone model

A summary of the model inputs derived from two-zone model sensitivity studies in Section 3.2.1 can be found in Table 1.

Table 1. Two-zone model inputs

	Shape factor				
Input	5	10	50	60	70
Compartment properties					
Height (m)	5	5	5	5	5
Width & length (m)	11.18	15.81	35.36	38.73	41.83
Compartment lining properties					
Thermal conductivity ($W.m^{-1}K^{-1}$)	0.01	0.01	0.01	0.01	0.01
Specific heat ($J.kg^{-1}K^{-1}$)	2000	2000	2000	2000	2000
Emissivity	1	1	1	1	1
Ventilation opening properties					
Width (m)	11.18	11.18	11.18	11.18	11.18
Height (m)	0.1	0.1	0.1	0.1	0.1
Fire properties					
Width & length (m)	0.221	0.277	0.620	0.680	0.734
Elevation (m)	0.022	0.031	0.070	0.077	0.083
Radiative energy loss fraction	0.01	0.01	0.01	0.01	0.01
Soot & CO_2 yields	0	0	0	0	0
Heat release rate (kW)	124	124	124	124	124

4.1.1 Input validation

Validating the usefulness and applicability of model inputs is possible through an energy conservation analysis. Energy conservation is a fundamental assumption for calculations throughout each two-zone simulation. Energy conservation was explored through determining the energy created by the fire through the heat release rate and calculating the total energy within the two-zone model system. Theoretical energy created by the fire was calculated as the heat release rate multiplied by the time since the model began in seconds. Two-zone model total energy was more difficult to determine and consisted of the energy in the upper and lower layers, energy escaping out of the vent and the net radiation to each of the floor, walls and ceiling.

The energy contained within the upper and lower layers was calculated at each time-step using

$$E_L = m_L c_p (T_L - T_0) \quad (39)$$

where E_L was the energy stored within the layer (J), m_L was the mass of air within the layer (kg), and T_L and T_0 were layer and ambient temperature (K) respectively. The majority of energy produced by the fire was captured within these two layers.

Energy escaping out of the vent occurred through heated lower layer air evacuating the compartment due to pressure gradients. Hot, upper layer smoke did not escape through the vent because the vent was located completely within the lower layer for the duration of the layer descent comparison. The energy contained within air escaping the compartment through the vent at each time step of the simulation was quantified using

$$E_v = c_p(T_{LL} - T_0)\dot{m}_v\delta t \quad (40)$$

where E_v was the energy leaving the vent (J), T_{LL} was the temperature of the lower layer (K), $\dot{m}_v$ was the mass flow of the vent (kg.s^{-1}), and δt was the timestep (s). Escaping vent flow energy totalled a small amount of energy because the temperature difference between the lower layer and outside was small, the compartment-exterior pressure gradients were small during the early stages of the two-zone model (where the comparison occurred), and the high energy upper layer remained far above the vent opening for the entire comparison.

Radiation from the fire, hot upper layer, relatively cool lower layer, and other surfaces within the compartment was balanced with the surface re-radiation within the two-zone model as a net radiation output using

$$E_{rad} = \dot{q}_s A_s \delta t \quad (41)$$

where E_{rad} was the energy absorbed by the walls due to radiation (J), $\dot{q}_s$ was the net radiation experienced by the particular surface (W.m^{-2}), and A_s was the surface area of the particular surface (m^2). Energy lost due to radiation was a small contribution to overall compartment energy due to the high emissivity and low thermal conductivity of the surfaces causing low net surface radiation (Table 1).

Total energy was calculated for each two-zone model. Theoretical energy comparison was undertaken using real-time because all models sharing the same heat release values encouraged direct comparison. As shape factor increased, the calculated energy within the compartment decreased relative to the theoretical energy, from near-perfect conservation with Shape Factor 5 through to Shape Factor 70 where significant energy losses from the system were unaccounted for (Figure 19). Energy losses were compared for the initial ninety seconds of simulation as this region encompassed the non-dimensional comparison regions for all shape factors. The energy losses were initially attributed to re-radiation from surfaces and the fire to carbon dioxide and water molecules within both layers due to their ability to experience induced dipoles which allowed them to absorb radiation. Carbon dioxide concentrations were constant at 0.032% throughout simulations with each shape factor. This value was low and constant due to the carbon dioxide yield being zero. Water vapour concentrations were approximately 1.5% throughout the two-zone simulations. It is possible that the energy losses were due to re-radiation of gases. However, due to the extremely low concentration of carbon dioxide and the small amount of water vapour, a small amount of the energy losses were likely to be dependent on gas re-radiation to the water vapour only. Other sources of energy loss were likely dependent on the increase in compartment volume or surface area as shape factor increased for the same fire size. The bounding compartment construction was not adiabatic and adiabatic surface conditions were not possible in the B-RISK two-zone model. Energy losses through the compartment walls was likely. As shape factor increased, the surface area of the walls, floor and ceiling all significantly increased which would have contributed to the increased

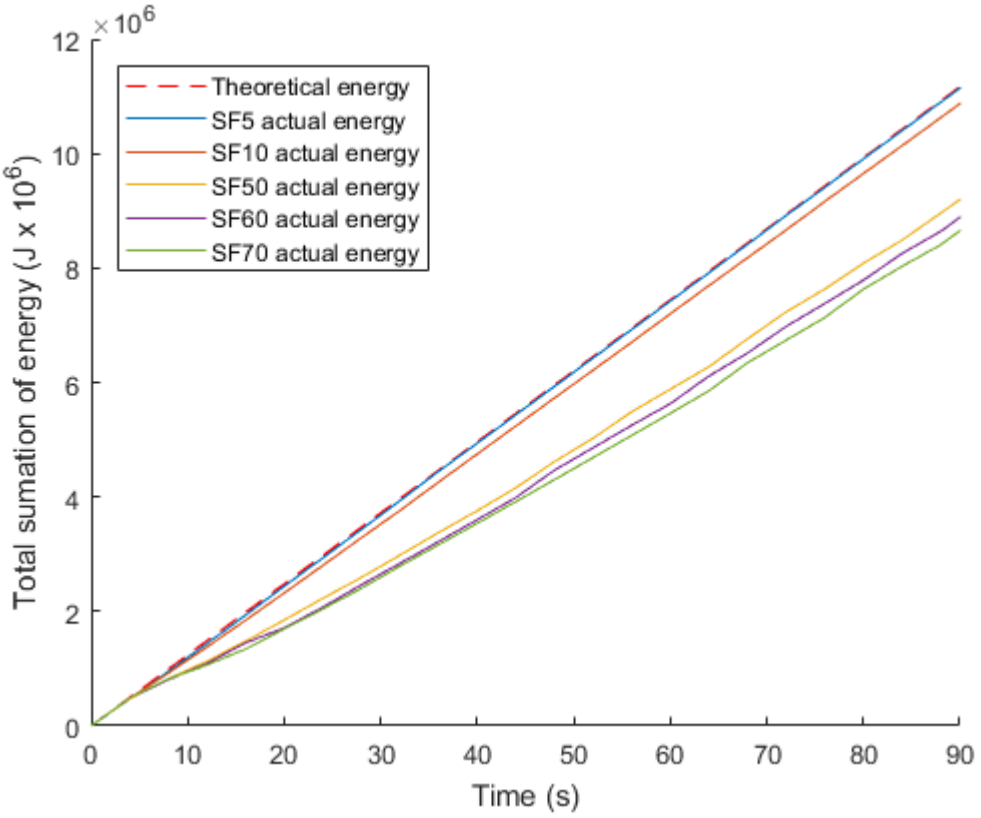

Figure 19. Calculated energy compared with theoretical energy produced by the fire in two-zone models of each shape factor.

amount of energy lost in these simulations. Further research is required to confirm the reason for the variation in energy conservation.

4.1.2 Layer height analysis

Comparing two-zone model layer height evolution showed behaviour that was close to independent of changes in all shape factor (Figure 20). The shape factor independence proves that the underlying two-zone approximation assumptions and using this particular derivation of the model inputs, produced layer height development behaviour that did not change significantly with a changing shape factor. However, in contrast, key assumptions, such as energy conservation, were found to not hold throughout every simulation. Assumptions crucial to determining the effectiveness of layer height evolution involved the instantaneous formation of a smoke layer, compartment construction, and energy conservation.

The smoke layer formation and ventilation assumptions caused similar behaviour between models of different shape factors.

The instantaneous smoke layer formation assumption did not account for variation in layer formation behaviour as may be expected in real compartment fires. Real fires have smoke transport lag and uniform smoke layers may not always form. The model's inability to take these situations into account could be caused by low buoyancy forces created by the small fire used in modelled compartments that were very wide compared to their height. Alternatively, it could be because these behaviours required a larger shape factor than 70 before layer formation issues, such as transport lag, were encountered.

The ventilation was sufficiently large to maintain fuel controlled burning without over-pressurisation of the compartment. The modelled ventilation opening was also short enough to

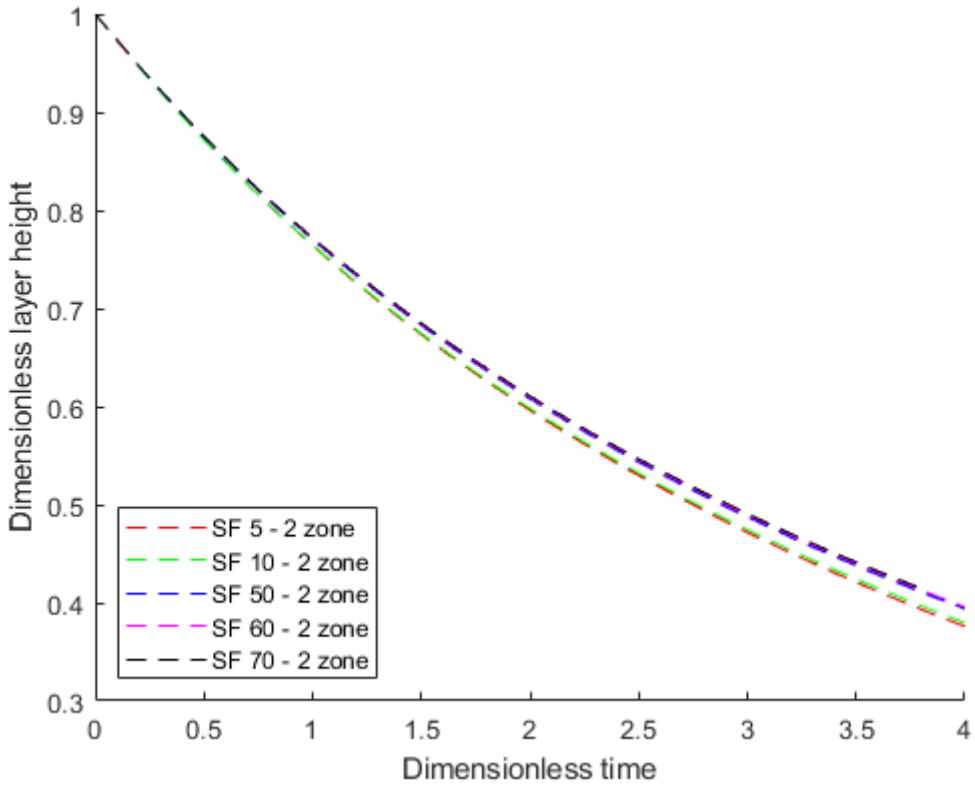

Figure 20. Layer heights calculated for each shape factor using the two-zone model.

remain below the smoke layer for the duration of the comparison period, meaning upper layer smoke was not lost through the vent.

The lack of energy conservation in all simulations except Shape Factor 5 caused a small variance in behaviour. Although energy conservation is an important element for understanding behavioural changes, the effect is considered relatively small. Therefore, the difference is inconsequential for the comparison of two-zone models and salt-water experiments within the scope of this research. Due to the inconsequential difference, a single two-zone model curve was chosen to compare with salt-water experiments. Shape Factor 5 was chosen due to reliable energy conservation.

4.2 Salt-water experiments

4.2.1 Overview

The water depth, source dye concentrations and source fluid densities for each shape factor are presented in Table 2.

Table 2. Salt-water experiment variables.

Shape factor	Water depth (m)	Source dye initial concentration (g m^{-3})	Source fluid density (kg m^{-3})
5	0.452	1.569	1.002
10	0.319	0.867	1.002
50	0.143	0.219	1.007
60	0.130	0.188	1.001
70	0.121	0.165	1.001

Before making interpretations from the experimental results, it was important to understand how a typical experiment progressed and how this process compared to idealised smoke layer evolution (Section 2.1). In reality, the salt-water used in all experiments travelled downward. To aid in comparison to rising smoke in fire compartments, analysis of the salt-water experiments is discussed as the salt-water rising into the freshwater, and all figures have been inverted to reflect this change.

Each experiment started with salt-water being injected into freshwater. The salt-water formed a buoyant-jet which transformed into a plume as it travelled towards the ceiling. The images collected during each experiment were processed and then analysed to gather depth averaged density deficit field data (Section 3.1.5). The processed images showed salt-water concentration on a spectrum with dark-blue corresponding to the freshwater and warm colour corresponding to an increasing concentration of salt-water. Dark-red colouring shows the highest concentration of salt-water, denoted by the largest depth integrated density difference. Salt-water injection created a cyan coloured line, corresponding to a depth integrated density deficit of approximately 0.046 kg.m^{-3}, that propagated upwards, fading towards the edges of the flow, where salt concentration was lowest (Figure 21). Until the layer was formed, these images provided qualitative results for discussion only.

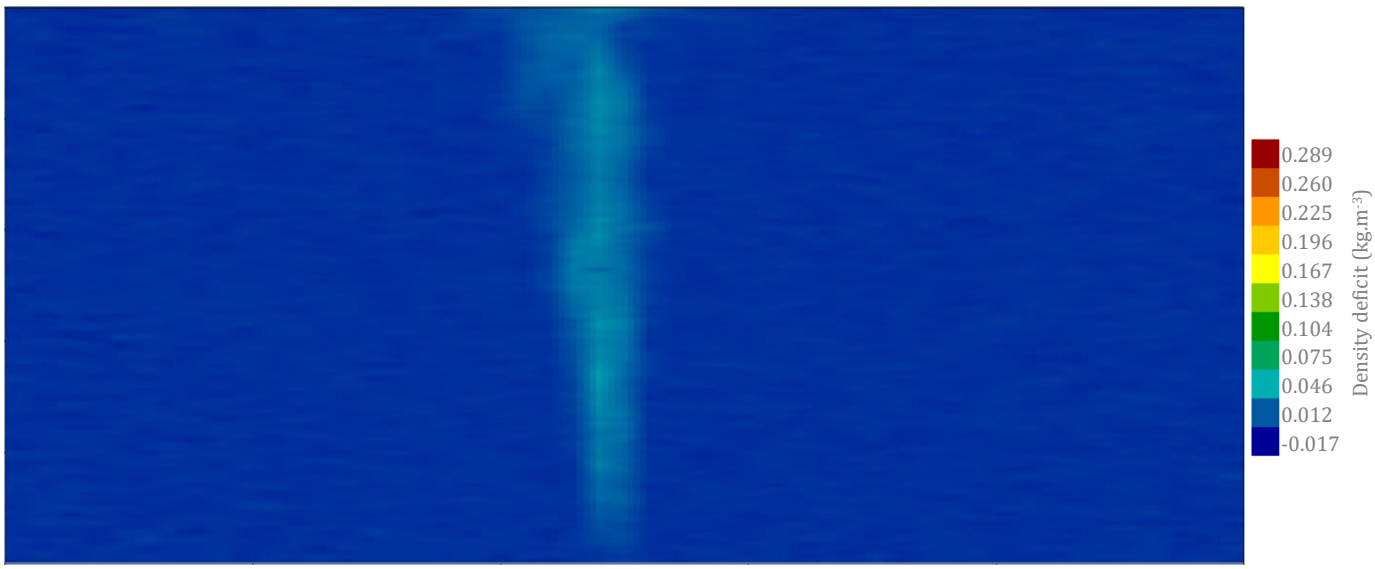

Figure 21. The plume rising to the ceiling. SF = 5, Experiment A, t = 0 s, t = 0*

As salt-water rose, impinged on the ceiling and began spreading radially, a depth integrated density deficit of approximately 0.138 kg.m^{-3} showed areas of relatively high salt concentration that had already become well established. The highest salt concentration was at the impingement point (Figure 22). The impingement point had a relatively high concentration because the processed experimental images were depth-integrated. When the salt-water spread radially, the salt-water depth in the top of the image was much deeper in the centre and thinner on the edges. As a result, light travelled through more salt in the centre of the tank compared to the edges and the concentration was measured as relatively high. The salt-water showed similar behaviour to a smoke plume impacting the ceiling and a ceiling jet travelling radially outward (Figure 1).

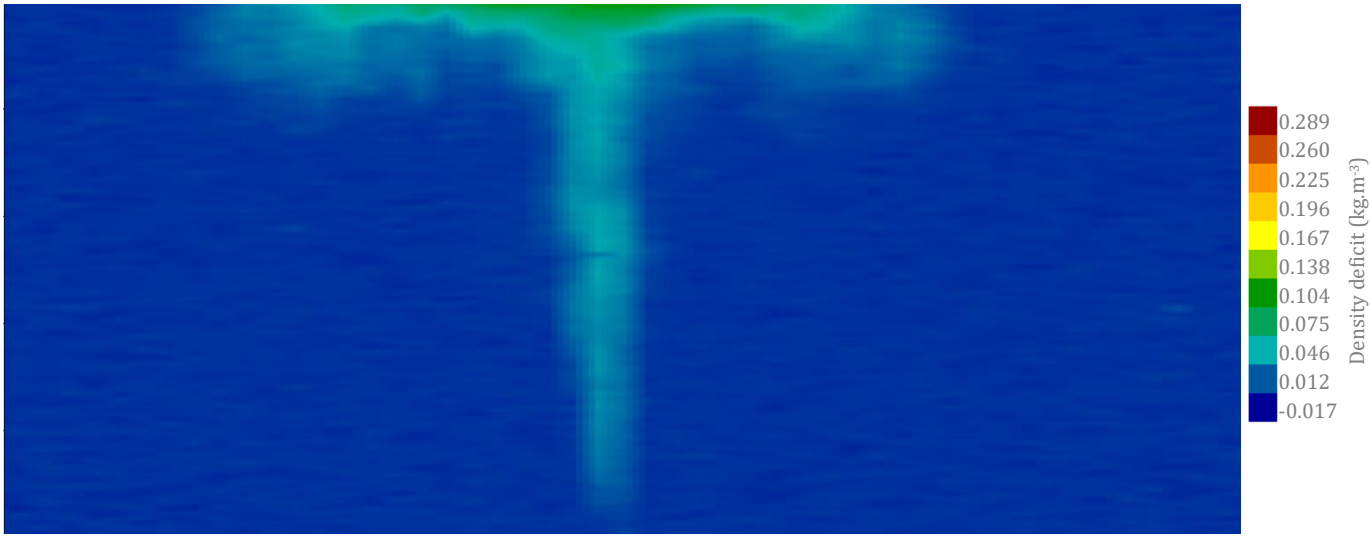

Figure 22. High salt concentration is shown at the ceiling as the plume impinges and spreads radially outward. SF = 5 Experiment A, t = 45 s, t = 0.25*

When the radially spreading salt-water impacted the walls, internal pressure gradients drove salt-water downwards (Figure 23). At this point, low concentrations were measured within the wall flows because the salt-water flow had only impinged on the sections of wall closest to the centre of each side of the tank. The salt-water showed similar behaviour to a smoke ceiling jet impacting the walls and travelling downward (Figure 2).

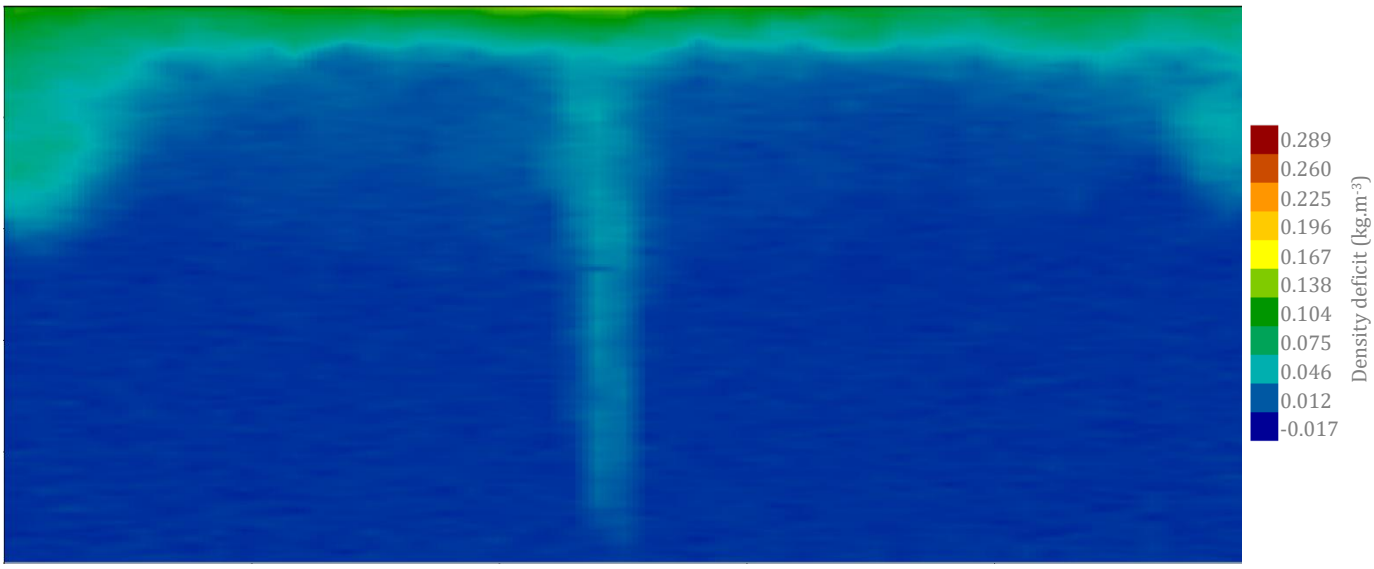

Figure 23. Salt-water impinging and flowing down walls. SF = 5 Experiment A, t = 96 s, t = 0.54*

Variations in pressure and buoyancy forced salt-water back towards the plume underneath the ceiling flow (Figure 24). These salt fronts, with approximate depth integrated density deficit of 0.104 kg.m^{-3}, had slightly lower concentrations of salt than the ceiling flows, with depth integrated density deficit approaching approximately 0.167 kg.m^{-3}. The salt fronts had lower salt concentrations than ceiling flows due to larger amounts of freshwater entrainment as the salt fronts travelled down the walls and back towards the plume. The salt-water showed similar behaviour to buoyancy driving smoke back towards the plume to form a smoke layer during a fire (as described in Figure 3).

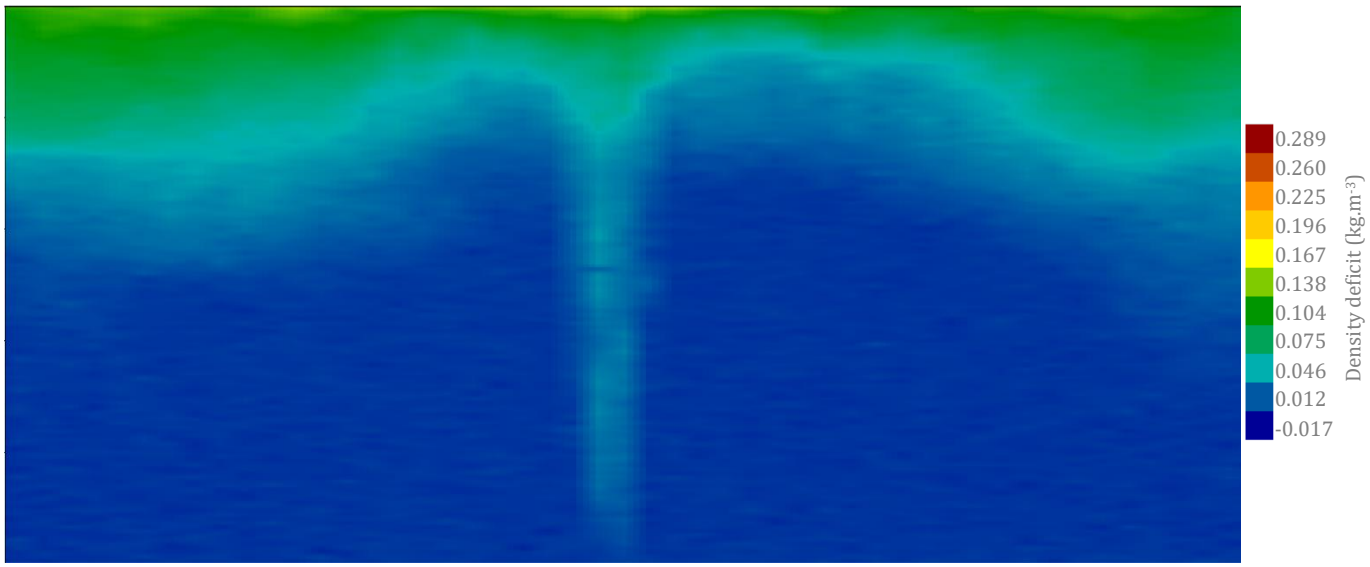

Figure 24. Salt-water flowing back towards plume. SF = 5 Experiment A, t = 144 s, t = 0.81*

Layer formation was complete when the salt-water fronts had travelled back to the plume (Figure 25). The fully-formed layer began lowering as more salt-water was injected. Layer height was not uniform across the tank, nor was layer salt-concentration shown by spatial variation in colour. Layer height variations propagated as momentum-driven waves at the bottom of the layer for a significant period of time (Figure 26). Regardless of the waves propagating along the layer interface, layer height dropped steadily as more salt-water was injected into the tank. As the layer dropped, the interface height became uniform throughout the

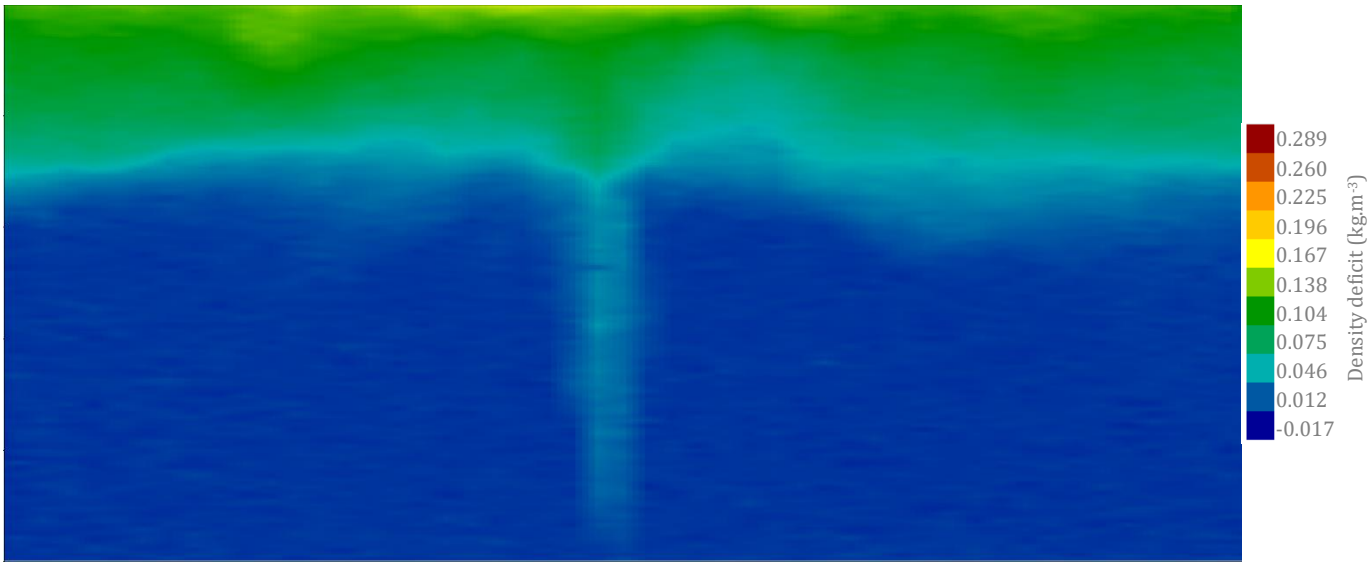

Figure 25. Layer has formed. SF = 5 Experiment A, t = 178 s, t = 1.0*

tank and significant vertical concentration gradients became more obvious, with high salt-concentration at the top of the tank and low concentration at the layer interface (Figure 27).

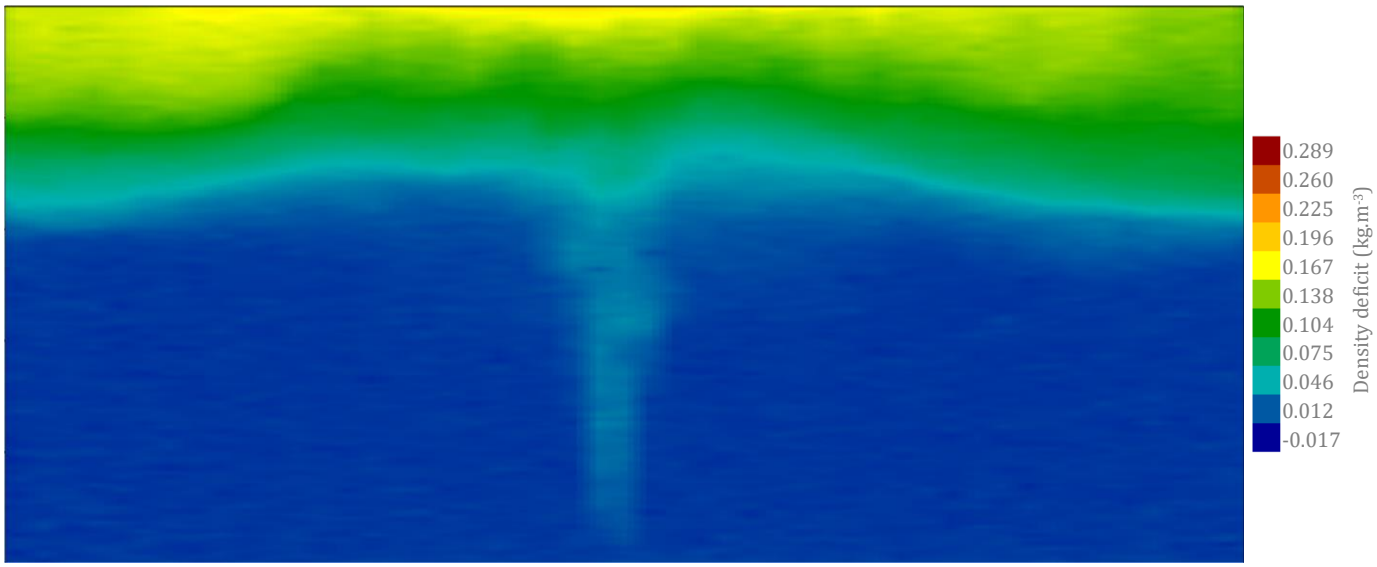

Figure 26. Layer interface waves propagating along the surface. SF = 5 Experiment A, t = 248 s, t = 1.39*

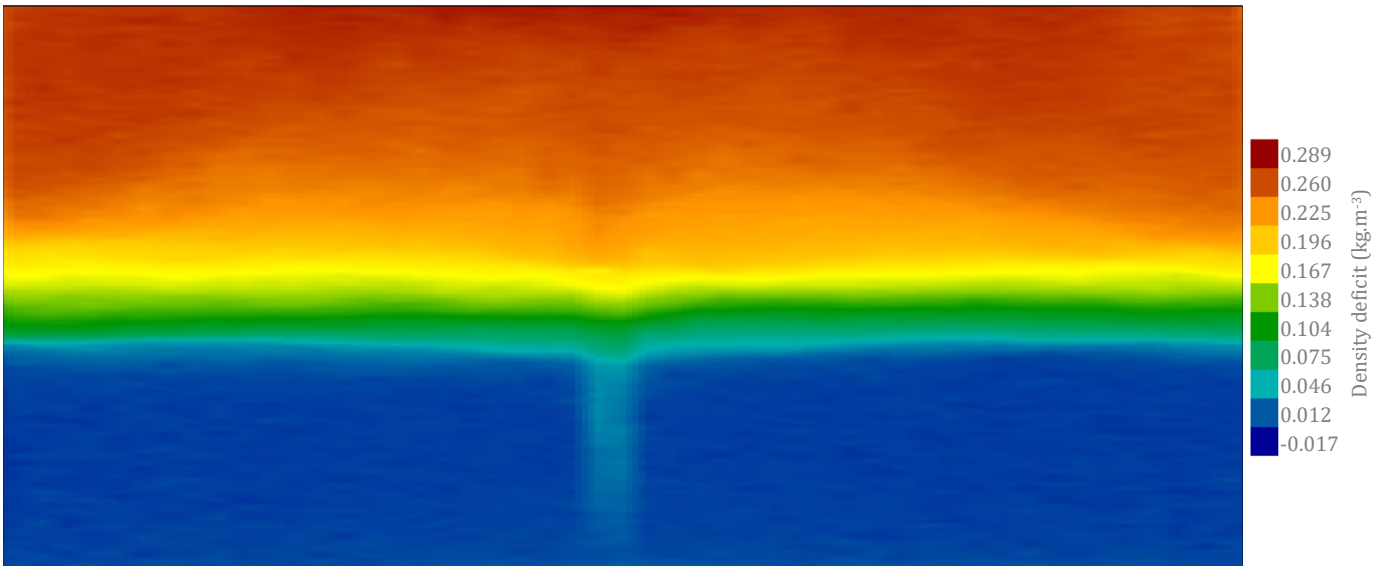

Figure 27. Layer gradient and interface consistency at experiment end. SF = 5 Experiment A, t = 811 s, t = 4.55*

4.2.2 Source conditions and flow regimes

The unique characteristics of each experiment were defined by the water depth and source conditions. Changing source conditions impacted flow characteristics and their ability to be compared to the two-zone model results. Source properties were governed by source Froude (Fr) and Reynolds (Re) numbers. Ideally, the source Froude number should be as close to 1 as possible to ensure a quick transition to buoyancy-driven flow. Source Reynolds number was to be maximised and ideally had a value above 2000 to ensure the flow regime was turbulent at the source. Source pipe diameter and source velocity governed these initial flow properties (Equations (21) & (26)). As source diameter increased, Re increased and Fr decreased. Therefore, a pipe diameter of 20 mm was chosen because it was the largest practical size and gave the best combination of Re and Fr. However, pipes of bigger sizes cause large zones of flow establishment and a turbulent regime may become impossible before ceiling impingement. Ideally pipe diameter should be very small and therefore larger diameter values were impractical. If flow increased, then consequently velocity also increased would lead to an increase in both Re and Fr for a particular source diameter.

The actual experimental flow rate was constant in all cases but differed from initial flow meter measurements throughout all experiments. Incorrect initial flow meter measurements may have been due to a poorly calibrated meter as the same experimental procedure was followed each experiment. Actual experimental flow rates were measured by tracking total water depth as a function of time. Increases in total water depth over time allowed calculation of a volume flux throughout each experiment and, by multiplying by tank cross-sectional area, a source in-flow rate. A large flow rate variance in the Shape Factor 5 (Experiment B) experiment and a smaller but still significant flow rate variance in the Shape Factor 70 became obvious when directly comparing measured and actual flows between all shape factor experiments (Figure

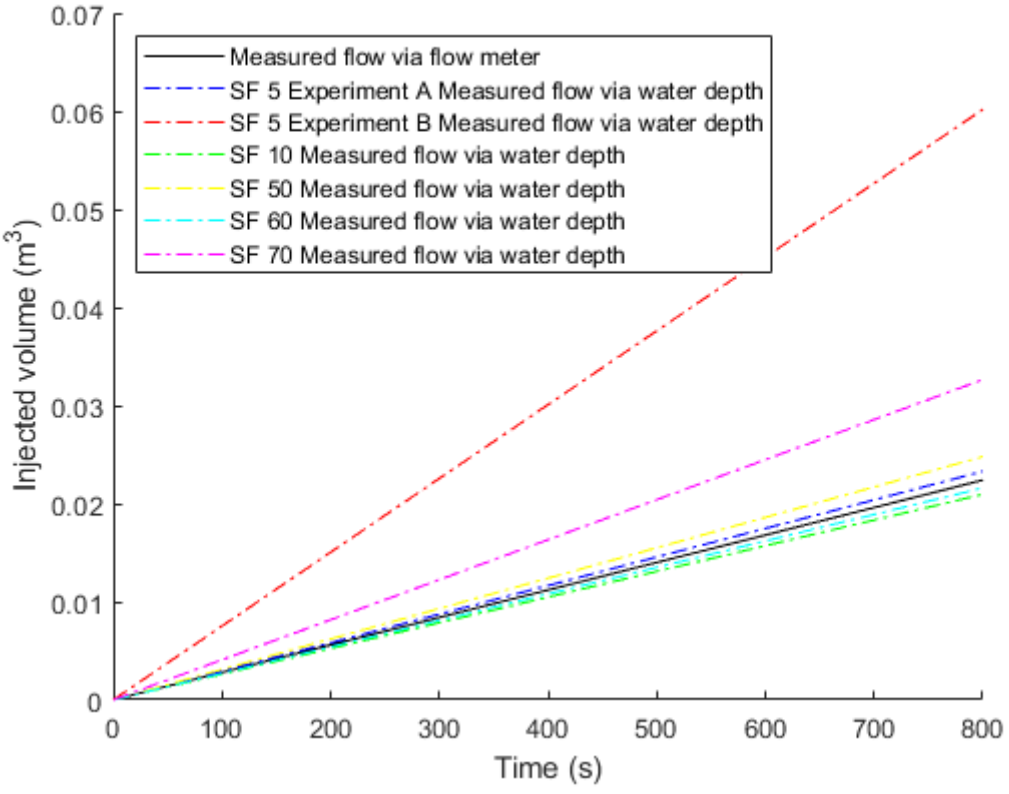

Figure 28. Comparison of measured and actual flow rates throughout each experiment as a function of time.

28). The flow rates deduced from changes in the water depth seemed robust and were used in all calculations.

Reynolds numbers, based on flow measured by water depth, within most of the experiments ranged from 1600 (Shape Factor 50) through to 2500 (Shape Factor 70) (Figure 30), with the exception of Shape Factor 5 (Experiment B). This experiment had a significantly higher *Re* value of 4600. Therefore, the amount of turbulent mixing present within the Shape Factor 5 (Experiment A), 10, 50 and 60 experiments was likely to represent a large portion of fully developed turbulent flow and the flow was approaching Reynolds, Prandtl, and Schmidt number independence. If Shape Factor 5 (Experiment B) and Shape Factor 70 experiments, the Reynolds number was greater than 2000, turbulent flows were fully developed and Reynolds, Prandtl, and Schmidt number independence was achieved.

Fr values approaching or below one were ideal, but not essential, for establishing a buoyancy-driven flow regime. The two-zone model assumed a plume-like flow occurred at the top of the fire, therefore the usefulness of the lab experiments depended on how close to the source similar conditions to plume-like flow existed in the tank. Froude numbers ranged from 2.5 for Shape Factor 5 (Experiment A) to 9.5 for Shape Factor 5 (Experiment B) (Figure 29). All experiments are approaching a Fr of 1 except Shape Factor 5 (Experiment B) (Figure 30). Investigating jet-plume flow regime dominance was essential for determining if Fr was sufficiently minimised to allow buoyancy forces to dominate close to the source. The flow exited the source as momentum-driven before transitioning to a flow regime where buoyancy and momentum effects were both important for characterising flow behaviour. As the flow travelled further from the source, the flow transitioned to be completely buoyancy-driven. The transition points between these flow regimes dictated the buoyant jet behaviour that occurred in each experiment. Comparing transition lengths with the transition to fully developed flow in each

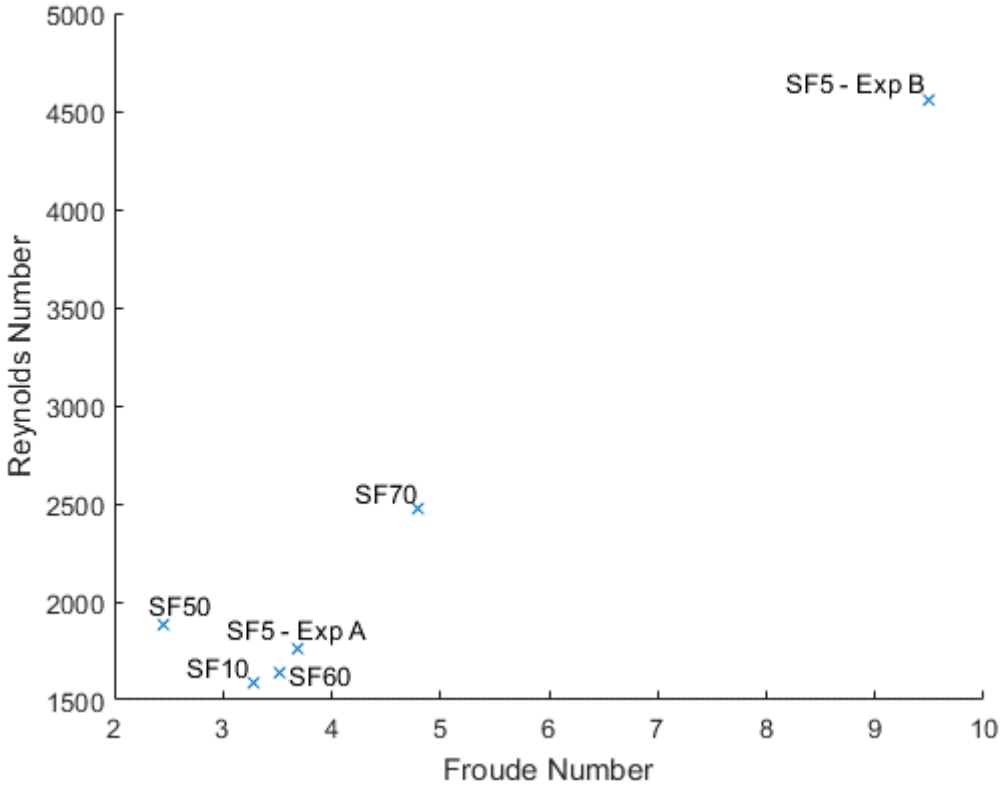

Figure 29. Comparison of initial Froude number and initial Reynolds number for all experiments.

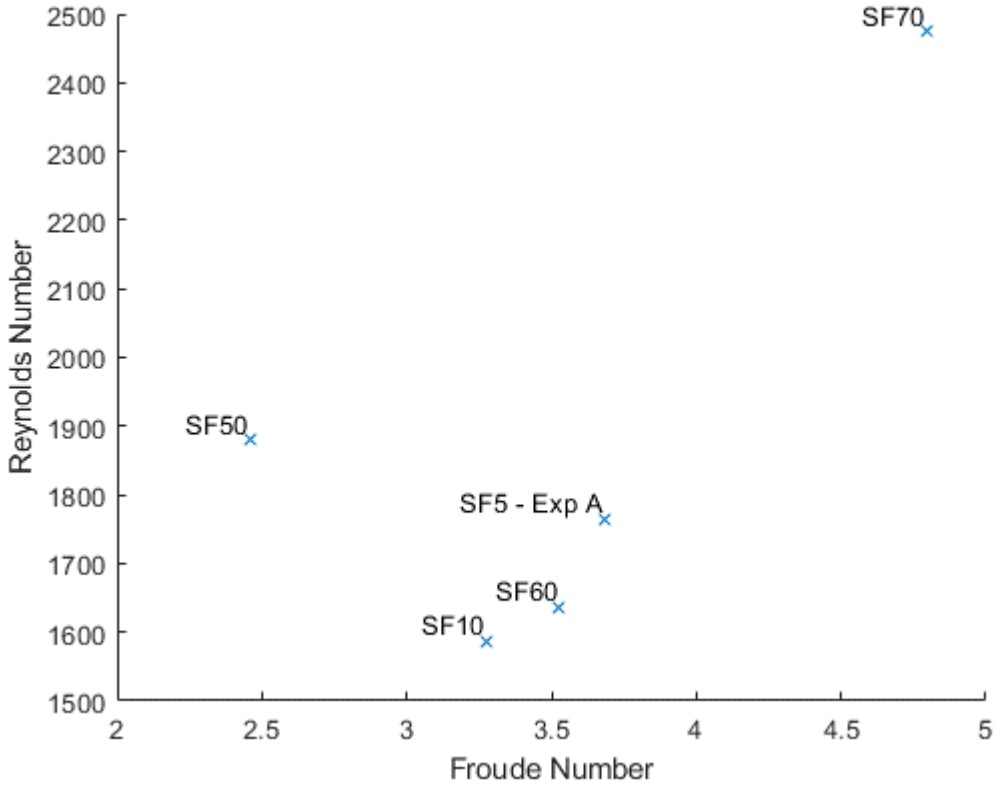

Figure 30. Close up comparison of initial Froude number and initial Reynolds number for all experiments except Shape Factor 5 Experiment B.

experiment allowed for analysis of the potential effects of flow regimes on experimental layer height results (Figure 31).

As shape factor increased, experimental water depth decreased, and the momentum-dominated portion of the flow increased significantly from 17% of the depth for Shape Factor 5 (Experiment A) through to 80% for Shape Factor 70 (Figure 31). The transition to fully buoyancy-driven, pure plume flow occurred in the Shape Factor 5 (Experiment A) through to Shape Factor 50 experiments. Shape Factor 60 and 70 experiments did not transition to completely buoyancy-driven flow before ceiling impingement because the source velocity was high, causing the length of plume transition to be too large relative to the depth of water. Reducing source velocity would have decreased Reynolds number and therefore the ability of the flow to develop turbulent mixing properties. Increasing the water depth would have required a much larger tank to maintain the high shape factors in these experiments.

When impinging on the ceiling, the shape factor 60 and 70 flow momentum was governed by the initial momentum at the source, compared to lower shape factor experiments which were governed by buoyancy driven momentum. However, as the ceiling jet travelled along the ceiling in these high shape factor experiments, the momentum became governed by the buoyancy driven momentum, which drove the flow characteristics. Due to the relatively low buoyancy-driven momentum, compared to the highly developed buoyancy driven momentum of low shape factor experiments, the velocity of the ceiling jet as it approached the wall and the velocity of the returning salt-water front would have been lower, causing a delay in smoke layer formation.

Due to the lower entrainment rate in momentum-driven flows than buoyancy-driven flows (Figure 6), when the layer formed it would have a significantly smaller volume (and therefore a

relatively high layer height at formation). However, the source flow has an initial volume flux which remains higher than buoyancy induced volume flux for some distance from the source. In shape factors 60 and 70 it was likely the source volume flux dominated the flow characteristics upon ceiling impingement, causing thicker layer heights upon formation.

As the layer lowered, the buoyancy dominated region became smaller and therefore less freshwater was entrained into the plume. With less freshwater being added to the layer, the rate of layer descent would be expected to decrease. The salt-water layer was likely to drop below the transition to buoyancy dominated flow in the Shape Factor 5 (Experiment B) and Shape Factor 50 experiments. This was likely to cause a reduction in freshwater entrainment and therefore a reduction in the rate of layer height descent towards the end of these experiments as discussed above for shape factor 60 and 70 experiments.

The source pipe was not oriented perfectly vertically and therefore there was some slight asymmetry in the flows within the tank. These small variances led to horizontal momentum in the salt-water flows. Horizontal momentum meant one side of the ceiling flows travelled more rapidly than the other as it approached the wall (Figure 22 & Figure 23).

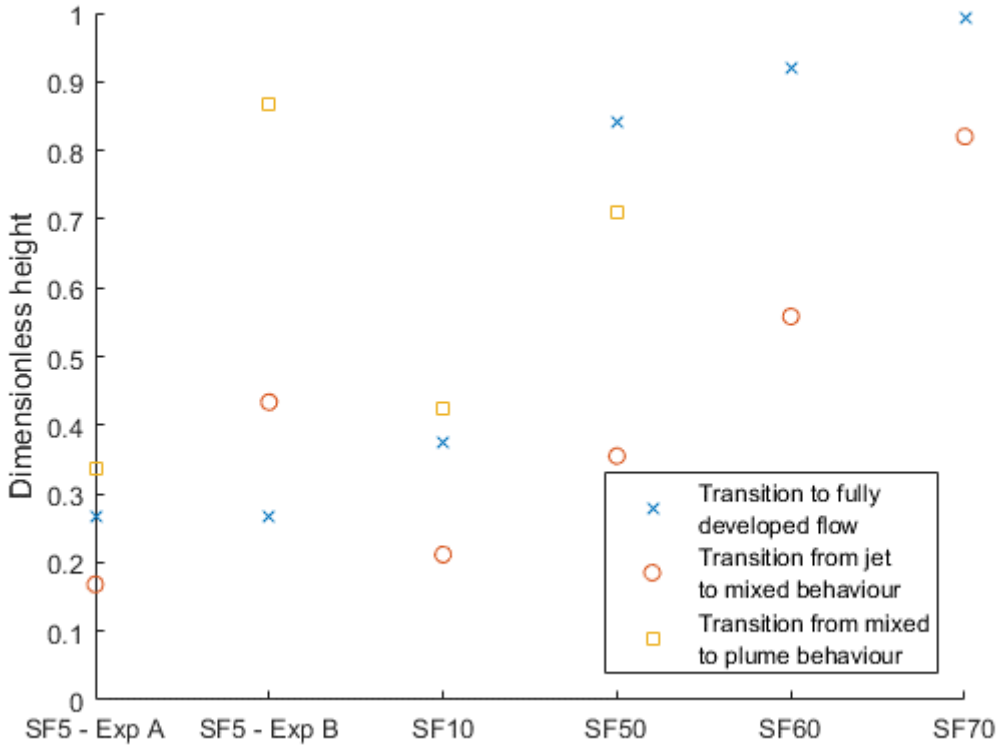

Figure 31. Comparison of dimensionless source flow characteristic length scales for different shape factor experiments.

4.2.3 Layer evolution

Upon leaving the source and impacting the ceiling, the buoyant salt-water travelled along the ceiling, down the walls, then back to the centre before forming a layer. The experiments were only comparable to the two-zone simulations once the layer had formed. We quantified the time scale of this process by tracking the salt front as it moved outward along the ceiling from the plume impingement point (Figure 32).

The smoke front was difficult to track on its return to the plume location. Time to layer formation was assumed to occur at twice the maximum time for wall impingement on the left and right sides. The time to wall impingement and therefore time to layer formation are shown in

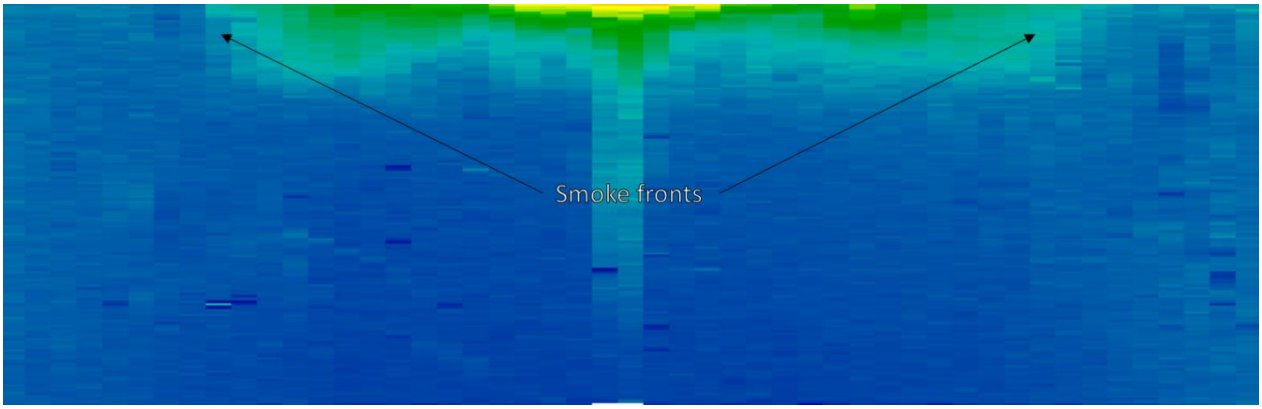

Figure 32. Intensity field (I(x,y)) at constant time displaying salt-water flow along the bottom of the tank near the beginning of SF = 10 experiment.

Table 3. Layer height development comparisons are more meaningful at times when all experiments had developed layers which is expected to be at $t^* = 0.48$.

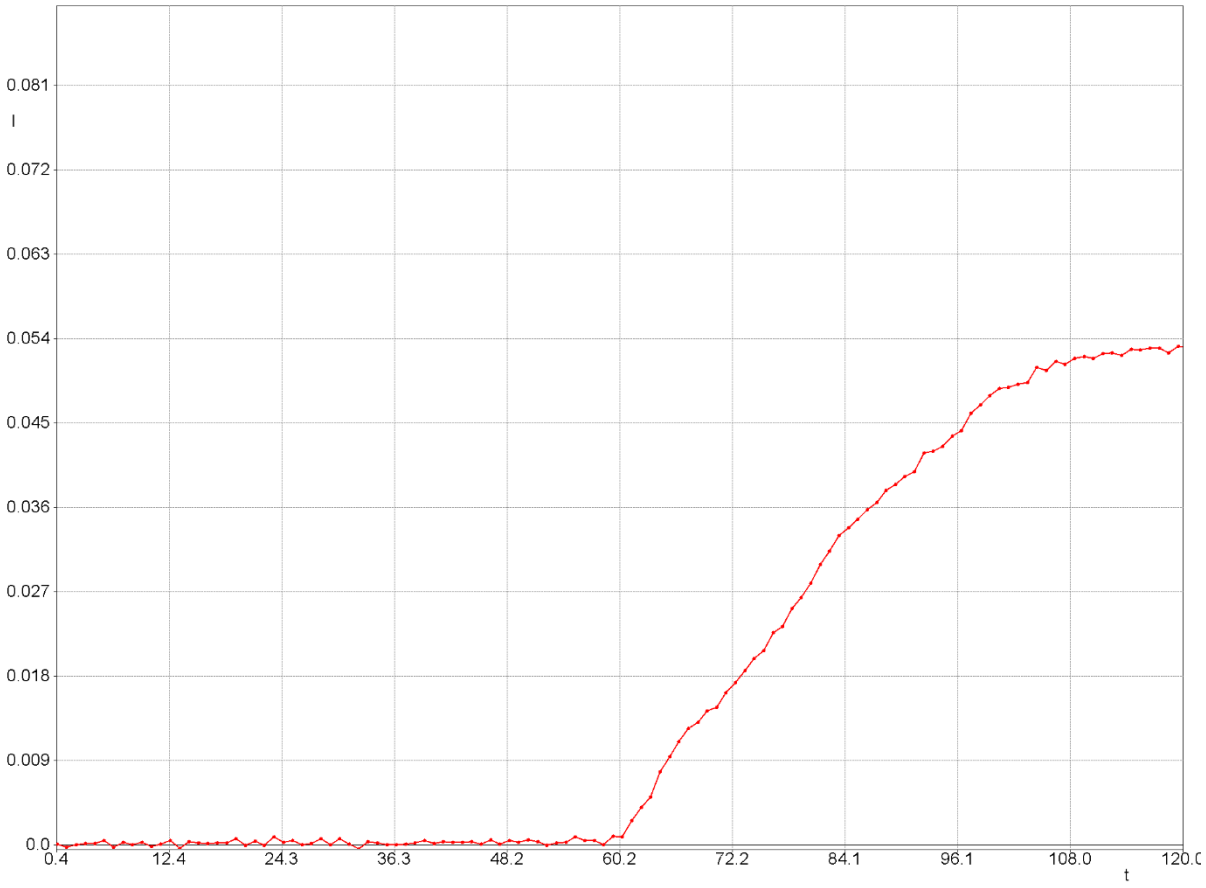

Figure 33. Intensity profiles at the side of the salt-water experiment tank showing an intensity increase at 59.4 s when salt-water impinges the wall.

Table 3. Layer formation times for each experiment.

Shape factor	Time of wall impingement				Time of layer formation	
	Left wall		Right wall			
	t (s)	t*	t (s)	t*	t (s)	t*
5 (Exp A)	38.9	0.22	42.0	0.24	84.0	0.48
10	49.9	0.22	40.0	0.17	98.8	0.44
50	38.9	0.14	42.2	0.15	84.4	0.30
60	48.0	0.11	55.0	0.13	110.0	0.26
70	34.4	0.09	38.0	0.10	76.0	0.20

Turbulence during layer formation caused waves to propagate along the layer interface. These waves were formed by high-density salt-water travelling inwards along the layer interface from the wall jets. As layer interface depth surpasses wall jet heights by a significant margin the waves become smaller and eventually become negligible in size. Although these waves allow increased entrainment into the upper layer, the amount of entrainment was miniscule as the waves were slow moving and non-breaking and therefore, they did not have a significant effect on the comparison with the two-zone model.

Vertical depth integrated density gradients were present as the layer descended through the tank (Figure 27). Investigation of characteristics of these gradients was undertaken by exploring the vertical depth averaged density deficit profiles throughout the water tank, from the central plume out to adjacent to the tank side (Figure 34). Profiles for other shape factors show the same trends and can be found in Appendix B. Horizontally throughout the tank, depth

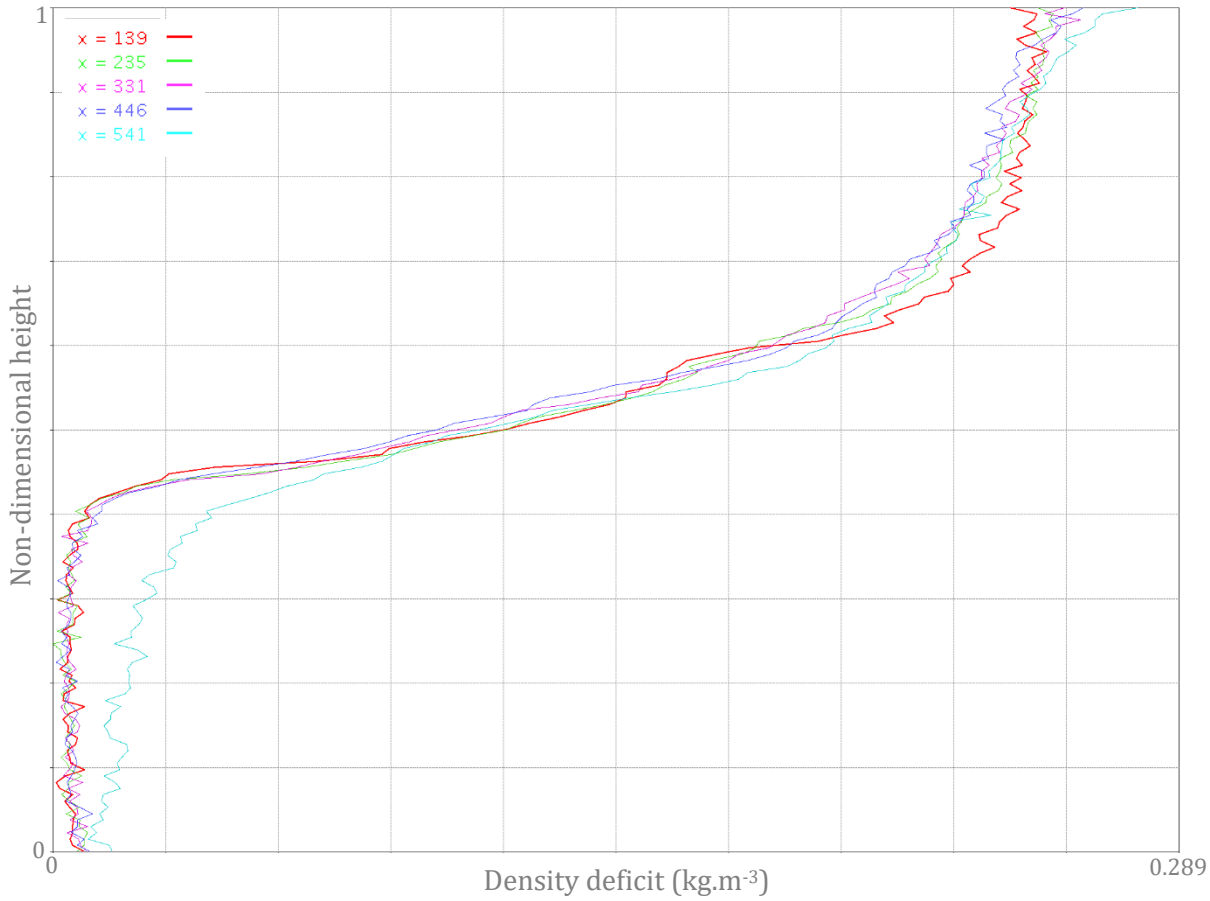

Figure 34. Full tank height vertical depth integrated density profiles for SF = 5 Experiment A from horizontal location x = 541 at the centre of the tank and plume and out to x = 139, which was immediately adjacent to the tank side.

averaged density deficit profiles were the same, independent of horizontal location except within the plume and at the tank sides. The salt-water plume travelled up, impacted the existing salt-water layer, continued upward, and travelled outward along the ceiling, down the wall and back inward to the plume, similar to during layer formation. The salt-water in this flow had higher salt concentrations than the surrounding fluid. This phenomenon was shown by the largest density excesses at the top of the tank (from the high concentration fluid travelling along the ceiling) and the high concentrations within the upper layer near the side of the tank. Densities adjacent to the wall of the tank up near the ceiling were within the wall jet and showed little change in concentration through the vertical extent of the wall jet. Wall jet concentrations appeared larger than plume concentrations because the depth averaged density deficit was measured throughout tank width. Wall jet phenomena occurred along the entire side of the tank whereas the plume only occurred through a smaller space in the tank centre.

4.2.4 Layer height development

Different methods for estimating non-dimensional experimental layer height from an averaged density deficit profile were discussed in Section 3.1.6. Each layer height methodology produced a different layer height estimate which was directly compared to a normalised density deficit profile where density deficit was defined as the difference in density between the diluted salt-water and the freshwater (Figure 35). This profile was normalised using the two-zone model upper layer density deficit. The integral ratio method (Section 3.1.7.2) calculated layer height as near to the lowest occurrence of salt-water in the layer. The least squares method (Section 3.1.7.3) calculated the layer height as occurring at about half the two-zone upper layer density deficit. Each of the N-percent estimates (Section 3.1.7.1) produced layer height estimates in between the values estimated by the integral method and the least squares method.

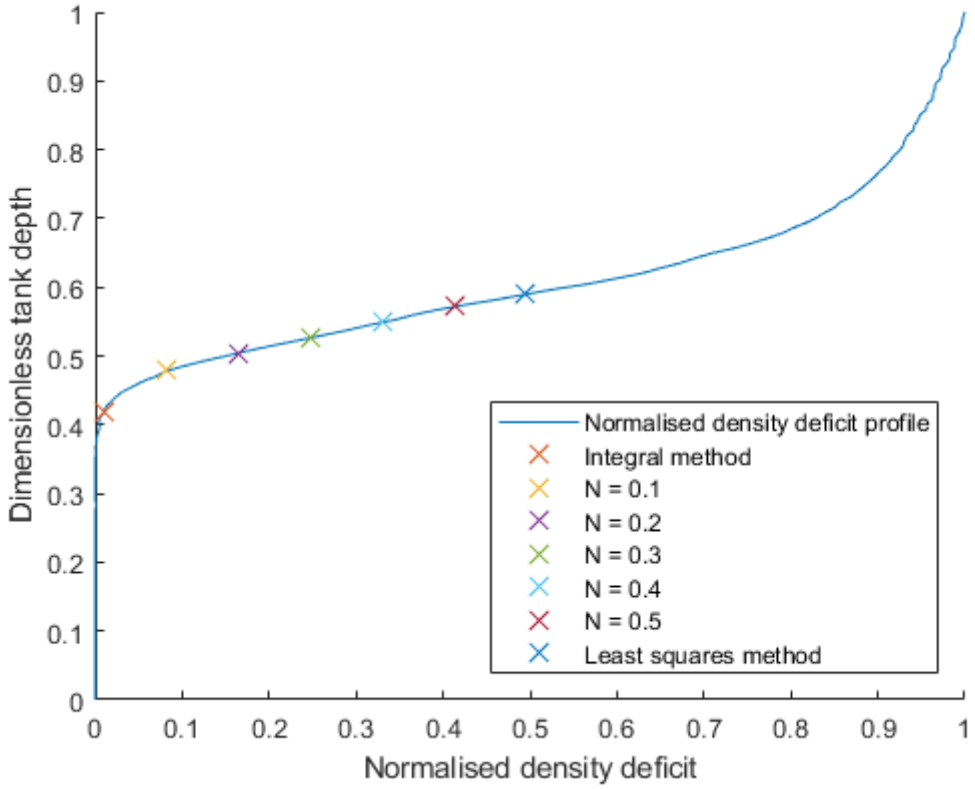

Figure 35. Layer height estimates shown against their corresponding normalised density deficit profile throughout the non-dimensionalised height. SF = 5 Experiment A, t = 534 s, t = 3.0*

Small changes in layer profile shape can have a disproportionately large impact on the layer height estimate. This is because the layer height estimates are calculated relative to the normalised layer density profile and therefore layer height estimates always occur at the same part of the shape of the profile and are not significantly affected by the magnitude of the normalised layer densities. Changes in depth integrated density profile shape throughout each experiment would have caused large shifts in the behaviour shown by each layer height method. Changes to sections of the depth integrated density profile would affect each layer height method behaviour differently. For the best comparison to the two-zone model layer heights it was important that the chosen layer height method provide a continuous layer height estimate through time with minimal fluctuations throughout each experiment from layer height formation and onwards for each shape factor.

The behaviour of each layer height method throughout the experiments were explored through looking at the depth integrated density deficit profile as a function of time, normalised using the maximum depth integrated density deficit. The maximum depth integrated density deficit at each time step was used to allow comparison as this maximum deficit increased throughout the experiment. The height through the tank was non-dimensionalised using layer thickness calculated using the investigated layer height method for exploration of the behaviour of the experiments around the layer interface.

The self-similarity of the profiles at each time step was of interest. Using the layer height method N = 0.2 to plot profiles for each experiment at various time steps illustrated the inapplicability of comparison between two-zone models and the experiments at early times while the layer was forming due to the only non-self-similar profile occurring at $t^* = 0.5$ (Figure 36). The region of these profiles around the layer height estimate were self-similar. The self-similarity meant, aside from during layer formation, the method always measured the same section of the normalised depth integrated density deficit profile and that N = 0.2 layer height method was applicable throughout all experiments. This result meant the N = 0.2 layer height method could be used to measure layer heights.

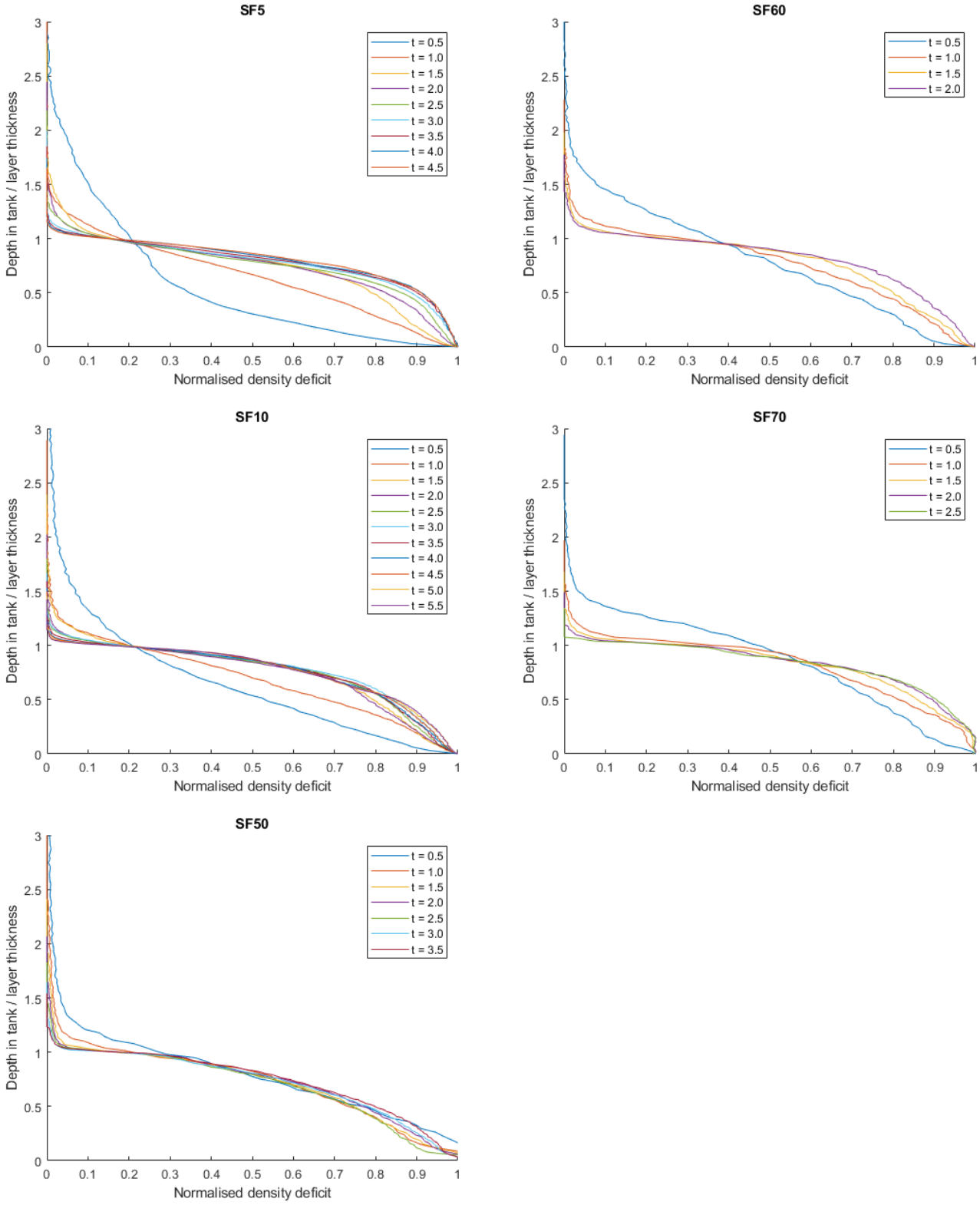

Figure 36. Normalised density deficit profiles using N = 0.2 layer height prediction throughout each experiment showing self-similarity after layer formation.

The N = 0.2 layer height method yielded self-similar and therefore useful results when non-dimensionalised and normalised density deficit profiles for each shape factor experiment were compared at a specific non-dimensionalised time (Figure 37). Due to self-similarity, the N = 0.2 method was expected to provide reliable layer height measurements between all the experiments.

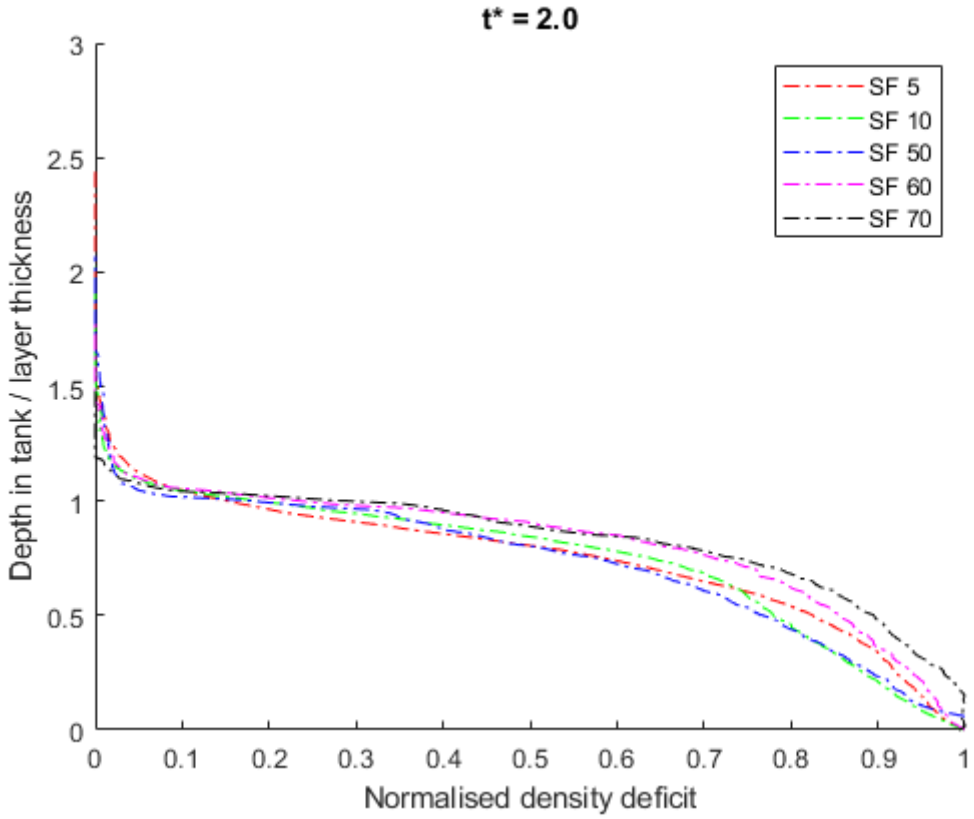

Figure 37. Normalised density deficit profiles throughout SF = 5 Experiment A, 10, 50, 60, & 70 experiments showing self-similarity between these experiments at t = 2.0.*

Due to the self-similarity throughout a SF = 5 experiment and between all experiments, it was expected that N = 0.2 results could be directly compared for all times (after layer formation) and between all experiments. The profile self-similarity was further investigated throughout all experiments at six separate time steps $t^* = 0.5, 0.7, 1.0, 1.5, 2.0, 2.5$ (Figure 38). The last comparison occurred at $t^* = 2.5$ because the Shape Factor 70 experiment ended. The N = 0.2 layer height method showed consistency and independence in all time frames and for all shape factors excluding $t^* = 0.5$. Due to the inconsistent behaviour at $t^* = 0.5$ it is unlikely that layer formation has completed for all shape factor experiments by $t^* = 0.48$ as estimated in Section 4.2.3. The difference in layer formation time is likely to be because the method described in Section 4.2.3 did not take into account the time for the wall jets to form and travel down the walls before the smoke front returned to the plume. It is also possible that the smoke front took longer to travel from the wall to the plume than from the impingement point to the wall, thereby taking a longer time for overall layer formation than estimated. Investigations defined the earliest occurrence of similar behaviour occurring for all shape factor experiments at $t^* = 0.7$ (Figure 38) and therefore salt-water layer formation was assumed to have completed by this non-dimensional time.

Figure 36 and Figure 38 were used to explore the appropriateness of the N = 0.2 layer height calculation method. the remaining N = 0.1 to N = 0.5, least squares, and integral ratio layer

height methods were explored with equivalent Figures in Figure 41 through Figure 52 within Appendix A. Through inspection N = 0.4, N = 0.5, least squares and integral ratio layer height methods produced profiles that were less appropriate for providing reliable calculated layer heights than the N = 0.2 profiles. Both N = 0.4 and N = 0.5 produced profiles for Shape Factor 60 and 70 experiments where it took longer than $t^* = 1$ for self-similarity to occur. Therefore N = 0.2 was better for the comparisons because it allowed at least $t^* = 0.3$ more time for comparison of the layer height results. The least squares method produced profiles for Shape Factor 5 and 10 experiments where it took longer than $t^* = 1$ for self-similarity to occur and similarly, N = 0.2 allowed more time for comparison of the layer height results. All of the layer heights calculated using the integral ratio method occurred adjacent to sharp changes in profile gradient. While the layer height occurring at a sharp increase in depth integrated density deficit made physical sense, small differences in profiles between experiments or time steps resulted in large changes in where, within the profile, the layer height was calculated. This caused large instabilities in the layer height calculation with no reliability between experiments.

Both N = 0.1 and N = 0.3 layer height calculation methods provided similar depth integrated density deficit profiles to N = 0.2 throughout the length of each experiment. N = 0.2 was chosen as it had previous been used by Cooper et al. (1982) and was the mean N value investigated that provided similar depth integrated density deficit profiles.

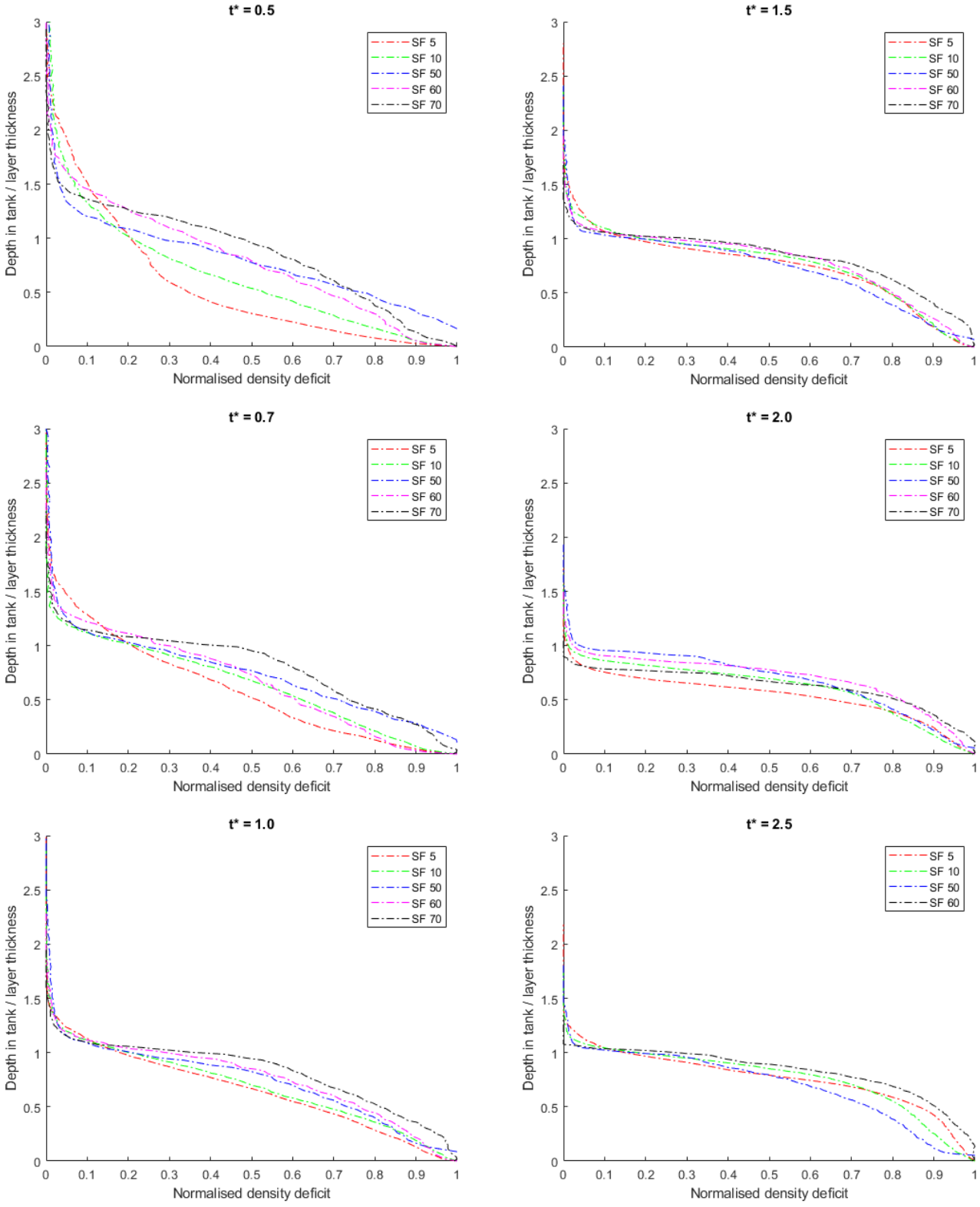

Figure 38. Development of self-similarity throughout all experiments at t = 0.5, 0.7, 1.0, 1.5, 2.0, & 2.5.*

4.2.5 Layer height analysis

Comparing experimental N = 0.2 layer height development from layer formation onwards showed significant variance between each shape factor (Figure 39). Figure 39 is the salt-water experiment equivalent of Figure 20 which showed the two-zone model layer height estimates within the same non-dimensional timeframe. It was expected that all salt-water experiment layer height curves became self-similar upon non-dimensionalisation. Changes in behaviour between shape factors may be due to a breakdown of the fundamental assumptions used in the salt-water setup, changes in geometry, or both.

For comparison to smoke plumes, it was assumed that the salt-water flows were fully established buoyancy-driven flows within a small distance of the source. This was true for experiments with Shape Factor 5 (Experiment A) and Shape Factor 10, where the transition to buoyancy-driven flow occurred close to the source. Shape Factor 5 (Experiment B) and Shape Factor 50 experiments became buoyancy-driven far from the source but before impinging the ceiling and formed salt-water layers with relatively similar layer heights. The same was not true of shape factors 60 and 70. These experiments showed significantly lower layer heights at formation. As previously discussed, it was expected that due to lower entrainment in the source flows in the jet-plume transition region that the layer would be significantly thinner upon formation in shape factors 60 and 70 which was obviously not the case. Further research is required to confirm why the thicker upper layer occurred.

The fully developed flow was expected to occur six source diameters downstream of the source (Fischer et al., 1979). The turbulent regime had only developed fully at this point. As experimental shape factors increased through 50, 60, and 70, the distance required to reach fully developed flow approached the ceiling. As the region of fully developed turbulent flow decreased in size for shape factors 50 through 70, the amount of freshwater entrained into the

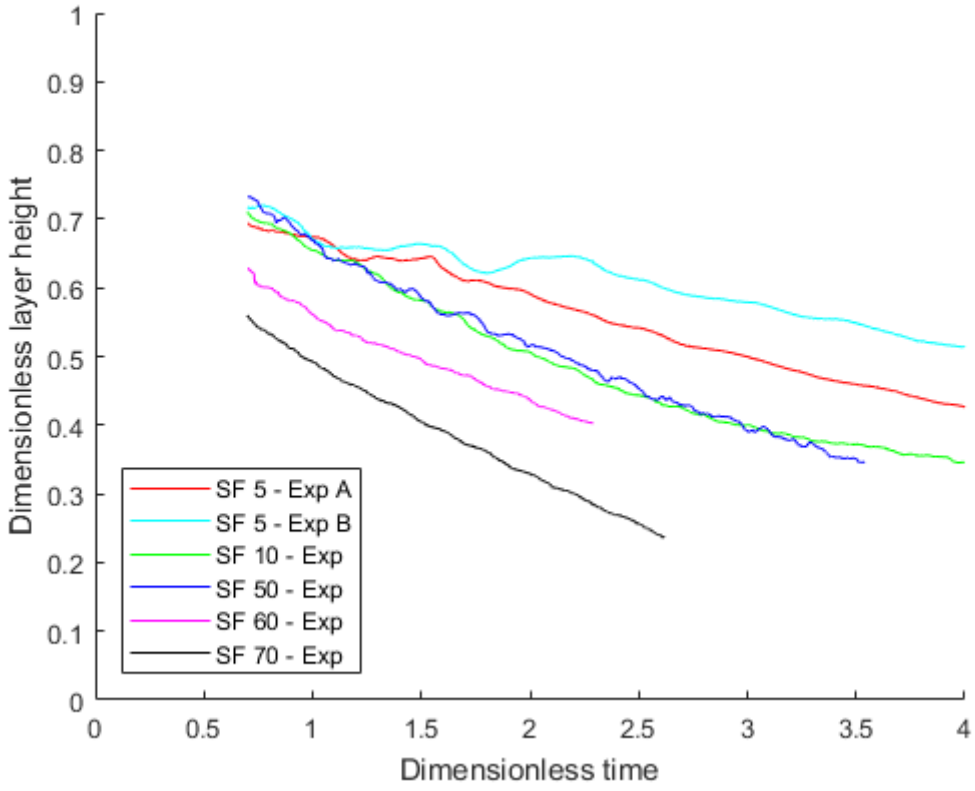

Figure 39. N = 0.2 layer heights calculated for each experiment including both SF5 experiments.

buoyant jet decreased significantly. Therefore the layer would be expected to be significantly thinner, resulting in a higher layer height. Figure 39 showed Shape Factor 50 having similar layer heights to lower shape factors and Shape Factors 60 and 70 showing increased layer thickness. Further research is required to confirm why the upper layer was thicker than expected.

Similarly, it was expected that as the salt-water layer descended through the plume transition point and beyond, the entrainment of freshwater into the buoyant jet would significantly decrease due to larger entrainment in buoyancy-driven flows. This phenomenon was expected to cause the layer height descent to slow due to less volume added. Evidence of layer height descent rate slowing over time existed in all shape factor experiments. However, the amount of change in descent rate was much smaller in all experiments than in the two-zone models. It was not clear why the change in descent rate was less significant in the salt-water experiments, further research is required to confirm why this has occurred.

4.3 Two-zone model and salt-water experiment layer height comparison

The two-zone model for Shape Factor 5, representing the behaviour seen with all modelled shape factors, was compared to the salt-water experiments (Figure 40). The two-zone model curves were represented by a single curve because the fundamental model behaviour did not change. The experiment layer height curves did not collapse onto one curve and therefore the development displayed behaviour that changed with shape factor, especially with Shape Factors 60 and 70. In comparing two-zone and salt-water layer heights a number of assumptions were made in attempt to allow the salt-water experiments to approximate the behaviour of the two-zone model. A breakdown of a number of these coupled assumptions likely contributed to the changes in experimental behaviour.

Heat release rate within the two-zone model was assumed to be constant throughout the simulation. For comparison, the injection rate of salt was required to be constant. Before each experiment, the source fluid was mixed thoroughly in a tank before being pumped into the pressure vessel to be injected into the tank. Once within the pressure vessel it was impractical to mix. It was only contained within the pressure vessel for a matter of hours and concentrations of dye and salt were very low, therefore the Carmoisine powder and salt were unlikely to precipitate out of solution. Both Carmoisine and salt were important as the Carmoisine changed the amount of light absorbed for measurement of the amount and location of salt-water and the salt created the buoyancy forces. To ensure the Carmoisine measurement was linearly dependent on the amount of salt-water added, the maximum concentration of powder was approximately 0.07 g m^{-3} which was significantly less than the maximum able to be added for accurate measurements, 0.12 g m^{-3} (Figure 8). Therefore, as the flow rate was

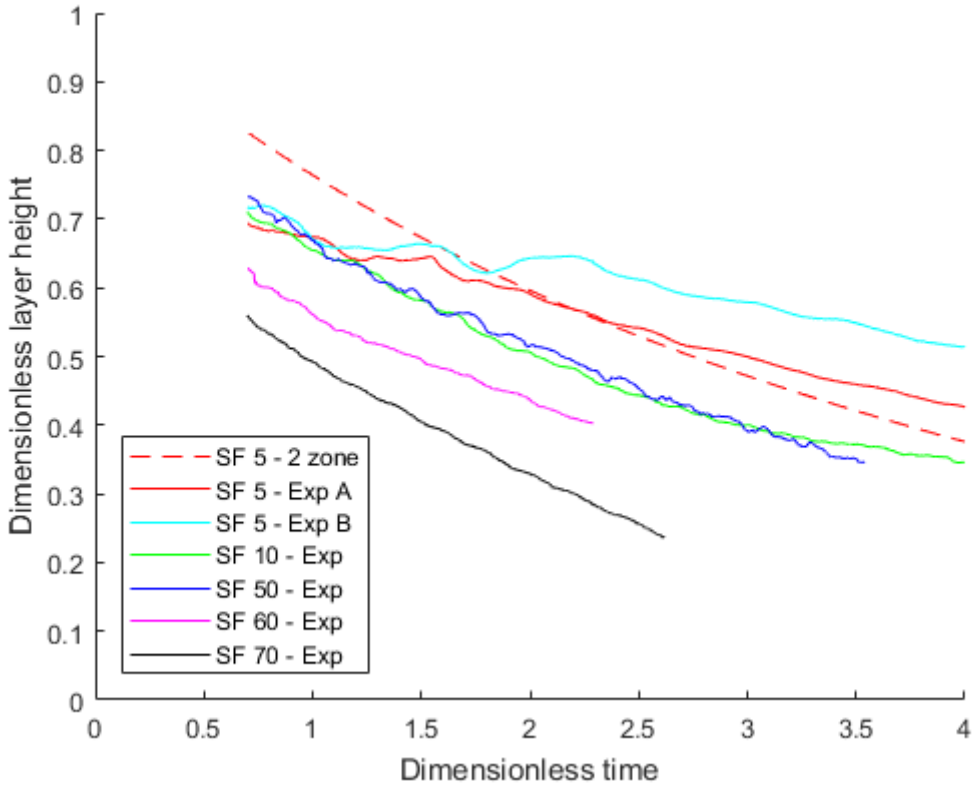

Figure 40. Comparison of layer height development between a two-zone model and salt-water experiments for Shape Factors 5, 10, 50, 60, and 70.

constant in every salt-water experiment (Figure 28), the assumption of constant salt injection rate was met and injection rate did not contribute to the changes in layer height behaviour.

Once injected the salt-water buoyant jet was assumed to approximate a pure plume in a real fire and therefore the fire within the two-zone model. This was discussed in Section 4.2.5. Neither Shape Factor 60 nor 70 became buoyancy-driven, and both had significantly different layer heights to the other experiments. The breakdown of this assumption may have contributed to changes in behaviour as shape factor increased.

A fundamental assumption was the buoyancy forces between smoke and air could be approximated by the density difference between salt-water and freshwater. Due to the distinctly similar flow characteristics observed between the experimental salt-water mixing phenomena (Section 4.2.1) and smoke layer evolution (Section 2.1) it was expected that salt-water modelling produced similar behaviour to an equivalent, real compartment fire. Therefore, the buoyancy forces were able to be approximated by salt-water well and it is unlikely that the difference in medium for producing buoyancy contributed to the changes in layer height behaviour.

As source fluid was injected during the experiment, it was assumed that fluid volume increase did not have a significant impact on the layer height predictions. In all cases, the salt-water layer interface did not approach the water surface and therefore the impact of volume increase at the free surface of the tank was negligible. The equivalent assumption in the two-zone model was that sufficient ventilation was provided to prevent over pressurisation. As discussed in Section 4.1.2, enough ventilation was provided to avoid over-pressurisation while ensuring the layer height did not reach the top of the vent. Avoidance of over-pressurisation meant that salt-water modelling overestimation of flow velocities due to pressure was unlikely and therefore did not contribute to changes in layer height behaviour.

In the two-zone model, the fire produces heat and smoke. Heat is absorbed by the surfaces of the room. Heat absorption was minimized through reducing the radiative heat loss coefficient to 0.01 and the emissivity of the surfaces being set to 1. In salt-water modelling, the walls cannot absorb salt and therefore even the small amount of heat absorbed by the walls in the two-zone model may have contributed a small amount to the changes in layer height behaviour through artificially high buoyancy near the boundaries. This buoyancy led to increased velocities near the boundaries. As the shape factor increased and the surface area of the walls increased, the amount of heat able to be absorbed by the walls would have increased significantly and the difference between the experiment and two-zone model also increased. The absorption of heat within the two-zone model may contribute to the greater layer height inconsistencies seen at larger shape factors.

A fundamental part of the two-zone approximation is the uniformity of the temperature of the hot, upper smoke layer and the cool, lower air layer. Throughout each salt-water experiment the lower, freshwater layer remained uniform in concentration. Large concentration gradients existed throughout the upper salt-water layer, with high concentrations at the ceiling and lower concentrations at the layer interface (Figure 27, Figure 34). In all experiments, the lower layer contained no significant salt concentrations. The high concentration gradient within the upper layer added significant difficulties in determining the layer height within the salt-water experiments as the layer interface was not explicit. Determining a layer height method that was reliable was difficult but the $N = 0.2$ method provided an acceptable level of behavioural consistency throughout all shape factors. Non-uniformity of the concentrations in the upper mixed layer of the salt-water experiments was likely to have contributed to the layer height inconsistencies because of the large impact on different methods for calculating layer height,

which were all based on the depth integrated density profiles. The depth integrated density profiles would change significantly based on the upper layer concentration gradient.

The N = 0.2 layer height method was chosen based on self-similarity of the depth integrated density profiles throughout time and the experiments of different shape factors. The choice of N = 0.2 is likely to have contributed significantly to the over-estimation of the layer thickness however it was the most appropriate methodology for these experiments and was therefore used. Further research is required to investigate alternate layer height methodologies.

Total energy within each experiment was based on energy within the equivalent two-zone model for any given non-dimensional time (Equation (19)). Scaling of the depth-integrated density deficit profiles was unlikely to have a large impact on layer height calculations as the layer height methods used were based on the shape of the profile rather than magnitude of the depth-integrated density deficits. Therefore, the energy scaling of the layer height profiles was unlikely to have contributed significantly to the changes in layer height behaviour, due to the self-similarity of the layer normalised density deficit profiles.

The salt-water experiments showed relatively small changes in behaviour for shape factors 5 through 50. These experiments were directly comparable to the two-zone model which showed minimal changes in behaviour for shape factors 5 through 70.

5 Conclusions

This research investigated the applicability and limitations of two-zone smoke movement models using salt-water physical experiments.

The salt-water experiments were used to investigate salt-water propagation when injected into freshwater within compartments of various geometric shape factors ($SF = A/H^2$, Equation (1)). The research concentrated on short, stout compartments with high shape factors. Light Attenuation was used to measure the density field throughout the experimental tank. The height of the interface between the salt-water and freshwater was found throughout each experiment. Similar layer height evolution behaviour was found for shape factors up to and including Shape Factor 50. Shape Factors 60 and 70 exhibited significant variations from layer height behaviour of the lower shape factors. The behavioural changes were likely due to difficulties in establishing buoyancy dominated flow with the experiment tank size used.

The two-zone model B-RISK was used to calculate the equivalent smoke layer interface location and temperature throughout time for full-size geometries with the same shape factors. The two-zone model and salt-water experiment layer heights and time scales were non-dimensionalised to allow comparisons to be made. Upon comparison of the layer height calculations from the two-zone model, it was shown that layer height behaviour within the simulations was similar for all shape factors.

Based on the behaviour exhibited by both the salt-water experiments and two-zone models, salt-water experiments were an appropriate method for validating two-zone models up to a shape factor of 50.

6 Bibliography

Alpert, R. (1975, November). Turbulent Ceiling-Jet Induced by Large-Scale Fires. *Combustion Science and Technology*, Vol. 11, pp. 197–213. https://doi.org/10.1080/00102207508946699

Birky, M., & Clarke, F. (1981). Inhalation of Toxic Products from Fires. *Bulletin of the New York Academy of Medicine*, Vol. 57, pp. 997–1013. Washington, D.C.: Centre for Fire Research, National Bureau of Standards.

Bong, W. (2011). *Limitations of Zone Models and CFD Models for Natural Smoke Filling in Large Spaces* (Master's Thesis). University of Canterbury, NZ.

Cenedese, C., & Dalziel, S. (1998, January). *Concentration and depth fields determined by the light transmitted through a dyed solution* (pp. 1–37). pp. 1–37. Cambridge, UK: University of Cambridge.

Chorin, A. (1969). On the convergence of discrete approximations to the Navier-Stokes equations. *Mathematics of Computation*, Vol. 23, p. 341. https://doi.org/10.1090/S0025-5718-1969-0242393-5

Clement, J. (2000). *Experimental Verification of the Fire Dynamics Simulator (FDS) Hydrodynamic Model* (Doctor of Philosophy Thesis). University of Canterbury, NZ.

Cooper, L. (1984). Smoke movement in rooms of fire involvement and adjacent spaces. *Fire Safety Journal*, Vol. 7, pp. 33–46. https://doi.org/10.1016/0379-7112(84)90006-7

Cooper, L., Harkleroad, M., Quintiere, J., & Rinkinen, W. (1982). An Experimental Study of Upper Hot Layer Stratification in Full-Scale Multiroom Fire Scenarios. *Journal of Heat Transfer*, Vol. 104, pp. 741–749. Washington, D.C.: American Society of Mechanical Engineers.

Fischer, H., List, J., Koh, R., Imberger, J., & Brooks, N. (1979). *Mixing in inland and coastal waters*. San Diego, CA: Academic Press.

Haynes, W., Lide, D., & Bruno, T. (Eds.). (2014). *CRC handbook of chemistry and physics*. Boca Raton, FL: Taylor & Francis Group.

He, Y., Fernando, A., & Luo, M. (1998). Determination of interface height from measured parameter profile in enclosure fire experiment. *Fire Safety Journal*, Vol. 31, pp. 19–38. Elsevier.

Karlsson, B., & Quintiere, J. (1999). *Enclosure Fire Dynamics*. https://doi.org/10.1201/9781420050219

Kikkert, G. (2006). *Buoyant jets with two and three-dimensional trajectories*. University of Canterbury, NZ.

Linden, P. (1999). The fluid Mechanics. *Annual Review of Fluid Mechanics*, pp. 201–238. https://doi.org/0066-4189/99/0115-0201

Lindholm, J., Brink, A., & Hupa, M. (2008). A guide to characterizing heat release rate measurement uncertainty for full-scale fire tests. *Fire and Materials*, Vol. 32, pp. 121–139. https://doi.org/10.1002/fam

McBryde, J. (2008). *Experimental and Numerical Modelling of Gravity Currents Preceding Backdrafts*. University of Canterbury.

Morton, B., Taylor, G., & Turner, J. (1956). Turbulent Gravitational Convection from Maintained and Instantaneous Sources. *Proceedings of the Royal Society of London. Series A, Mathematical and Physical Sciences*, Vol. 234, pp. 1–23. London, UK: Royal Society.

Mowrer, F. (2016). Enclosure Smoke Filling and Fire-Generated Environmental Conditions. In M. Hurley, D. Gottuk, J. Hall, K. Harada, E. Kuligowski, M. Puchovsky, … C. Wieczorek (Eds.),

SFPE Handbook of Fire Protection Engineering (pp. 1066–1101). https://doi.org/10.1007/978-1-4939-2565-0_33

Nokes, R. (2016, January). *System Theory and Design (Version 2.05)*. Christchurch, New Zealand.

Olenick, S. M., & Carpenter, D. J. (2003). An Updated International Survey of Computer Models for Fire and Smoke. *Journal of Fire Protection Engineering*, *13*, 87–110. https://doi.org/10.1177/104239103033367

Onate, E., & Idelsohn, S. (1992). A comparison between finite element and finite volume methods in CFD. *Computational Fluid Dynamics '92; Proceedings of the European Computational Fluid Dynamics Conference*, *1* & *2*, 93–100. Brussels, Belgium.

Partridge, J., & Linden, P. (2013). Validity of thermally-driven small-scale ventilated filling box models. *Experiments in Fluids*, Vol. 54. https://doi.org/10.1007/s00348-013-1613-4

Peacock, R. D., McGrattan, K. B., Forney, G. P., & Reneke, P. A. (2017). *NIST Technical Note 1889v3 CFAST – Consolidated Fire and Smoke Transport. Volume 3: Verification and Validation Guide*. *3*(Version 7). https://doi.org/10.6028/NIST.TN.1889v1

Peacock, R., McGratten, K., Reneke, P., & Forney, G. (2015). *CFAST – Consolidated Model of Fire Growth and Smoke Transport (Version 7) Volume 2: User's Guide* (Vol. 3). Vol. 3. https://doi.org/10.6028/NIST.TN.1889v2

Quintiere, J. (1989). Scaling applications in fire research. *Fire Safety Journal*, Vol. 15, pp. 3–29. https://doi.org/10.1016/0379-7112(89)90045-3

Reynolds, O. (1895). On the Dynamical Theory of Incompressible Viscous Fluids and the Determination of the Criterion. *Philosophical Transactions of the Royal Society of London*, Vol. 186, pp. 123–164. London, UK: Royal Society.

Ricou, F., & Spalding, D. (1961). Measurements of entrainment by axisymmetrical turbulent jets. *Journal of Fluid Mechanics*, *11*(1), 21–32. https://doi.org/10.1017/S0022112061000834

Röwekamp, M., Dreisbach, J., Klein-Heßling, W., McGratten, K., Miles, S., Plys, M., & Riese, O. (2008). *International Collaborative Fire Modeling Project (ICFMP) Summary of Benchmark Exercises No. 1 to 5*.

Smagorinsky, J. (1963). General Circulation Experiments With the Primitive Equations. *Monthly Weather Review*, Vol. 91, pp. 99–164. https://doi.org/10.1175/1520-0493(1963)091<0099:GCEWTP>2.3.CO;2

Steckler, K., Baum, H., & Quintiere, A. (1986). Salt Water Modeling of Fire Induced Flows in Multicompartment Enclosures. *Twenty-First Symposium (International) on Combustion/The Combustion Institute*, Vol. 21, pp. 143–149. Gaithersburg, MD, USA: Elsevier.

Steckler, K., Quintiere, J., & Rinkinen, W. (1982). Flow induced by fire in a compartment. *Ninteenth Symposium (International) on Combustion/The Combustion Institute*, *19*(1), 913–920. https://doi.org/10.1016/S0082-0784(82)80267-1

Tavelli, S., Rota, R., & Derudi, M. (2014). A Critical Comparison Between CFD and Zone Models for the Consequence Analysis of Fires in Congested Environments. *Chemical Engineering Transactions*, Vol. 36, pp. 247–252. https://doi.org/10.3303/CET1436042

Wade, C., Baker, G., Frank, K., Harrison, R., & Spearpoint, M. (2016). *B-RISK 2016 user guide and technical manual*. Wellington, NZ: Building Research Association of New Zealand.

Wade, C., & Robbins, A. (2008). *Smoke filling in large spaces using BRANZFIRE* (Vol. 195). Wellington, NZ: BRANZ.

Yao, X. (2006). Characterization of fire induced flow transport along ceilings using salt-water modeling (Doctor of Philosophy Thesis). University of Maryland.

Yao, X., & Marshall, A. (2007). Quantitative Salt-Water Modeling of Fire-Induced Flows for Convective Heat Transfer Model Development. *Journal of Heat Transfer*, Vol. 129, p. 1373.

https://doi.org/10.1115/1.2754943

Zukoski, E. (1978). Development of a stratified ceiling layer in the early stages of a closed room fire. *Fire and Materials*, Vol. 2, pp. 54–62. https://doi.org/10.1002/fam.810020203

7 Appendix A – Layer height methodology

7.1 N-percentage – 0.1

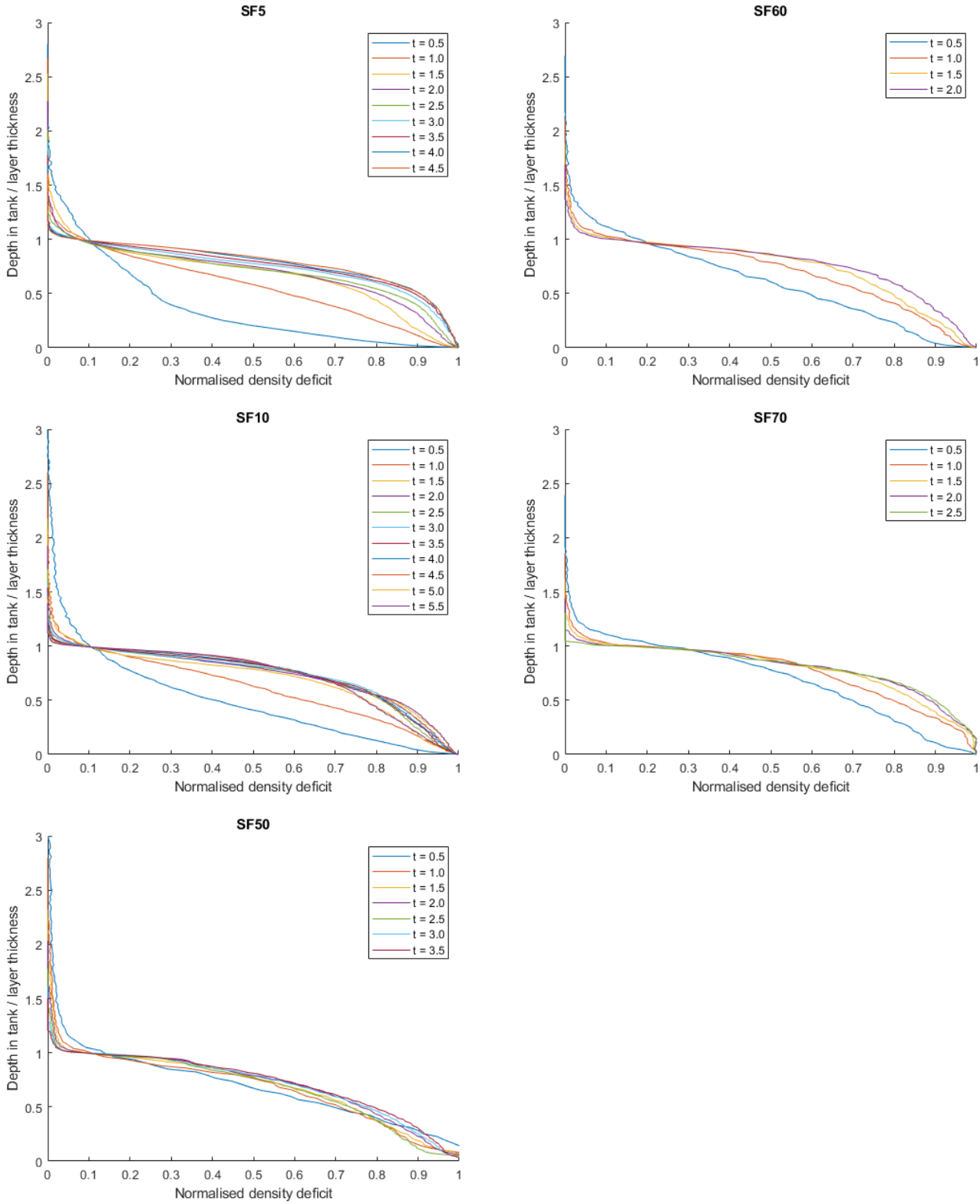

Figure 41. Normalised density deficit profiles using N = 0.1 layer height prediction throughout each experiment showing self-similarity after layer formation.

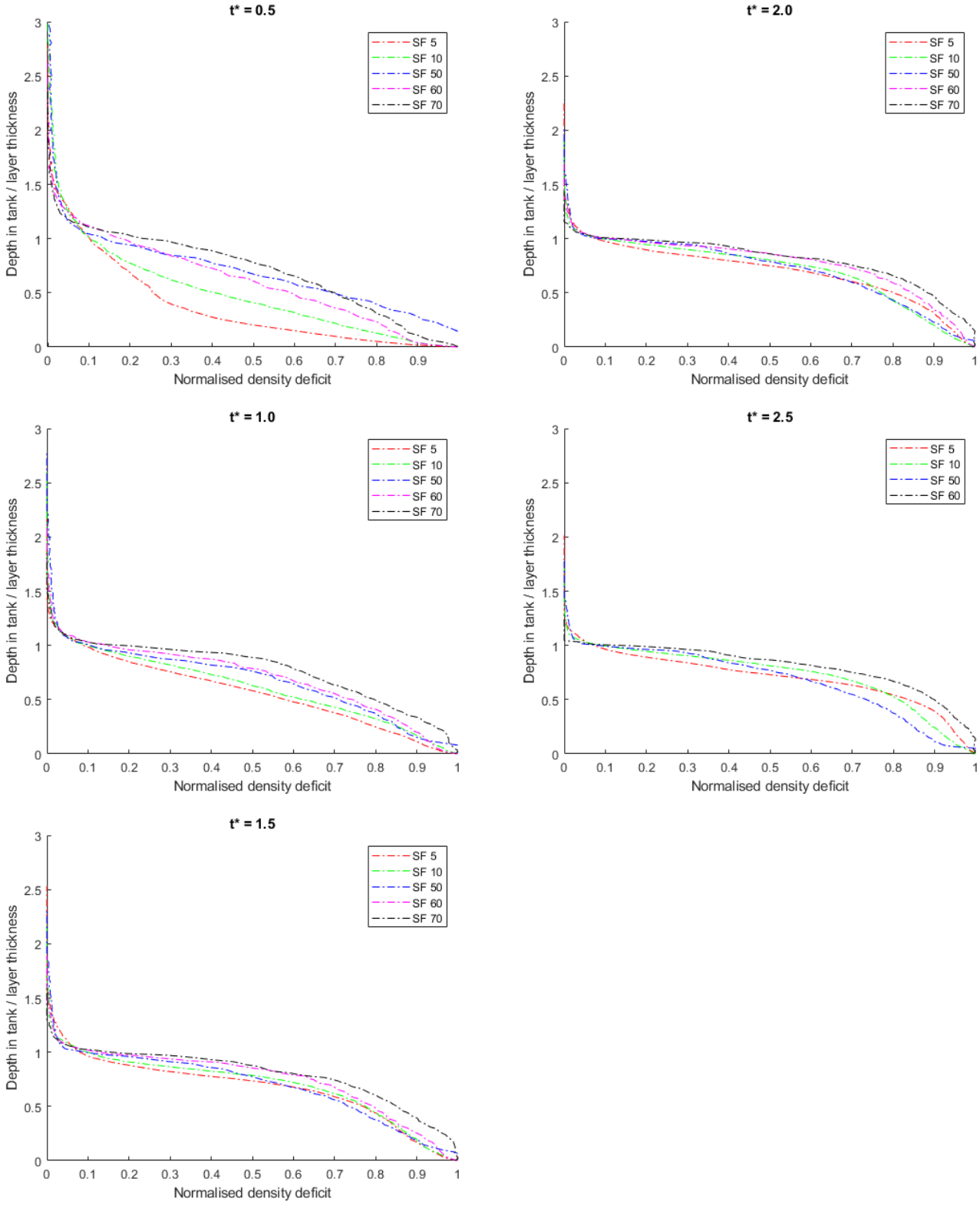

Figure 42. Development of self-similarity throughout all experiments at t = 0.5, 1.0, 1.5, 2.0, & 2.5 using N = 0.1 layer height method.*

7.2 N-percentage – 0.3

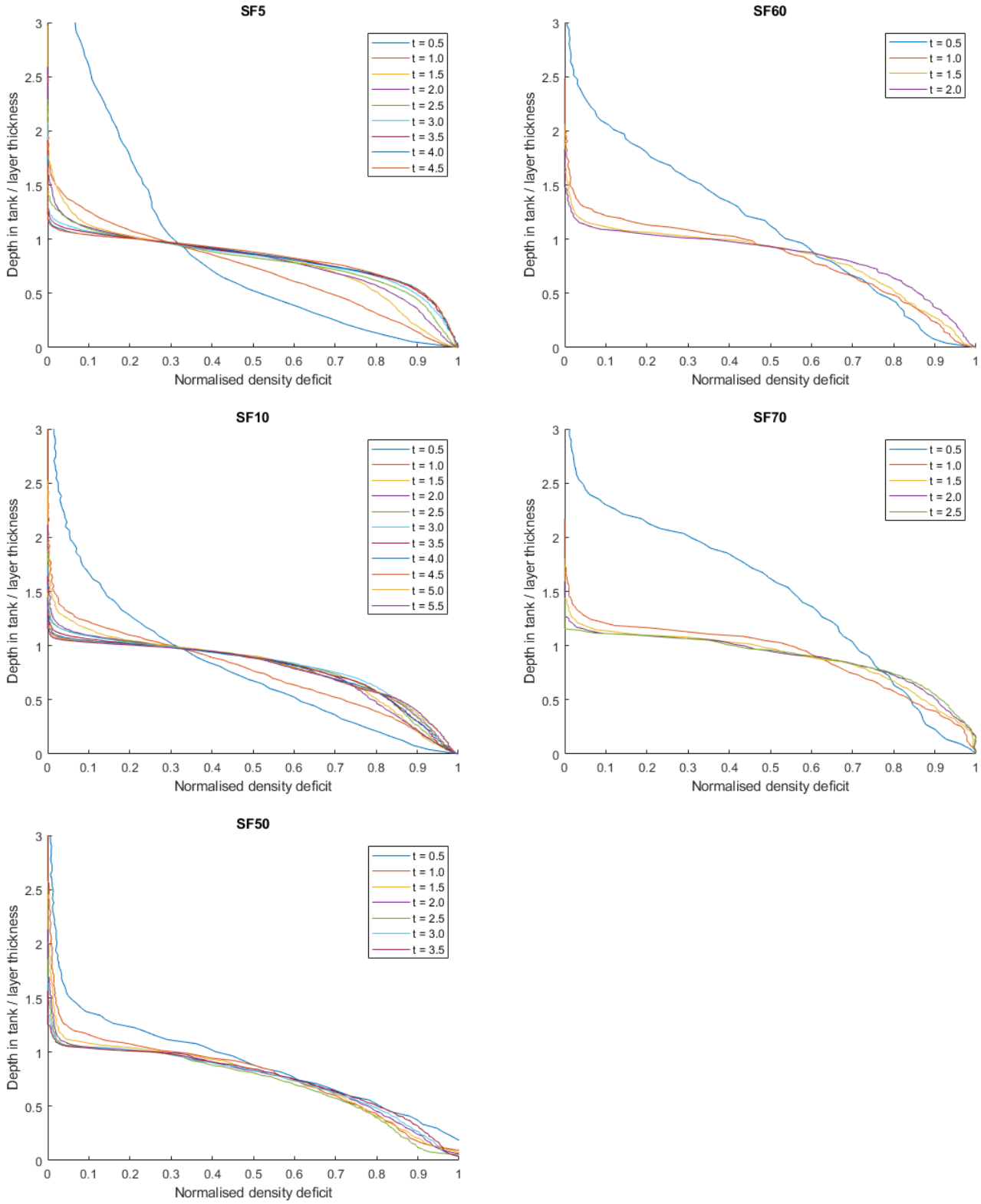

Figure 43. Normalised density deficit profiles using N = 0.3 layer height prediction throughout each experiment showing self-similarity after layer formation.

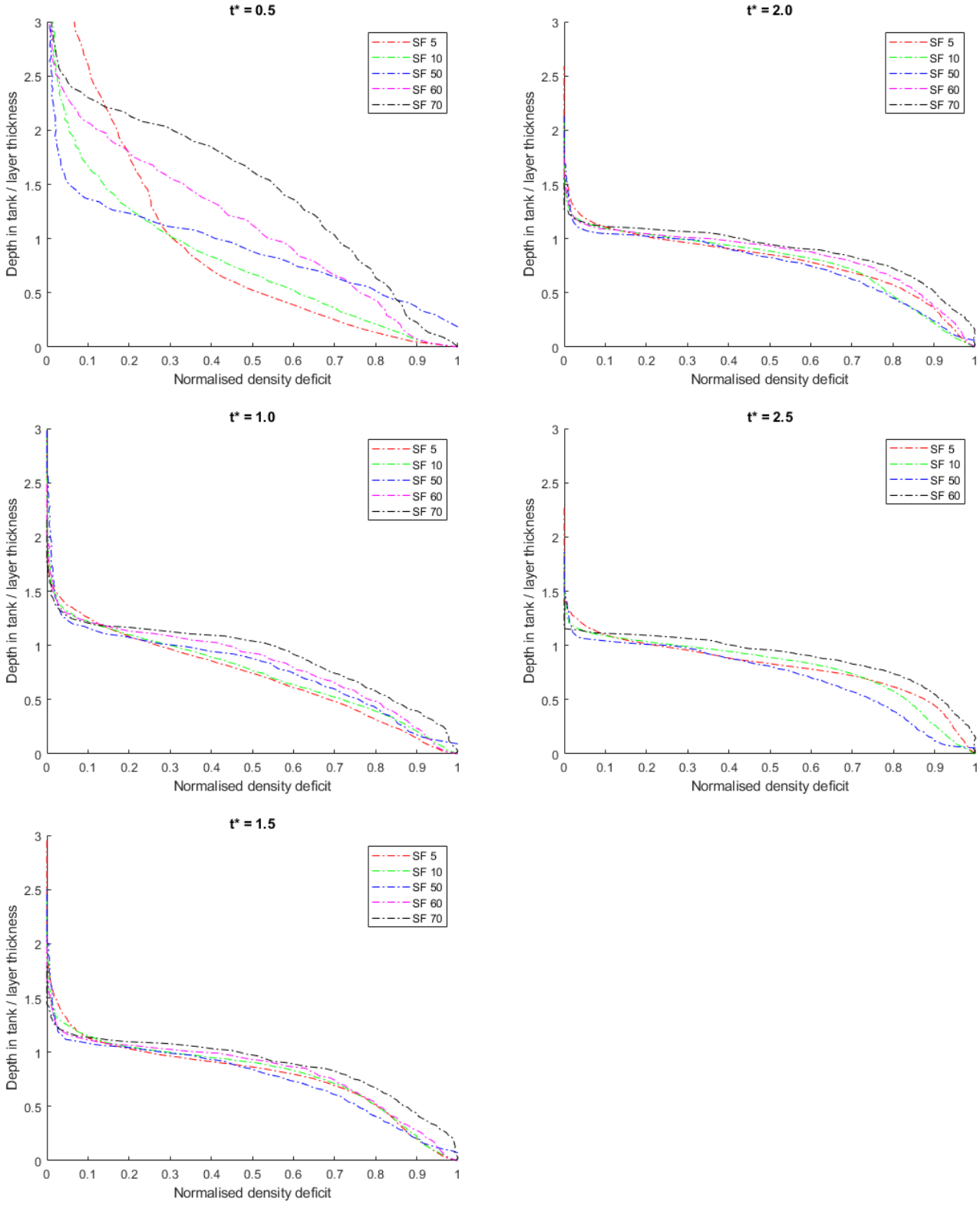

Figure 44. Development of self-similarity throughout all experiments at t = 0.5, 1.0, 1.5, 2.0, & 2.5 using N = 0.3 layer height method*

7.3 N-percentage – 0.4

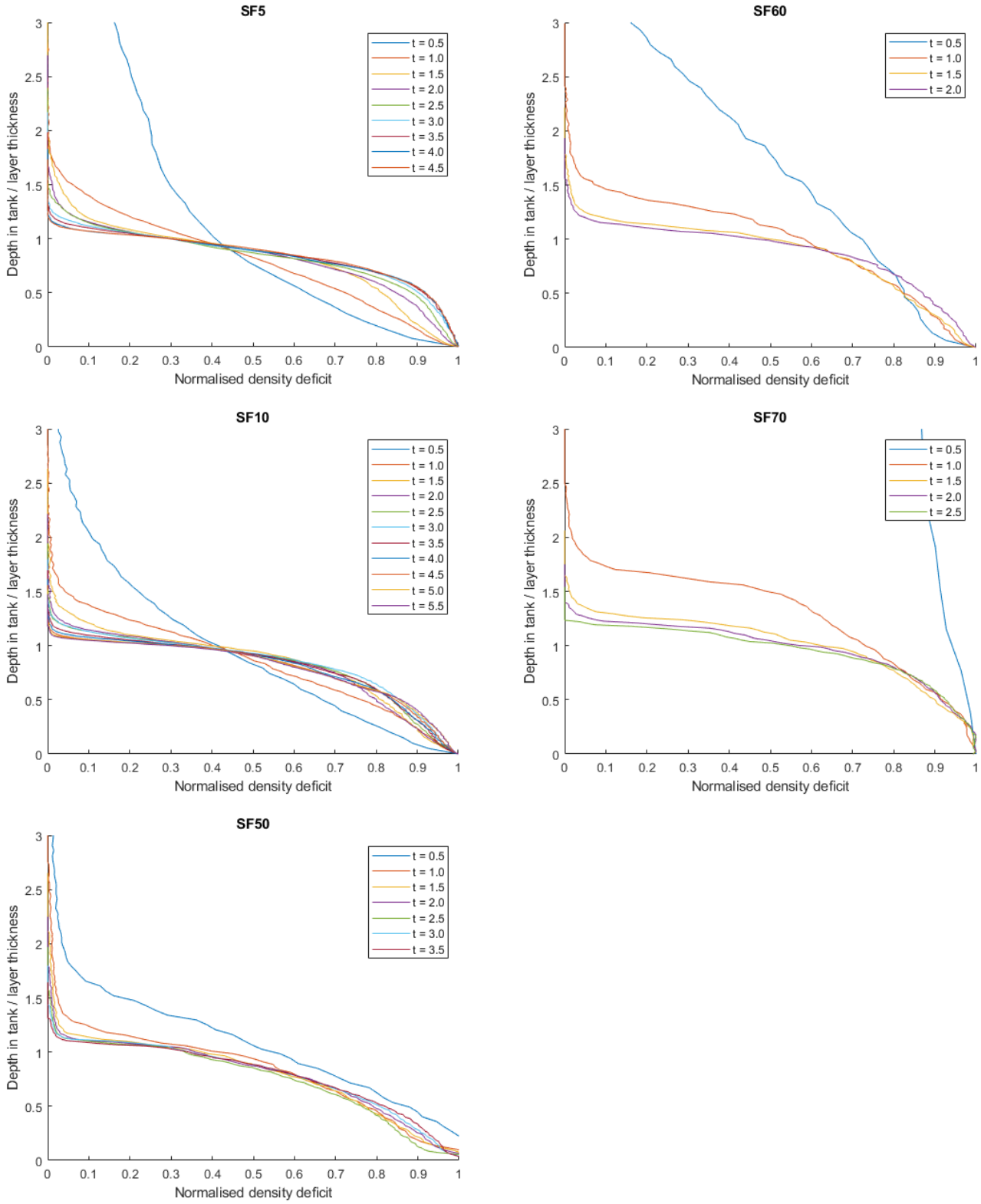

Figure 45. Normalised density deficit profiles using N = 0.4 layer height prediction throughout each experiment showing self-similarity after layer formation.

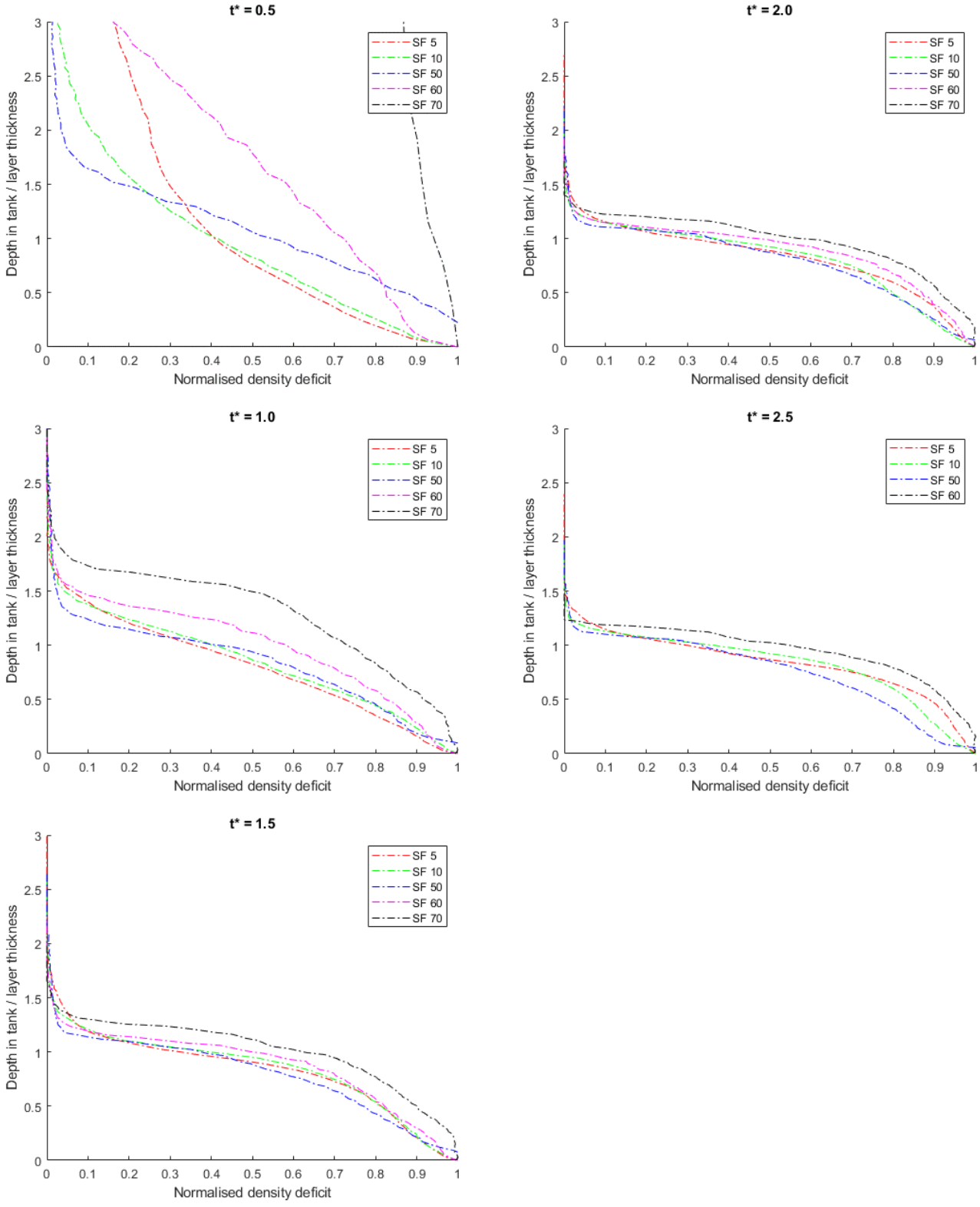

Figure 46. Development of self-similarity throughout all experiments at t = 0.5, 1.0, 1.5, 2.0, & 2.5 using N = 0.4 layer height method*

7.4 N-percentage – 0.5

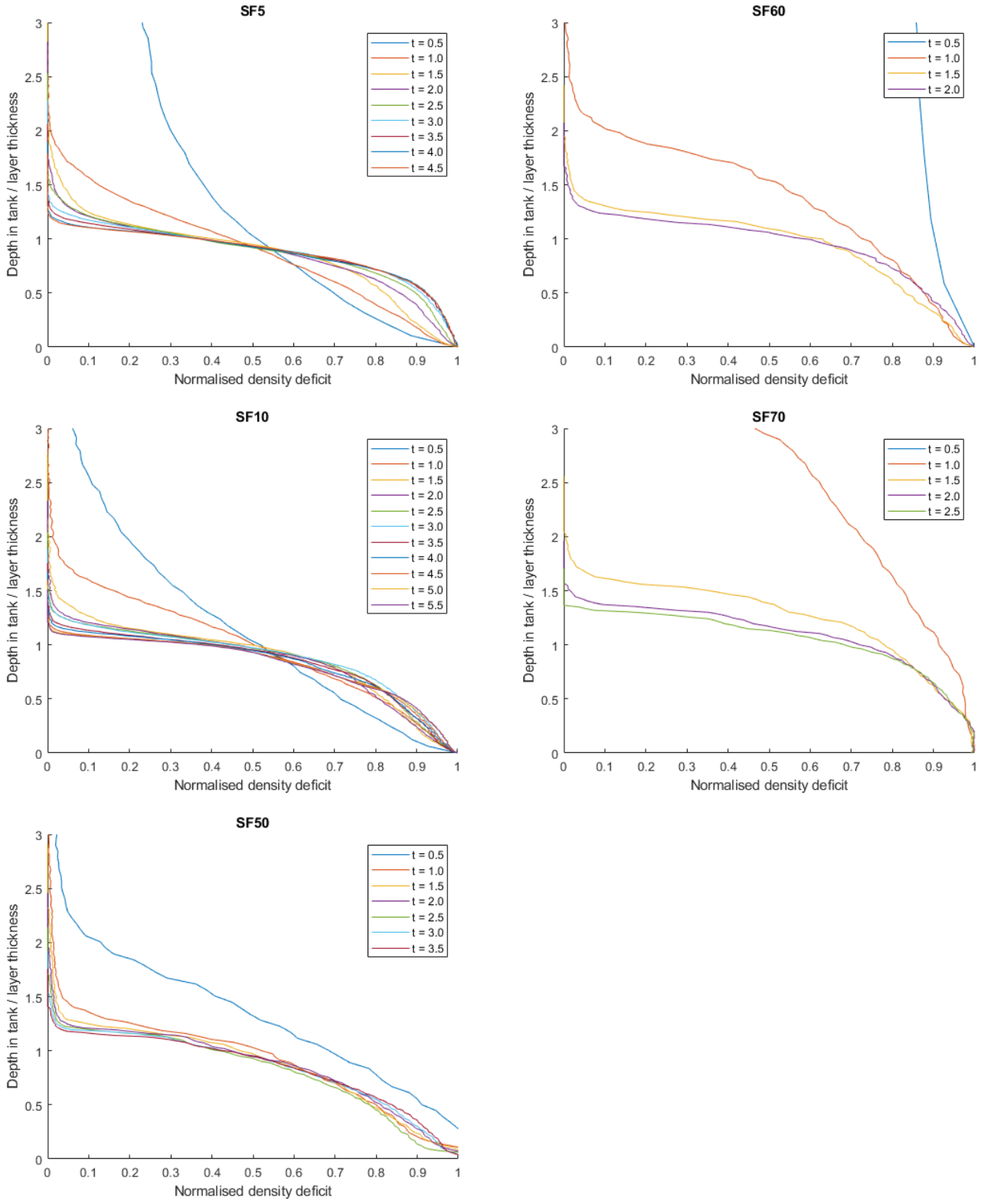

Figure 47. Normalised density deficit profiles using N = 0.5 layer height prediction throughout each experiment showing self-similarity after layer formation.

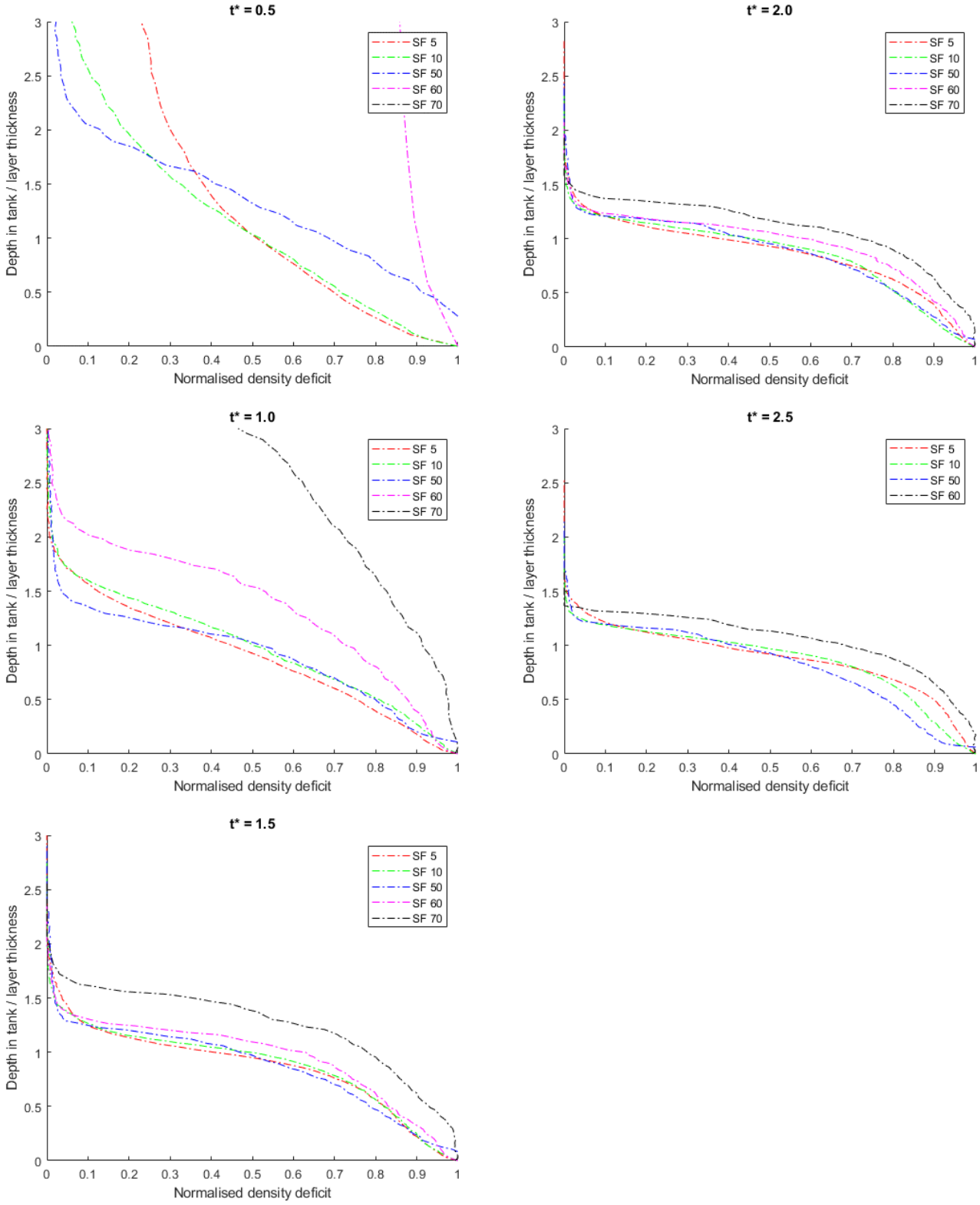

Figure 48. Development of self-similarity throughout all experiments at t = 0.5, 1.0, 1.5, 2.0, & 2.5 using N = 0.5 layer height method*

7.5 Least squares

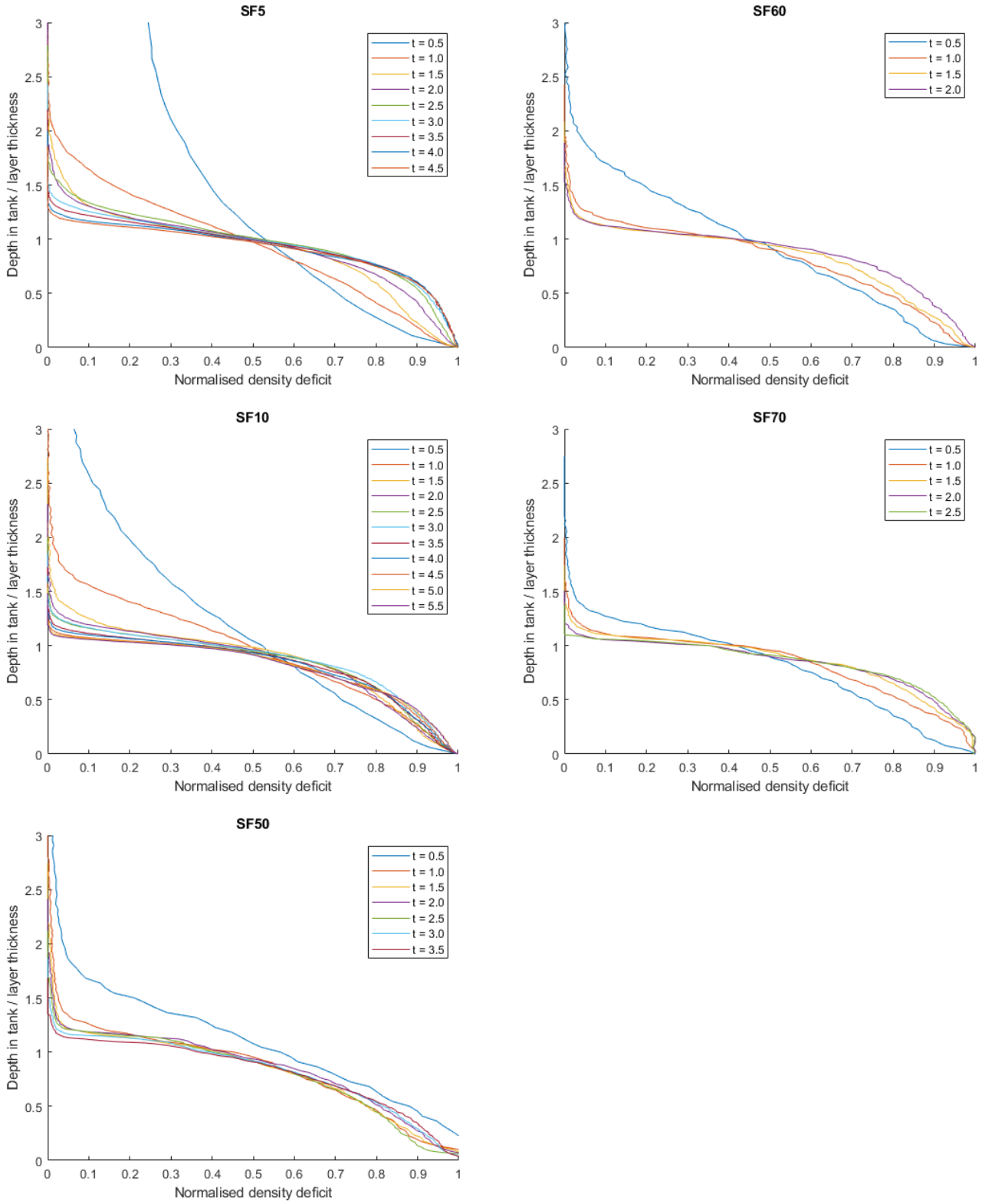

Figure 49. Normalised density deficit profiles using least squares layer height prediction throughout each experiment showing self-similarity after layer formation.

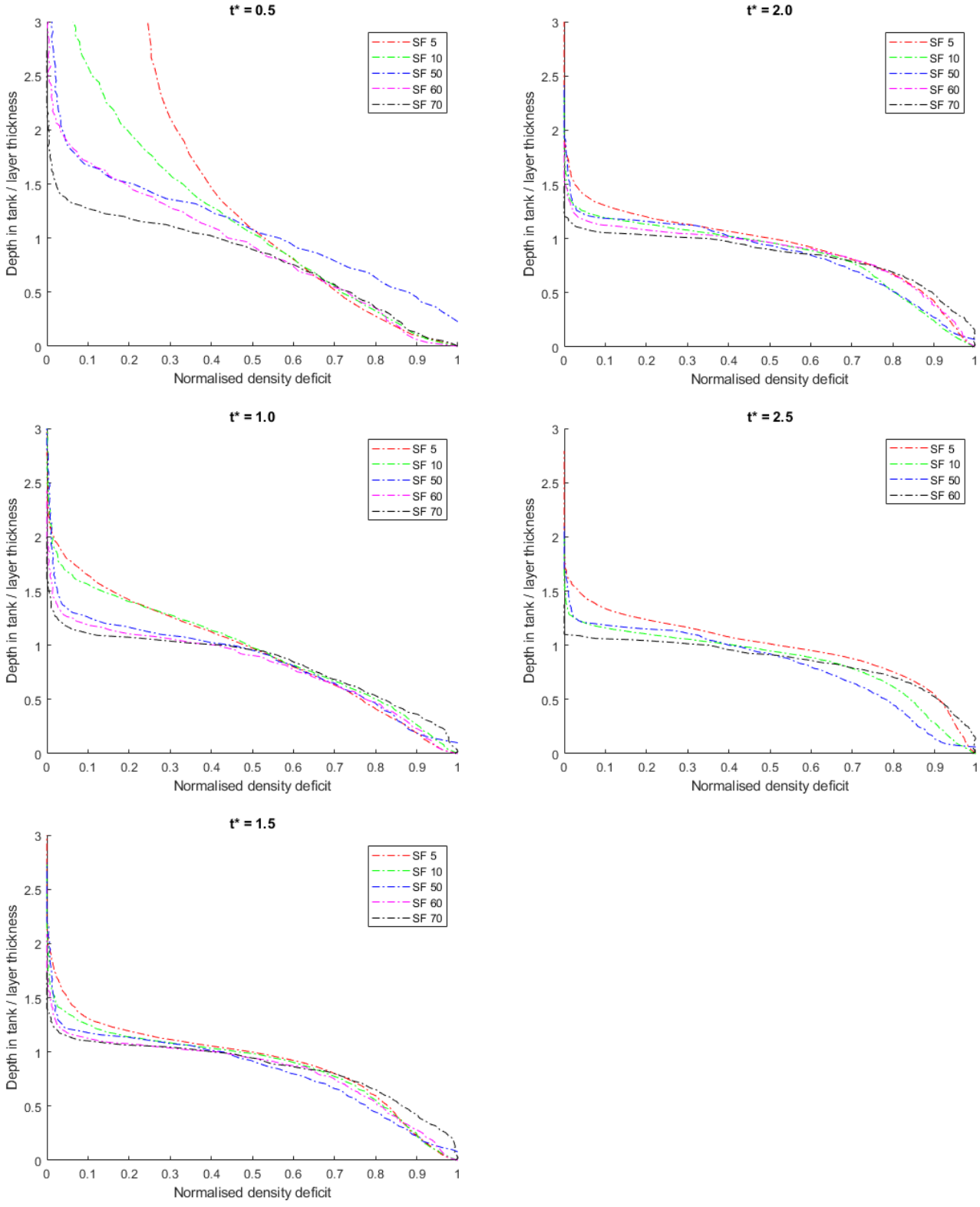

Figure 50. Development of self-similarity throughout all experiments at t = 0.5, 1.0, 1.5, 2.0, & 2.5 using the least squares layer height method*

7.6 Integral ratio

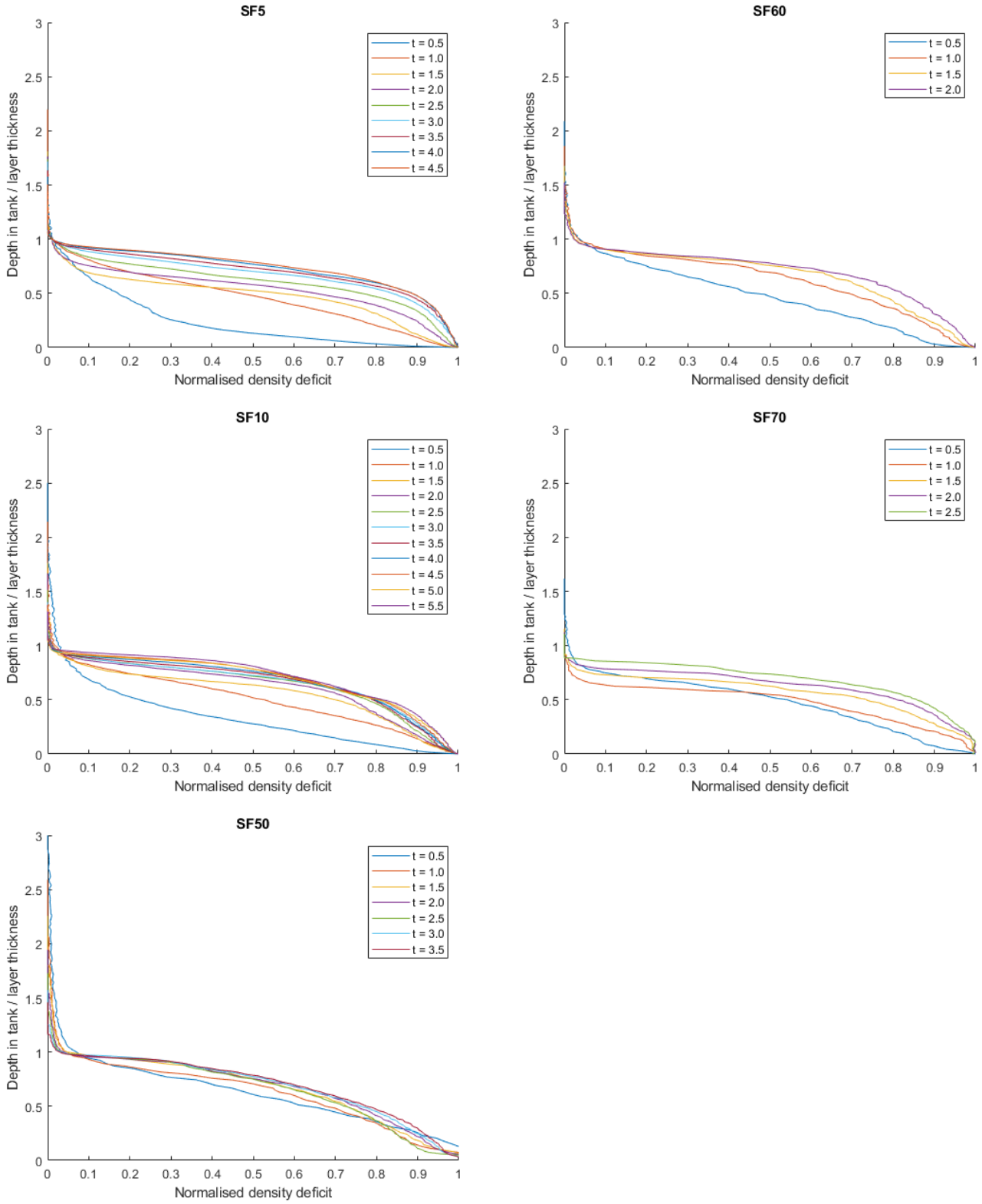

Figure 51. Normalised density deficit profiles using integral ratio layer height prediction throughout each experiment showing self-similarity after layer formation.

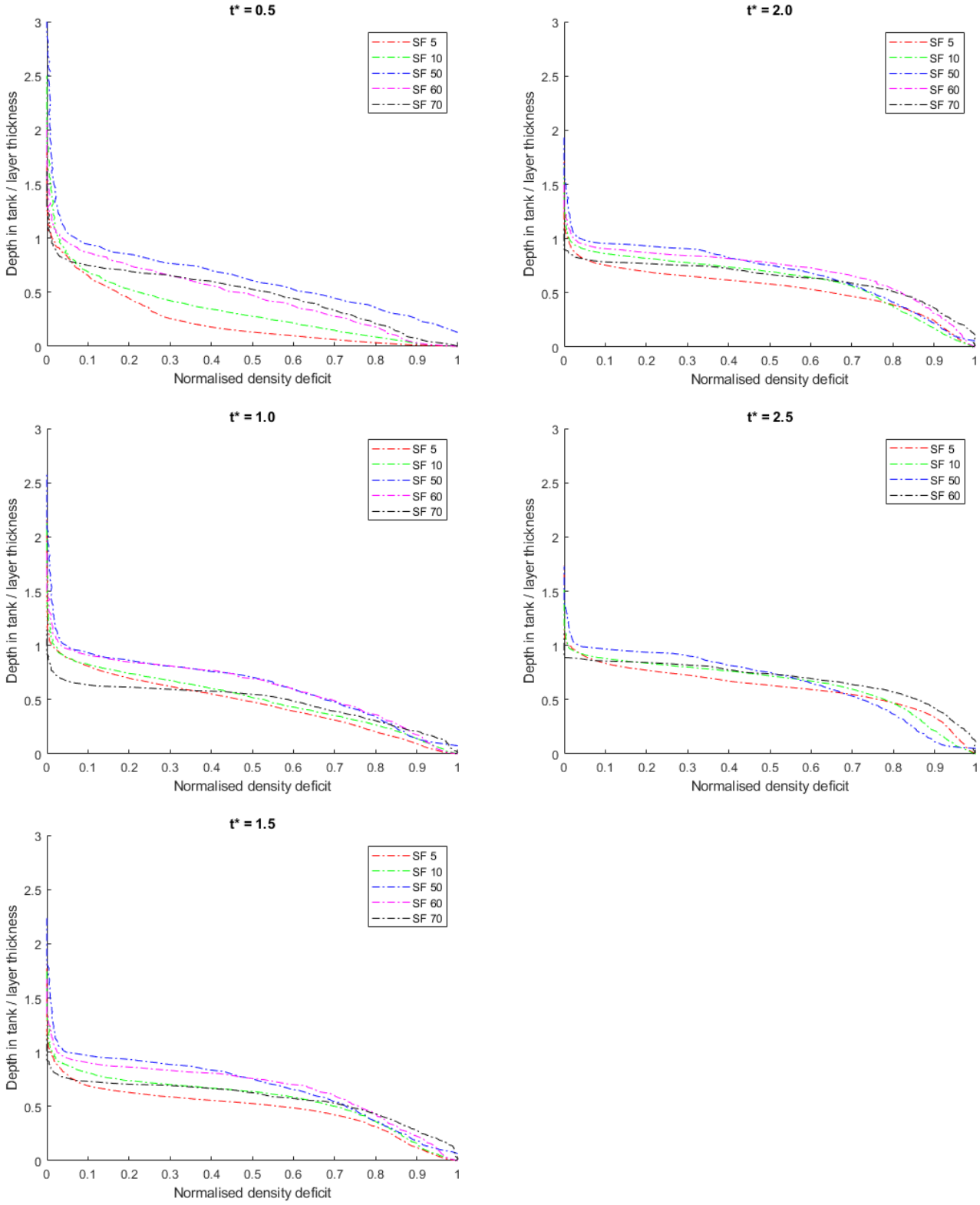

Figure 52. Development of self-similarity throughout all experiments at t = 0.5, 1.0, 1.5, 2.0, & 2.5 using the integral ratio layer height method*

8 Appendix B – Vertical depth integrated density deficit profiles

8.1 Shape Factor 10

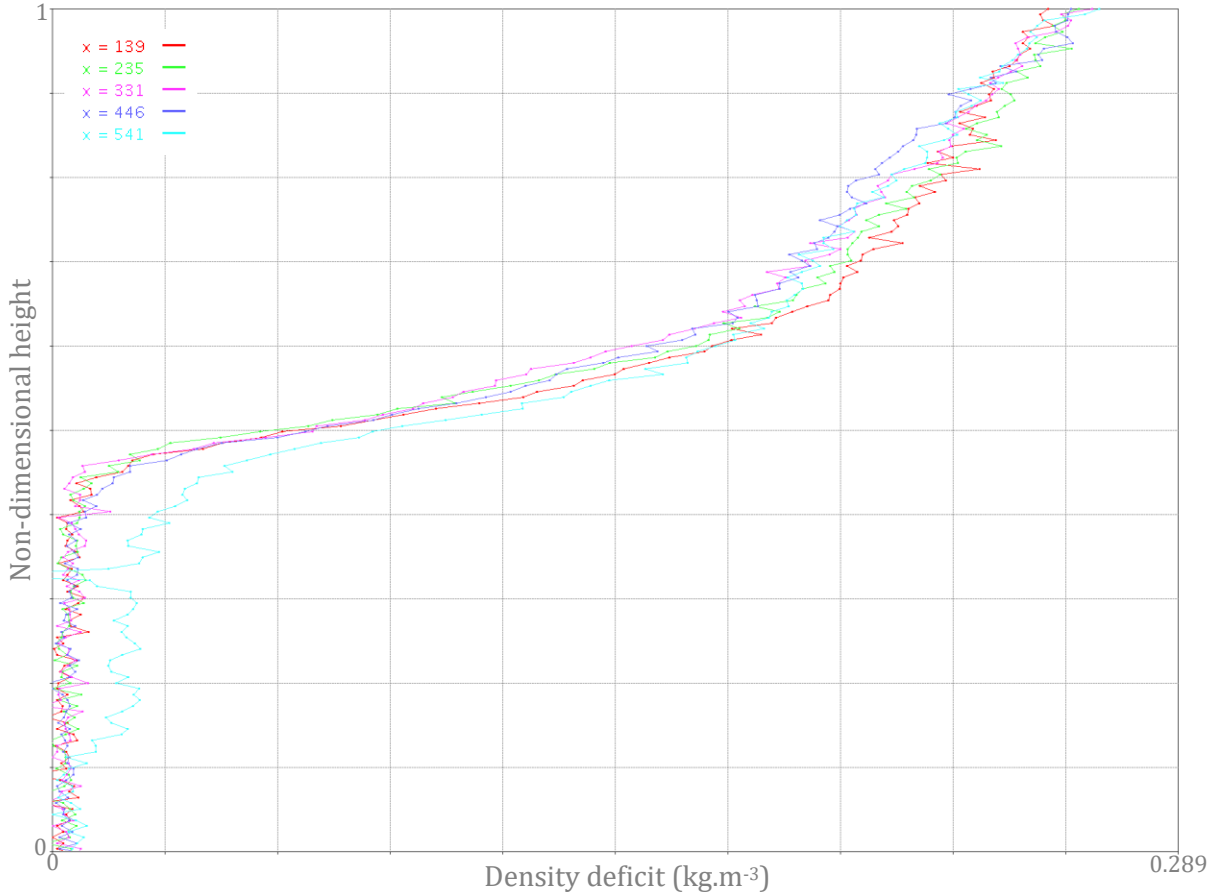

Figure 53. Full tank height vertical depth integrated density profiles for SF = 10 from horizontal location x = 541 at the centre of the tank and plume and out to x = 139, which was immediately adjacent to the tank side.

8.2 Shape Factor 50

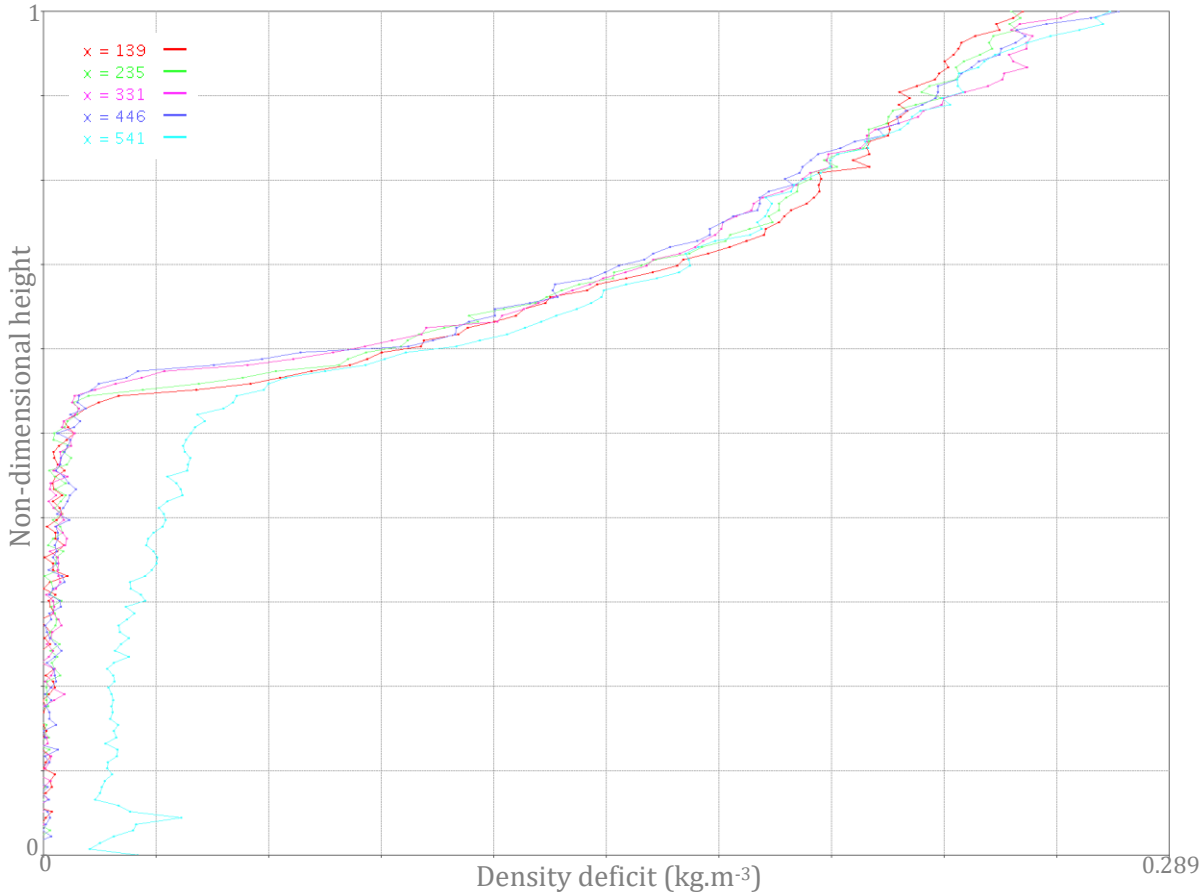

Figure 54. Full tank height vertical depth integrated density profiles for SF = 50 from horizontal location x = 541 at the centre of the tank and plume and out to x = 139, which was immediately adjacent to the tank side.

8.3 Shape Factor 60

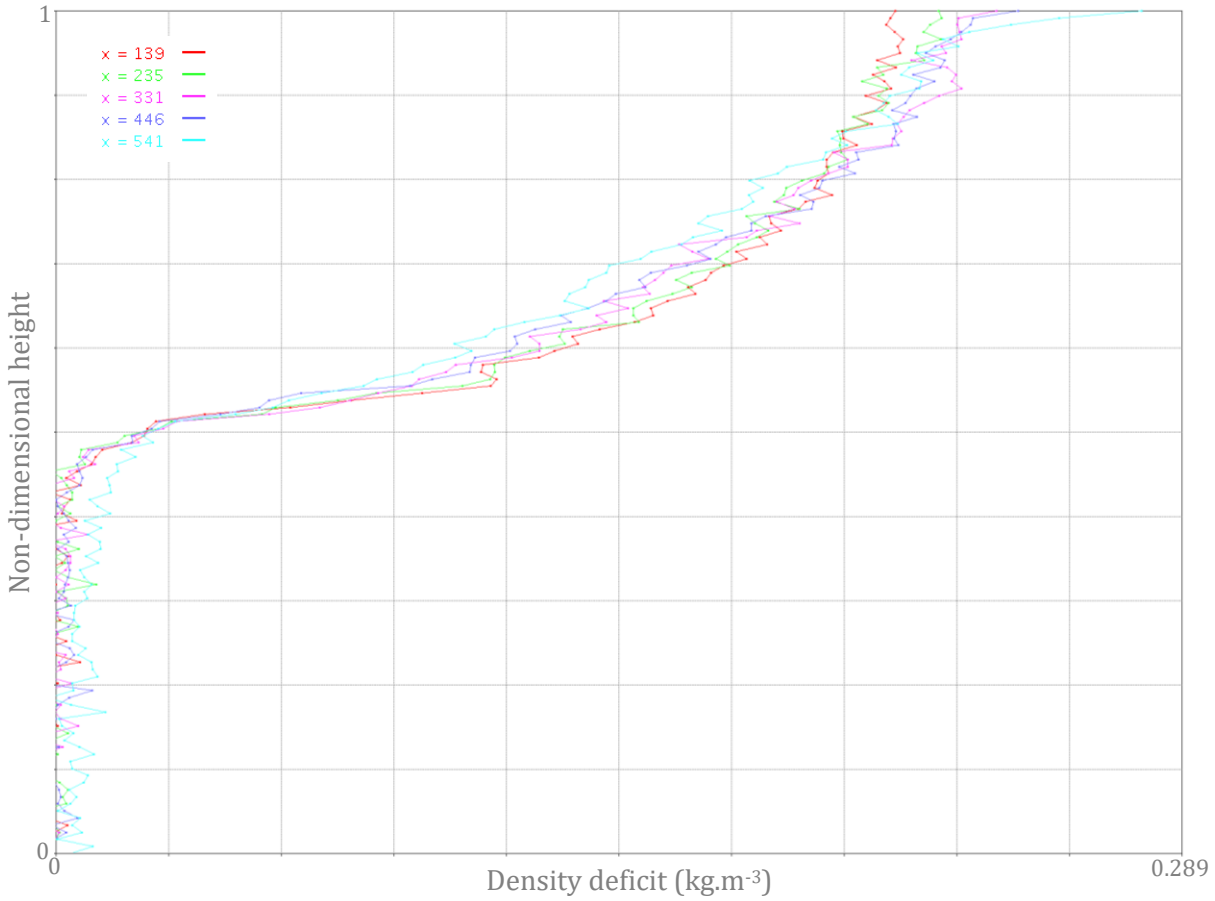

Figure 55. Full tank height vertical depth integrated density profiles for SF = 60 from horizontal location x = 541 at the centre of the tank and plume and out to x = 139, which was immediately adjacent to the tank side.

8.4 Shape Factor 70

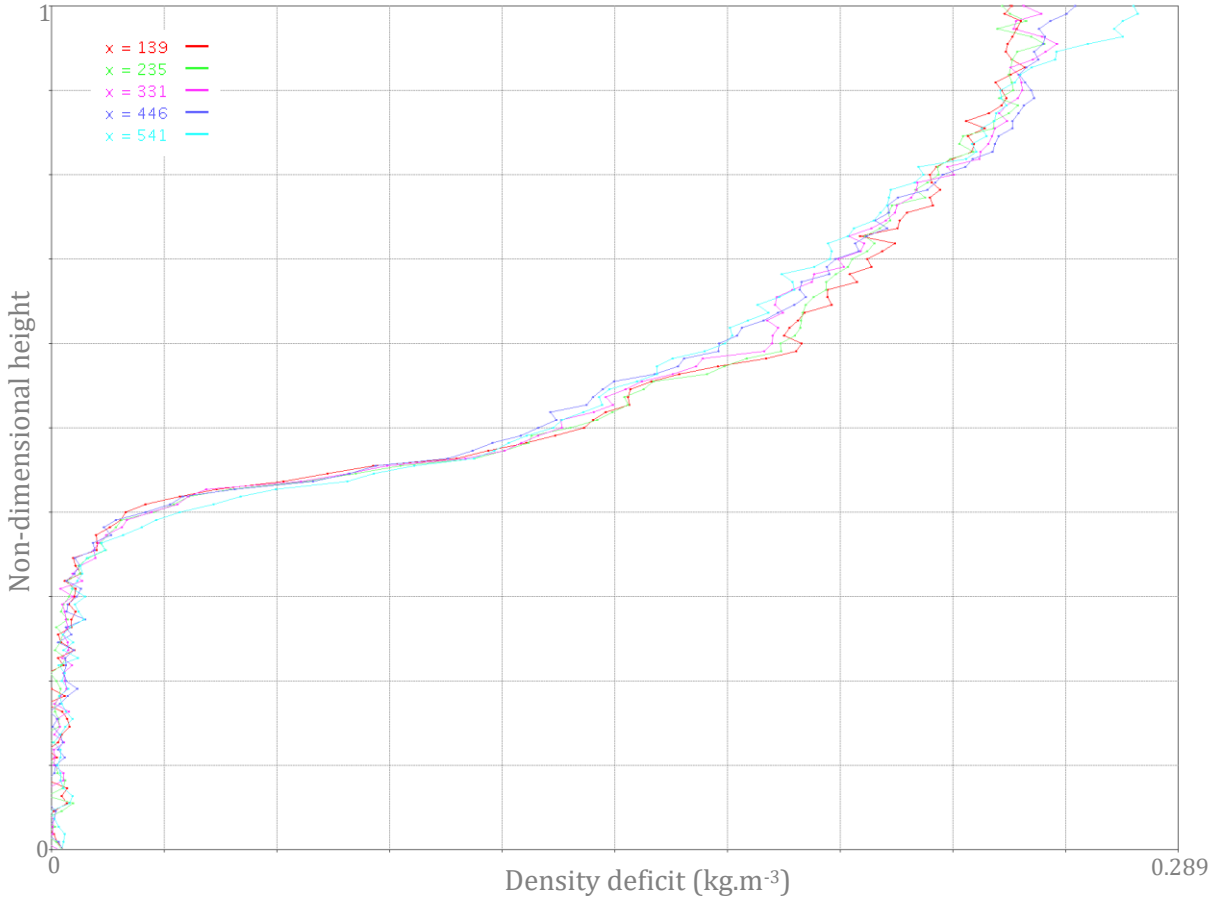

Figure 56. Full tank height vertical depth integrated density profiles for SF = 70 from horizontal location x = 541 at the centre of the tank and plume and out to x = 139, which was immediately adjacent to the tank side.

9 Appendix C – Two-zone model (B-RISK) example results log

VERIFIED PDF CREATED BY B-RISK : 8/13/2019 6:27:03 PM

August 13, 2019 18:27:03
B-RISK Fire Simulator and Design Fire Tool (Ver 2018.04)

Input Filename : input1.xml
Base File : C:\Users\Peter M\Documents\B-RISK\riskdata\basemodel_20190716_SF5_001\basemodel_20190716_SF5_001.xml

User Mode : Risk Simulator
Simulation Time = 180.00 seconds.
Initial Time-Step = 1.00 seconds.

```
======================================================================
Description of Rooms
======================================================================
Room 1 : room
         Room Length (m) =                              11.18
         Room Width (m) =                               11.18
         Maximum Room Height (m) =                      5.00
         Minimum Room Height (m) =                      5.00
         Floor Elevation (m) =                          0.000
         Absolute X Position (m) =                      0.000
         Absolute Y Position (m) =                      0.000
         Room 1 has a flat ceiling.
         Shape Factor (Af/H^2) =                        5.0

         Wall Surface is AThesisMaterial
         Wall Density (kg/m3) =                         10.0
         Wall Conductivity (W/m.K) =                    0.010
         Wall Specific Heat (J/kg.K) =                  2000
         Wall Emissivity =                              1.00
         Wall Thickness (mm) =                          100.0
         SQROOT Thermal Inertia (J.m-2.s-1/2.K-1) =     14

         Ceiling Surface is AThesisMaterial
         Ceiling Density (kg/m3) =                      10.0
         Ceiling Conductivity (W/m.K) =                 0.010
         Ceiling Specific Heat (J/kg.K) =               2000
         Ceiling Emissivity =                           1.00
         Ceiling Thickness (mm) =                       100.0
         SQROOT Thermal Inertia (J.m-2.s-1/2.K-1) =     14

         Floor Surface is AThesisMaterial
         Floor Density (kg/m3) =                        10.0
         Floor Conductivity (W/m.K) =                   0.010
         Floor Specific Heat (J/kg.K) =                 2000
         Floor Emissivity =                             1.00
         Floor Thickness = (mm)                         100.0
         SQROOT Thermal Inertia (J.m-2.s-1/2.K-1) =     14

======================================================================
Wall Vents
======================================================================
Vent  1 : vent label
                  From room 1 to 2
                  Left  face of room 1
                  Offset (m) =                          0.000
                  Vent Width (m) =                      11.180
                  Vent Height (m) =                     0.100
                  Vent Sill Height (m) =                0.000
                  Vent Soffit Height (m) =              0.100
                  Opening Time (sec) =                  0
                  Closing Time (sec) =                  0
                  Discharge Coefficient (-) =           1.000

======================================================================
Ceiling/Floor Vents
======================================================================
======================================================================
Ambient Conditions
======================================================================
```

```
Interior Temp (C) =                                     24.0
Exterior Temp (C) =                                     15.0
Relative Humidity (%) =                                 50

=====================================================================
Tenability Parameters
=====================================================================
Monitoring Height for Visibility and FED (m) =          2.00
Asphyxiant gas model =                                  FED(CO) C/VM2
Visibility calculations assume:                         reflective signs
Egress path segments for FED calculations
1. Start Time (sec)                                     0
1. End Time (sec)                                       600
1. Room                                                 1
2. Start Time (sec)                                     0
2. End Time (sec)                                       0
2. Room                                                 0
3. Start Time (sec)                                     0
3. End Time (sec)                                       0
3. Room                                                 0

=====================================================================
Sprinkler / Detector Parameters
=====================================================================
         Ceiling Jet model used is NIST JET.
         Sprinkler System Reliability                   1.000
         Sprinkler Probability of Suppression           0.000
         Sprinkler Cooling Coefficient                  1.000

=====================================================================
Smoke Detector Parameters
=====================================================================
         Smoke Detection System Reliability             1.000


=====================================================================
Mechanical Ventilation (to/from outside)
=====================================================================
Mechanical Ventilation not installed.
         Mech ventilation system reliability            1.000


=====================================================================
Description of the Fire
=====================================================================
CO Yield pre-flashover(g/g) =                           0.040
Soot Alpha Coefficient =                                2.50
Smoke Epsilon Coefficient =                             1.20
Flame Emission Coefficient (1/m) =                      0.80
Fuel - Carbon Moles                                     1.00
Fuel - Hydrogen Moles                                   2.00
Fuel - Oxygen Moles                                     0.50
Fuel - Nitrogen Moles                                   0.00
Stoichiometric air/fuel ratio                           6.1

Burning objects are manually positioned in room.
Enhanced burning submodel is                            OFF

Burning Object No 1
description
              Located in Room                           1
              Energy Yield (kJ/g) =                     20.0
              CO2 Yield (kg/kg fuel) =                  0.000
              HCN Yield (kg/kg fuel) =                  0.000
              H2O Yield (kg/kg fuel) =                  0.818
              Soot Yield (kg/kg fuel) =                 0.000
              Heat Release Rate Per Unit Area (kW/m2) =  250.0
              Radiant Loss Fraction =                   0.01
              Fire Elevation (m) =                      0.022
              Fire Object Length (m) =                  0.196
              Fire Object Width (m) =                   0.196
              Fire Object Height (m) =                  0.000
              Location, X-coordinate (m) =              3.000
```

```
              Location, Y-coordinate (m) =                2.000
              Fire Location (for entrainment) =           CENTRE
              Plume behaviour is                          UNDISTURBED

              Time (sec)              Heat Release (kW)
               0                      0
               1                      124
               1800                   124

=====================================================================
Postflashover Inputs
=====================================================================
Postflashover model is OFF.


=====================================================================
Results from Fire Simulation
=====================================================================

0 min    00 sec
         (0 sec)                     Room 1    Outside

         Layer (m)                   5.000
         Upper Temp (C)              24.0
         Lower Temp (C)              24.0
         HRR (kW)                    0.0
         Visibility (m) at 2m        20+
         FED gases on egress path = 0.000
         FED thermal on egress path = 0.000

0 min    01 sec
         (1 sec)                     Room 1    Outside

         Layer (m)                   4.970
         Upper Temp (C)              35.9
         Lower Temp (C)              24.0
         HRR (kW)                    124.1
         Visibility (m) at 2m        20+
         FED gases on egress path = 0.000
         FED thermal on egress path = 0.000

0 min    02 sec
         (2 sec)                     Room 1    Outside

         Layer (m)                   4.928
         Upper Temp (C)              40.9
         Lower Temp (C)              24.0
         HRR (kW)                    124.1
         Visibility (m) at 2m        20+
         FED gases on egress path = 0.000
         FED thermal on egress path = 0.000

0 min    03 sec
         (3 sec)                     Room 1    Outside

         Layer (m)                   4.887
         Upper Temp (C)              42.3
         Lower Temp (C)              24.0
         HRR (kW)                    124.1
         Visibility (m) at 2m        20+
         FED gases on egress path = 0.000
         FED thermal on egress path = 0.000

0 min    04 sec
         (4 sec)                     Room 1    Outside

         Layer (m)                   4.847
         Upper Temp (C)              43.0
         Lower Temp (C)              24.0
         HRR (kW)                    124.1
         Visibility (m) at 2m        20+
         FED gases on egress path = 0.000
         FED thermal on egress path = 0.000
```

```
0 min    05 sec
         (5 sec)                      Room 1    Outside

         Layer (m)                    4.807
         Upper Temp (C)               43.5
         Lower Temp (C)               24.0
         HRR (kW)                     124.1
         Visibility (m) at 2m         20+
         FED gases on egress path = 0.000
         FED thermal on egress path = 0.000

0 min    06 sec
         (6 sec)                      Room 1    Outside

         Layer (m)                    4.767
         Upper Temp (C)               43.9
         Lower Temp (C)               24.0
         HRR (kW)                     124.1
         Visibility (m) at 2m         20+
         FED gases on egress path = 0.000
         FED thermal on egress path = 0.000

0 min    07 sec
         (7 sec)                      Room 1    Outside

         Layer (m)                    4.728
         Upper Temp (C)               44.2
         Lower Temp (C)               24.0
         HRR (kW)                     124.1
         Visibility (m) at 2m         20+
         FED gases on egress path = 0.000
         FED thermal on egress path = 0.000

0 min    08 sec
         (8 sec)                      Room 1    Outside

         Layer (m)                    4.689
         Upper Temp (C)               44.4
         Lower Temp (C)               24.0
         HRR (kW)                     124.1
         Visibility (m) at 2m         20+
         FED gases on egress path = 0.000
         FED thermal on egress path = 0.000

0 min    09 sec
         (9 sec)                      Room 1    Outside

         Layer (m)                    4.651
         Upper Temp (C)               44.7
         Lower Temp (C)               24.0
         HRR (kW)                     124.1
         Visibility (m) at 2m         20+
         FED gases on egress path = 0.000
         FED thermal on egress path = 0.000

0 min    10 sec
         (10 sec)                     Room 1    Outside

         Layer (m)                    4.613
         Upper Temp (C)               44.9
         Lower Temp (C)               24.0
         HRR (kW)                     124.1
         Visibility (m) at 2m         20+
         FED gases on egress path = 0.000
         FED thermal on egress path = 0.000

0 min    11 sec
         (11 sec)                     Room 1    Outside

         Layer (m)                    4.575
         Upper Temp (C)               45.1
         Lower Temp (C)               24.0
```

```
        HRR (kW)                    124.1
        Visibility (m) at 2m        20+
        FED gases on egress path = 0.000
        FED thermal on egress path = 0.000

0 min   12 sec
        (12 sec)                    Room 1    Outside

        Layer (m)                   4.538
        Upper Temp (C)              45.3
        Lower Temp (C)              24.0
        HRR (kW)                    124.1
        Visibility (m) at 2m        20+
        FED gases on egress path = 0.000
        FED thermal on egress path = 0.000

0 min   13 sec
        (13 sec)                    Room 1    Outside

        Layer (m)                   4.501
        Upper Temp (C)              45.5
        Lower Temp (C)              24.0
        HRR (kW)                    124.1
        Visibility (m) at 2m        20+
        FED gases on egress path = 0.000
        FED thermal on egress path = 0.000

0 min   14 sec
        (14 sec)                    Room 1    Outside

        Layer (m)                   4.465
        Upper Temp (C)              45.7
        Lower Temp (C)              24.0
        HRR (kW)                    124.1
        Visibility (m) at 2m        20+
        FED gases on egress path = 0.000
        FED thermal on egress path = 0.000

0 min   15 sec
        (15 sec)                    Room 1    Outside

        Layer (m)                   4.429
        Upper Temp (C)              45.9
        Lower Temp (C)              24.0
        HRR (kW)                    124.1
        Visibility (m) at 2m        20+
        FED gases on egress path = 0.000
        FED thermal on egress path = 0.000

0 min   16 sec
        (16 sec)                    Room 1    Outside

        Layer (m)                   4.394
        Upper Temp (C)              46.0
        Lower Temp (C)              24.1
        HRR (kW)                    124.1
        Visibility (m) at 2m        20+
        FED gases on egress path = 0.000
        FED thermal on egress path = 0.000

0 min   17 sec
        (17 sec)                    Room 1    Outside

        Layer (m)                   4.359
        Upper Temp (C)              46.2
        Lower Temp (C)              24.1
        HRR (kW)                    124.1
        Visibility (m) at 2m        20+
        FED gases on egress path = 0.000
        FED thermal on egress path = 0.000

0 min   18 sec
        (18 sec)                    Room 1    Outside
```

```
        Layer (m)                   4.324
        Upper Temp (C)              46.4
        Lower Temp (C)              24.1
        HRR (kW)                    124.1
        Visibility (m) at 2m        20+
        FED gases on egress path = 0.000
        FED thermal on egress path = 0.000

0 min   19 sec
        (19 sec)                    Room 1    Outside

        Layer (m)                   4.290
        Upper Temp (C)              46.5
        Lower Temp (C)              24.1
        HRR (kW)                    124.1
        Visibility (m) at 2m        20+
        FED gases on egress path = 0.000
        FED thermal on egress path = 0.000

0 min   20 sec
        (20 sec)                    Room 1    Outside

        Layer (m)                   4.256
        Upper Temp (C)              46.7
        Lower Temp (C)              24.1
        HRR (kW)                    124.1
        Visibility (m) at 2m        20+
        FED gases on egress path = 0.000
        FED thermal on egress path = 0.000

0 min   21 sec
        (21 sec)                    Room 1    Outside

        Layer (m)                   4.223
        Upper Temp (C)              46.8
        Lower Temp (C)              24.1
        HRR (kW)                    124.1
        Visibility (m) at 2m        20+
        FED gases on egress path = 0.000
        FED thermal on egress path = 0.000

0 min   22 sec
        (22 sec)                    Room 1    Outside

        Layer (m)                   4.190
        Upper Temp (C)              47.0
        Lower Temp (C)              24.1
        HRR (kW)                    124.1
        Visibility (m) at 2m        20+
        FED gases on egress path = 0.000
        FED thermal on egress path = 0.000

0 min   23 sec
        (23 sec)                    Room 1    Outside

        Layer (m)                   4.157
        Upper Temp (C)              47.1
        Lower Temp (C)              24.1
        HRR (kW)                    124.1
        Visibility (m) at 2m        20+
        FED gases on egress path = 0.000
        FED thermal on egress path = 0.000

0 min   24 sec
        (24 sec)                    Room 1    Outside

        Layer (m)                   4.124
        Upper Temp (C)              47.3
        Lower Temp (C)              24.1
        HRR (kW)                    124.1
        Visibility (m) at 2m        20+
        FED gases on egress path = 0.000
```

```
        FED thermal on egress path = 0.000

0 min   25 sec
        (25 sec)                    Room 1    Outside

        Layer (m)                   4.092
        Upper Temp (C)              47.4
        Lower Temp (C)              24.1
        HRR (kW)                    124.1
        Visibility (m) at 2m        20+
        FED gases on egress path = 0.000
        FED thermal on egress path = 0.000

0 min   26 sec
        (26 sec)                    Room 1    Outside

        Layer (m)                   4.061
        Upper Temp (C)              47.5
        Lower Temp (C)              24.1
        HRR (kW)                    124.1
        Visibility (m) at 2m        20+
        FED gases on egress path = 0.000
        FED thermal on egress path = 0.000

0 min   27 sec
        (27 sec)                    Room 1    Outside

        Layer (m)                   4.029
        Upper Temp (C)              47.7
        Lower Temp (C)              24.1
        HRR (kW)                    124.1
        Visibility (m) at 2m        20+
        FED gases on egress path = 0.000
        FED thermal on egress path = 0.000

0 min   28 sec
        (28 sec)                    Room 1    Outside

        Layer (m)                   3.998
        Upper Temp (C)              47.8
        Lower Temp (C)              24.1
        HRR (kW)                    124.1
        Visibility (m) at 2m        20+
        FED gases on egress path = 0.000
        FED thermal on egress path = 0.000

0 min   29 sec
        (29 sec)                    Room 1    Outside

        Layer (m)                   3.967
        Upper Temp (C)              48.0
        Lower Temp (C)              24.1
        HRR (kW)                    124.1
        Visibility (m) at 2m        20+
        FED gases on egress path = 0.000
        FED thermal on egress path = 0.000

0 min   30 sec
        (30 sec)                    Room 1    Outside

        Layer (m)                   3.937
        Upper Temp (C)              48.1
        Lower Temp (C)              24.2
        HRR (kW)                    124.1
        Visibility (m) at 2m        20+
        FED gases on egress path = 0.000
        FED thermal on egress path = 0.000

0 min   31 sec
        (31 sec)                    Room 1    Outside

        Layer (m)                   3.907
        Upper Temp (C)              48.3
```

```
         Lower Temp (C)               24.2
         HRR (kW)                     124.1
         Visibility (m) at 2m         20+
         FED gases on egress path = 0.000
         FED thermal on egress path = 0.000

0 min    32 sec
         (32 sec)                     Room 1    Outside

         Layer (m)                    3.877
         Upper Temp (C)               48.4
         Lower Temp (C)               24.2
         HRR (kW)                     124.1
         Visibility (m) at 2m         20+
         FED gases on egress path = 0.000
         FED thermal on egress path = 0.000

0 min    33 sec
         (33 sec)                     Room 1    Outside

         Layer (m)                    3.848
         Upper Temp (C)               48.5
         Lower Temp (C)               24.2
         HRR (kW)                     124.1
         Visibility (m) at 2m         20+
         FED gases on egress path = 0.000
         FED thermal on egress path = 0.000

0 min    34 sec
         (34 sec)                     Room 1    Outside

         Layer (m)                    3.818
         Upper Temp (C)               48.7
         Lower Temp (C)               24.2
         HRR (kW)                     124.1
         Visibility (m) at 2m         20+
         FED gases on egress path = 0.000
         FED thermal on egress path = 0.000

0 min    35 sec
         (35 sec)                     Room 1    Outside

         Layer (m)                    3.790
         Upper Temp (C)               48.8
         Lower Temp (C)               24.2
         HRR (kW)                     124.1
         Visibility (m) at 2m         20+
         FED gases on egress path = 0.000
         FED thermal on egress path = 0.000

0 min    36 sec
         (36 sec)                     Room 1    Outside

         Layer (m)                    3.761
         Upper Temp (C)               49.0
         Lower Temp (C)               24.2
         HRR (kW)                     124.1
         Visibility (m) at 2m         20+
         FED gases on egress path = 0.000
         FED thermal on egress path = 0.000

0 min    37 sec
         (37 sec)                     Room 1    Outside

         Layer (m)                    3.733
         Upper Temp (C)               49.1
         Lower Temp (C)               24.2
         HRR (kW)                     124.1
         Visibility (m) at 2m         20+
         FED gases on egress path = 0.000
         FED thermal on egress path = 0.000

0 min    38 sec
```

```
        (38 sec)                    Room 1    Outside

        Layer (m)                   3.705
        Upper Temp (C)              49.2
        Lower Temp (C)              24.2
        HRR (kW)                    124.1
        Visibility (m) at 2m        20+
        FED gases on egress path = 0.000
        FED thermal on egress path = 0.000

0 min   39 sec
        (39 sec)                    Room 1    Outside

        Layer (m)                   3.677
        Upper Temp (C)              49.4
        Lower Temp (C)              24.2
        HRR (kW)                    124.1
        Visibility (m) at 2m        20+
        FED gases on egress path = 0.000
        FED thermal on egress path = 0.000

0 min   40 sec
        (40 sec)                    Room 1    Outside

        Layer (m)                   3.649
        Upper Temp (C)              49.5
        Lower Temp (C)              24.2
        HRR (kW)                    124.1
        Visibility (m) at 2m        20+
        FED gases on egress path = 0.000
        FED thermal on egress path = 0.000

0 min   41 sec
        (41 sec)                    Room 1    Outside

        Layer (m)                   3.622
        Upper Temp (C)              49.6
        Lower Temp (C)              24.2
        HRR (kW)                    124.1
        Visibility (m) at 2m        20+
        FED gases on egress path = 0.000
        FED thermal on egress path = 0.000

0 min   42 sec
        (42 sec)                    Room 1    Outside

        Layer (m)                   3.595
        Upper Temp (C)              49.8
        Lower Temp (C)              24.3
        HRR (kW)                    124.1
        Visibility (m) at 2m        20+
        FED gases on egress path = 0.000
        FED thermal on egress path = 0.000

0 min   43 sec
        (43 sec)                    Room 1    Outside

        Layer (m)                   3.569
        Upper Temp (C)              49.9
        Lower Temp (C)              24.3
        HRR (kW)                    124.1
        Visibility (m) at 2m        20+
        FED gases on egress path = 0.000
        FED thermal on egress path = 0.000

0 min   44 sec
        (44 sec)                    Room 1    Outside

        Layer (m)                   3.542
        Upper Temp (C)              50.0
        Lower Temp (C)              24.3
        HRR (kW)                    124.1
        Visibility (m) at 2m        20+
```

```
        FED gases on egress path = 0.000
        FED thermal on egress path = 0.000

0 min   45 sec
        (45 sec)                    Room 1    Outside

        Layer (m)                   3.516
        Upper Temp (C)              50.2
        Lower Temp (C)              24.3
        HRR (kW)                    124.1
        Visibility (m) at 2m        20+
        FED gases on egress path = 0.000
        FED thermal on egress path = 0.000

0 min   46 sec
        (46 sec)                    Room 1    Outside

        Layer (m)                   3.490
        Upper Temp (C)              50.3
        Lower Temp (C)              24.3
        HRR (kW)                    124.1
        Visibility (m) at 2m        20+
        FED gases on egress path = 0.000
        FED thermal on egress path = 0.000

0 min   47 sec
        (47 sec)                    Room 1    Outside

        Layer (m)                   3.465
        Upper Temp (C)              50.4
        Lower Temp (C)              24.3
        HRR (kW)                    124.1
        Visibility (m) at 2m        20+
        FED gases on egress path = 0.000
        FED thermal on egress path = 0.000

0 min   48 sec
        (48 sec)                    Room 1    Outside

        Layer (m)                   3.439
        Upper Temp (C)              50.6
        Lower Temp (C)              24.3
        HRR (kW)                    124.1
        Visibility (m) at 2m        20+
        FED gases on egress path = 0.000
        FED thermal on egress path = 0.000

0 min   49 sec
        (49 sec)                    Room 1    Outside

        Layer (m)                   3.414
        Upper Temp (C)              50.7
        Lower Temp (C)              24.3
        HRR (kW)                    124.1
        Visibility (m) at 2m        20+
        FED gases on egress path = 0.000
        FED thermal on egress path = 0.000

0 min   50 sec
        (50 sec)                    Room 1    Outside

        Layer (m)                   3.389
        Upper Temp (C)              50.9
        Lower Temp (C)              24.3
        HRR (kW)                    124.1
        Visibility (m) at 2m        20+
        FED gases on egress path = 0.000
        FED thermal on egress path = 0.000

0 min   51 sec
        (51 sec)                    Room 1    Outside

        Layer (m)                   3.365
```

```
        Upper Temp (C)               51.0
        Lower Temp (C)               24.4
        HRR (kW)                     124.1
        Visibility (m) at 2m         20+
        FED gases on egress path = 0.000
        FED thermal on egress path = 0.000

0 min   52 sec
        (52 sec)                     Room 1    Outside

        Layer (m)                    3.340
        Upper Temp (C)               51.1
        Lower Temp (C)               24.4
        HRR (kW)                     124.1
        Visibility (m) at 2m         20+
        FED gases on egress path = 0.000
        FED thermal on egress path = 0.000

0 min   53 sec
        (53 sec)                     Room 1    Outside

        Layer (m)                    3.316
        Upper Temp (C)               51.3
        Lower Temp (C)               24.4
        HRR (kW)                     124.1
        Visibility (m) at 2m         20+
        FED gases on egress path = 0.000
        FED thermal on egress path = 0.000

0 min   54 sec
        (54 sec)                     Room 1    Outside

        Layer (m)                    3.292
        Upper Temp (C)               51.4
        Lower Temp (C)               24.4
        HRR (kW)                     124.1
        Visibility (m) at 2m         20+
        FED gases on egress path = 0.000
        FED thermal on egress path = 0.000

0 min   55 sec
        (55 sec)                     Room 1    Outside

        Layer (m)                    3.268
        Upper Temp (C)               51.5
        Lower Temp (C)               24.4
        HRR (kW)                     124.1
        Visibility (m) at 2m         20+
        FED gases on egress path = 0.000
        FED thermal on egress path = 0.000

0 min   56 sec
        (56 sec)                     Room 1    Outside

        Layer (m)                    3.245
        Upper Temp (C)               51.7
        Lower Temp (C)               24.4
        HRR (kW)                     124.1
        Visibility (m) at 2m         20+
        FED gases on egress path = 0.000
        FED thermal on egress path = 0.000

0 min   57 sec
        (57 sec)                     Room 1    Outside

        Layer (m)                    3.221
        Upper Temp (C)               51.8
        Lower Temp (C)               24.4
        HRR (kW)                     124.1
        Visibility (m) at 2m         20+
        FED gases on egress path = 0.000
        FED thermal on egress path = 0.000
```

```
0 min    58 sec
         (58 sec)                      Room 1    Outside

         Layer (m)                     3.198
         Upper Temp (C)                51.9
         Lower Temp (C)                24.4
         HRR (kW)                      124.1
         Visibility (m) at 2m          20+
         FED gases on egress path = 0.000
         FED thermal on egress path = 0.000

0 min    59 sec
         (59 sec)                      Room 1    Outside

         Layer (m)                     3.175
         Upper Temp (C)                52.1
         Lower Temp (C)                24.5
         HRR (kW)                      124.1
         Visibility (m) at 2m          20+
         FED gases on egress path = 0.000
         FED thermal on egress path = 0.000

1 min    00 sec
         (60 sec)                      Room 1    Outside

         Layer (m)                     3.153
         Upper Temp (C)                52.2
         Lower Temp (C)                24.5
         HRR (kW)                      124.1
         Visibility (m) at 2m          20+
         FED gases on egress path = 0.000
         FED thermal on egress path = 0.000

1 min    01 sec
         (61 sec)                      Room 1    Outside

         Layer (m)                     3.130
         Upper Temp (C)                52.4
         Lower Temp (C)                24.5
         HRR (kW)                      124.1
         Visibility (m) at 2m          20+
         FED gases on egress path = 0.000
         FED thermal on egress path = 0.000

1 min    02 sec
         (62 sec)                      Room 1    Outside

         Layer (m)                     3.108
         Upper Temp (C)                52.5
         Lower Temp (C)                24.5
         HRR (kW)                      124.1
         Visibility (m) at 2m          20+
         FED gases on egress path = 0.000
         FED thermal on egress path = 0.000

1 min    03 sec
         (63 sec)                      Room 1    Outside

         Layer (m)                     3.086
         Upper Temp (C)                52.6
         Lower Temp (C)                24.5
         HRR (kW)                      124.1
         Visibility (m) at 2m          20+
         FED gases on egress path = 0.000
         FED thermal on egress path = 0.000

1 min    04 sec
         (64 sec)                      Room 1    Outside

         Layer (m)                     3.064
         Upper Temp (C)                52.8
         Lower Temp (C)                24.5
         HRR (kW)                      124.1
```

```
         Visibility (m) at 2m          20+
         FED gases on egress path = 0.000
         FED thermal on egress path = 0.000

1 min    05 sec
         (65 sec)                      Room 1    Outside

         Layer (m)                     3.042
         Upper Temp (C)                52.9
         Lower Temp (C)                24.5
         HRR (kW)                      124.1
         Visibility (m) at 2m          20+
         FED gases on egress path = 0.000
         FED thermal on egress path = 0.000

1 min    06 sec
         (66 sec)                      Room 1    Outside

         Layer (m)                     3.021
         Upper Temp (C)                53.0
         Lower Temp (C)                24.6
         HRR (kW)                      124.1
         Visibility (m) at 2m          20+
         FED gases on egress path = 0.000
         FED thermal on egress path = 0.000

1 min    07 sec
         (67 sec)                      Room 1    Outside

         Layer (m)                     2.999
         Upper Temp (C)                53.2
         Lower Temp (C)                24.6
         HRR (kW)                      124.1
         Visibility (m) at 2m          20+
         FED gases on egress path = 0.000
         FED thermal on egress path = 0.000

1 min    08 sec
         (68 sec)                      Room 1    Outside

         Layer (m)                     2.978
         Upper Temp (C)                53.3
         Lower Temp (C)                24.6
         HRR (kW)                      124.1
         Visibility (m) at 2m          20+
         FED gases on egress path = 0.000
         FED thermal on egress path = 0.000

1 min    09 sec
         (69 sec)                      Room 1    Outside

         Layer (m)                     2.957
         Upper Temp (C)                53.4
         Lower Temp (C)                24.6
         HRR (kW)                      124.1
         Visibility (m) at 2m          20+
         FED gases on egress path = 0.000
         FED thermal on egress path = 0.000

1 min    10 sec
         (70 sec)                      Room 1    Outside

         Layer (m)                     2.936
         Upper Temp (C)                53.6
         Lower Temp (C)                24.6
         HRR (kW)                      124.1
         Visibility (m) at 2m          20+
         FED gases on egress path = 0.000
         FED thermal on egress path = 0.000

1 min    11 sec
         (71 sec)                      Room 1    Outside
```

```
        Layer (m)                   2.916
        Upper Temp (C)              53.7
        Lower Temp (C)              24.6
        HRR (kW)                    124.1
        Visibility (m) at 2m        20+
        FED gases on egress path = 0.000
        FED thermal on egress path = 0.000

1 min   12 sec
        (72 sec)                    Room 1    Outside

        Layer (m)                   2.895
        Upper Temp (C)              53.9
        Lower Temp (C)              24.6
        HRR (kW)                    124.1
        Visibility (m) at 2m        20+
        FED gases on egress path = 0.000
        FED thermal on egress path = 0.000

1 min   13 sec
        (73 sec)                    Room 1    Outside

        Layer (m)                   2.875
        Upper Temp (C)              54.0
        Lower Temp (C)              24.7
        HRR (kW)                    124.1
        Visibility (m) at 2m        20+
        FED gases on egress path = 0.000
        FED thermal on egress path = 0.000

1 min   14 sec
        (74 sec)                    Room 1    Outside

        Layer (m)                   2.855
        Upper Temp (C)              54.1
        Lower Temp (C)              24.7
        HRR (kW)                    124.1
        Visibility (m) at 2m        20+
        FED gases on egress path = 0.000
        FED thermal on egress path = 0.000

1 min   15 sec
        (75 sec)                    Room 1    Outside

        Layer (m)                   2.835
        Upper Temp (C)              54.3
        Lower Temp (C)              24.7
        HRR (kW)                    124.1
        Visibility (m) at 2m        20+
        FED gases on egress path = 0.000
        FED thermal on egress path = 0.000

1 min   16 sec
        (76 sec)                    Room 1    Outside

        Layer (m)                   2.816
        Upper Temp (C)              54.4
        Lower Temp (C)              24.7
        HRR (kW)                    124.1
        Visibility (m) at 2m        20+
        FED gases on egress path = 0.000
        FED thermal on egress path = 0.000

1 min   17 sec
        (77 sec)                    Room 1    Outside

        Layer (m)                   2.796
        Upper Temp (C)              54.5
        Lower Temp (C)              24.7
        HRR (kW)                    124.1
        Visibility (m) at 2m        20+
        FED gases on egress path = 0.000
        FED thermal on egress path = 0.000
```

```
1 min    18 sec
         (78 sec)                      Room 1    Outside

         Layer (m)                     2.777
         Upper Temp (C)                54.7
         Lower Temp (C)                24.7
         HRR (kW)                      124.1
         Visibility (m) at 2m          20+
         FED gases on egress path = 0.000
         FED thermal on egress path = 0.000

1 min    19 sec
         (79 sec)                      Room 1    Outside

         Layer (m)                     2.757
         Upper Temp (C)                54.8
         Lower Temp (C)                24.8
         HRR (kW)                      124.1
         Visibility (m) at 2m          20+
         FED gases on egress path = 0.000
         FED thermal on egress path = 0.000

1 min    20 sec
         (80 sec)                      Room 1    Outside

         Layer (m)                     2.738
         Upper Temp (C)                55.0
         Lower Temp (C)                24.8
         HRR (kW)                      124.1
         Visibility (m) at 2m          20+
         FED gases on egress path = 0.000
         FED thermal on egress path = 0.000

1 min    21 sec
         (81 sec)                      Room 1    Outside

         Layer (m)                     2.720
         Upper Temp (C)                55.1
         Lower Temp (C)                24.8
         HRR (kW)                      124.1
         Visibility (m) at 2m          20+
         FED gases on egress path = 0.000
         FED thermal on egress path = 0.000

1 min    22 sec
         (82 sec)                      Room 1    Outside

         Layer (m)                     2.701
         Upper Temp (C)                55.2
         Lower Temp (C)                24.8
         HRR (kW)                      124.1
         Visibility (m) at 2m          20+
         FED gases on egress path = 0.000
         FED thermal on egress path = 0.000

1 min    23 sec
         (83 sec)                      Room 1    Outside

         Layer (m)                     2.682
         Upper Temp (C)                55.4
         Lower Temp (C)                24.8
         HRR (kW)                      124.1
         Visibility (m) at 2m          20+
         FED gases on egress path = 0.000
         FED thermal on egress path = 0.000

1 min    24 sec
         (84 sec)                      Room 1    Outside

         Layer (m)                     2.664
         Upper Temp (C)                55.5
         Lower Temp (C)                24.9
```

```
        HRR (kW)                      124.1
        Visibility (m) at 2m          20+
        FED gases on egress path = 0.000
        FED thermal on egress path = 0.000

1 min   25 sec
        (85 sec)                      Room 1    Outside

        Layer (m)                     2.645
        Upper Temp (C)                55.6
        Lower Temp (C)                24.9
        HRR (kW)                      124.1
        Visibility (m) at 2m          20+
        FED gases on egress path = 0.000
        FED thermal on egress path = 0.000

1 min   26 sec
        (86 sec)                      Room 1    Outside

        Layer (m)                     2.627
        Upper Temp (C)                55.8
        Lower Temp (C)                24.9
        HRR (kW)                      124.1
        Visibility (m) at 2m          20+
        FED gases on egress path = 0.000
        FED thermal on egress path = 0.000

1 min   27 sec
        (87 sec)                      Room 1    Outside

        Layer (m)                     2.609
        Upper Temp (C)                55.9
        Lower Temp (C)                24.9
        HRR (kW)                      124.1
        Visibility (m) at 2m          20+
        FED gases on egress path = 0.000
        FED thermal on egress path = 0.000

1 min   28 sec
        (88 sec)                      Room 1    Outside

        Layer (m)                     2.591
        Upper Temp (C)                56.0
        Lower Temp (C)                24.9
        HRR (kW)                      124.1
        Visibility (m) at 2m          20+
        FED gases on egress path = 0.000
        FED thermal on egress path = 0.000

1 min   29 sec
        (89 sec)                      Room 1    Outside

        Layer (m)                     2.574
        Upper Temp (C)                56.2
        Lower Temp (C)                24.9
        HRR (kW)                      124.1
        Visibility (m) at 2m          20+
        FED gases on egress path = 0.000
        FED thermal on egress path = 0.000

1 min   30 sec
        (90 sec)                      Room 1    Outside

        Layer (m)                     2.556
        Upper Temp (C)                56.3
        Lower Temp (C)                25.0
        HRR (kW)                      124.1
        Visibility (m) at 2m          20+
        FED gases on egress path = 0.000
        FED thermal on egress path = 0.000

1 min   31 sec
        (91 sec)                      Room 1    Outside
```

```
        Layer (m)                   2.539
        Upper Temp (C)              56.5
        Lower Temp (C)              25.0
        HRR (kW)                    124.1
        Visibility (m) at 2m        20+
        FED gases on egress path = 0.000
        FED thermal on egress path = 0.000

1 min   32 sec
        (92 sec)                    Room 1    Outside

        Layer (m)                   2.522
        Upper Temp (C)              56.6
        Lower Temp (C)              25.0
        HRR (kW)                    124.1
        Visibility (m) at 2m        20+
        FED gases on egress path = 0.000
        FED thermal on egress path = 0.000

1 min   33 sec
        (93 sec)                    Room 1    Outside

        Layer (m)                   2.504
        Upper Temp (C)              56.7
        Lower Temp (C)              25.0
        HRR (kW)                    124.1
        Visibility (m) at 2m        20+
        FED gases on egress path = 0.000
        FED thermal on egress path = 0.000

1 min   34 sec
        (94 sec)                    Room 1    Outside

        Layer (m)                   2.487
        Upper Temp (C)              56.9
        Lower Temp (C)              25.1
        HRR (kW)                    124.1
        Visibility (m) at 2m        20+
        FED gases on egress path = 0.000
        FED thermal on egress path = 0.000

1 min   35 sec
        (95 sec)                    Room 1    Outside

        Layer (m)                   2.471
        Upper Temp (C)              57.0
        Lower Temp (C)              25.1
        HRR (kW)                    124.1
        Visibility (m) at 2m        20+
        FED gases on egress path = 0.000
        FED thermal on egress path = 0.000

1 min   36 sec
        (96 sec)                    Room 1    Outside

        Layer (m)                   2.454
        Upper Temp (C)              57.1
        Lower Temp (C)              25.1
        HRR (kW)                    124.1
        Visibility (m) at 2m        20+
        FED gases on egress path = 0.000
        FED thermal on egress path = 0.000

1 min   37 sec
        (97 sec)                    Room 1    Outside

        Layer (m)                   2.437
        Upper Temp (C)              57.3
        Lower Temp (C)              25.1
        HRR (kW)                    124.1
        Visibility (m) at 2m        20+
        FED gases on egress path = 0.000
```

```
        FED thermal on egress path = 0.000

1 min   38 sec
        (98 sec)                    Room 1    Outside

        Layer (m)                   2.421
        Upper Temp (C)              57.4
        Lower Temp (C)              25.1
        HRR (kW)                    124.1
        Visibility (m) at 2m        20+
        FED gases on egress path = 0.000
        FED thermal on egress path = 0.000

1 min   39 sec
        (99 sec)                    Room 1    Outside

        Layer (m)                   2.404
        Upper Temp (C)              57.6
        Lower Temp (C)              25.2
        HRR (kW)                    124.1
        Visibility (m) at 2m        20+
        FED gases on egress path = 0.000
        FED thermal on egress path = 0.000

1 min   40 sec
        (100 sec)                   Room 1    Outside

        Layer (m)                   2.388
        Upper Temp (C)              57.7
        Lower Temp (C)              25.2
        HRR (kW)                    124.1
        Visibility (m) at 2m        20+
        FED gases on egress path = 0.000
        FED thermal on egress path = 0.000

1 min   41 sec
        (101 sec)                   Room 1    Outside

        Layer (m)                   2.372
        Upper Temp (C)              57.8
        Lower Temp (C)              25.2
        HRR (kW)                    124.1
        Visibility (m) at 2m        20+
        FED gases on egress path = 0.000
        FED thermal on egress path = 0.000

1 min   42 sec
        (102 sec)                   Room 1    Outside

        Layer (m)                   2.356
        Upper Temp (C)              58.0
        Lower Temp (C)              25.2
        HRR (kW)                    124.1
        Visibility (m) at 2m        20+
        FED gases on egress path = 0.000
        FED thermal on egress path = 0.000

1 min   43 sec
        (103 sec)                   Room 1    Outside

        Layer (m)                   2.340
        Upper Temp (C)              58.1
        Lower Temp (C)              25.2
        HRR (kW)                    124.1
        Visibility (m) at 2m        20+
        FED gases on egress path = 0.000
        FED thermal on egress path = 0.000

1 min   44 sec
        (104 sec)                   Room 1    Outside

        Layer (m)                   2.324
        Upper Temp (C)              58.3
```

```
        Lower Temp (C)                25.3
        HRR (kW)                      124.1
        Visibility (m) at 2m          20+
        FED gases on egress path = 0.000
        FED thermal on egress path = 0.000

1 min   45 sec
        (105 sec)                     Room 1    Outside

        Layer (m)                     2.309
        Upper Temp (C)                58.4
        Lower Temp (C)                25.3
        HRR (kW)                      124.1
        Visibility (m) at 2m          20+
        FED gases on egress path = 0.000
        FED thermal on egress path = 0.000

1 min   46 sec
        (106 sec)                     Room 1    Outside

        Layer (m)                     2.293
        Upper Temp (C)                58.5
        Lower Temp (C)                25.3
        HRR (kW)                      124.1
        Visibility (m) at 2m          20+
        FED gases on egress path = 0.000
        FED thermal on egress path = 0.000

1 min   47 sec
        (107 sec)                     Room 1    Outside

        Layer (m)                     2.278
        Upper Temp (C)                58.7
        Lower Temp (C)                25.3
        HRR (kW)                      124.1
        Visibility (m) at 2m          20+
        FED gases on egress path = 0.000
        FED thermal on egress path = 0.000

1 min   48 sec
        (108 sec)                     Room 1    Outside

        Layer (m)                     2.263
        Upper Temp (C)                58.8
        Lower Temp (C)                25.4
        HRR (kW)                      124.1
        Visibility (m) at 2m          20+
        FED gases on egress path = 0.000
        FED thermal on egress path = 0.000

1 min   49 sec
        (109 sec)                     Room 1    Outside

        Layer (m)                     2.247
        Upper Temp (C)                58.9
        Lower Temp (C)                25.4
        HRR (kW)                      124.1
        Visibility (m) at 2m          20+
        FED gases on egress path = 0.000
        FED thermal on egress path = 0.000

1 min   50 sec
        (110 sec)                     Room 1    Outside

        Layer (m)                     2.232
        Upper Temp (C)                59.1
        Lower Temp (C)                25.4
        HRR (kW)                      124.1
        Visibility (m) at 2m          20+
        FED gases on egress path = 0.000
        FED thermal on egress path = 0.000

1 min   51 sec
```

```
        (111 sec)                   Room 1    Outside

        Layer (m)                   2.217
        Upper Temp (C)              59.2
        Lower Temp (C)              25.4
        HRR (kW)                    124.1
        Visibility (m) at 2m        20+
        FED gases on egress path = 0.000
        FED thermal on egress path = 0.000

1 min   52 sec
        (112 sec)                   Room 1    Outside

        Layer (m)                   2.203
        Upper Temp (C)              59.4
        Lower Temp (C)              25.5
        HRR (kW)                    124.1
        Visibility (m) at 2m        20+
        FED gases on egress path = 0.000
        FED thermal on egress path = 0.000

1 min   53 sec
        (113 sec)                   Room 1    Outside

        Layer (m)                   2.188
        Upper Temp (C)              59.5
        Lower Temp (C)              25.5
        HRR (kW)                    124.1
        Visibility (m) at 2m        20+
        FED gases on egress path = 0.000
        FED thermal on egress path = 0.000

1 min   54 sec
        (114 sec)                   Room 1    Outside

        Layer (m)                   2.173
        Upper Temp (C)              59.6
        Lower Temp (C)              25.5
        HRR (kW)                    124.1
        Visibility (m) at 2m        20+
        FED gases on egress path = 0.000
        FED thermal on egress path = 0.000

1 min   55 sec
        (115 sec)                   Room 1    Outside

        Layer (m)                   2.159
        Upper Temp (C)              59.8
        Lower Temp (C)              25.5
        HRR (kW)                    124.1
        Visibility (m) at 2m        20+
        FED gases on egress path = 0.000
        FED thermal on egress path = 0.000

1 min   56 sec
        (116 sec)                   Room 1    Outside

        Layer (m)                   2.144
        Upper Temp (C)              59.9
        Lower Temp (C)              25.6
        HRR (kW)                    124.1
        Visibility (m) at 2m        20+
        FED gases on egress path = 0.000
        FED thermal on egress path = 0.000

1 min   57 sec
        (117 sec)                   Room 1    Outside

        Layer (m)                   2.130
        Upper Temp (C)              60.1
        Lower Temp (C)              25.6
        HRR (kW)                    124.1
        Visibility (m) at 2m        20+
```

```
        FED gases on egress path = 0.000
        FED thermal on egress path = 0.000

1 min   58 sec
        (118 sec)                   Room 1    Outside

        Layer (m)                   2.116
        Upper Temp (C)              60.2
        Lower Temp (C)              25.6
        HRR (kW)                    124.1
        Visibility (m) at 2m        20+
        FED gases on egress path = 0.000
        FED thermal on egress path = 0.001

1 min   59 sec
        (119 sec)                   Room 1    Outside

        Layer (m)                   2.102
        Upper Temp (C)              60.3
        Lower Temp (C)              25.7
        HRR (kW)                    124.1
        Visibility (m) at 2m        20+
        FED gases on egress path = 0.000
        FED thermal on egress path = 0.001

2 min   00 sec
        (120 sec)                   Room 1    Outside

        Layer (m)                   2.088
        Upper Temp (C)              60.5
        Lower Temp (C)              25.7
        HRR (kW)                    124.1
        Visibility (m) at 2m        20+
        FED gases on egress path = 0.000
        FED thermal on egress path = 0.001

2 min   01 sec
        (121 sec)                   Room 1    Outside

        Layer (m)                   2.074
        Upper Temp (C)              60.6
        Lower Temp (C)              25.7
        HRR (kW)                    124.1
        Visibility (m) at 2m        20+
        FED gases on egress path = 0.000
        FED thermal on egress path = 0.001

2 min   02 sec
        (122 sec)                   Room 1    Outside

        Layer (m)                   2.060
        Upper Temp (C)              60.7
        Lower Temp (C)              25.7
        HRR (kW)                    124.1
        Visibility (m) at 2m        20+
        FED gases on egress path = 0.000
        FED thermal on egress path = 0.001

2 min   03 sec
        (123 sec)                   Room 1    Outside

        Layer (m)                   2.046
        Upper Temp (C)              60.9
        Lower Temp (C)              25.8
        HRR (kW)                    124.1
        Visibility (m) at 2m        20+
        FED gases on egress path = 0.000
        FED thermal on egress path = 0.001

2 min   04 sec
        (124 sec)                   Room 1    Outside

        Layer (m)                   2.033
```

```
         Upper Temp (C)               61.0
         Lower Temp (C)               25.8
         HRR (kW)                     124.1
         Visibility (m) at 2m         20+
         FED gases on egress path = 0.000
         FED thermal on egress path = 0.001

2 min    05 sec
         (125 sec)                    Room 1    Outside

         Layer (m)                    2.019
         Upper Temp (C)               61.1
         Lower Temp (C)               25.8
         HRR (kW)                     124.1
         Visibility (m) at 2m         20+
         FED gases on egress path = 0.000
         FED thermal on egress path = 0.001

2 min    06 sec
         (126 sec)                    Room 1    Outside

         Layer (m)                    2.006
         Upper Temp (C)               61.3
         Lower Temp (C)               25.9
         HRR (kW)                     124.1
         Visibility (m) at 2m         20+
         FED gases on egress path = 0.000
         FED thermal on egress path = 0.001

2 min    07 sec
         (127 sec)                    Room 1    Outside

         Layer (m)                    1.993
         Upper Temp (C)               61.4
         Lower Temp (C)               25.9
         HRR (kW)                     124.1
         Visibility (m) at 2m         20+
         FED gases on egress path = 0.000
         FED thermal on egress path = 0.001

2 min    08 sec
         (128 sec)                    Room 1    Outside

         Layer (m)                    1.979
         Upper Temp (C)               61.6
         Lower Temp (C)               25.9
         HRR (kW)                     124.1
         Visibility (m) at 2m         20+
         FED gases on egress path = 0.000
         FED thermal on egress path = 0.001

2 min    09 sec
         (129 sec)                    Room 1    Outside

         Layer (m)                    1.966
         Upper Temp (C)               61.7
         Lower Temp (C)               25.9
         HRR (kW)                     124.1
         Visibility (m) at 2m         20+
         FED gases on egress path = 0.000
         FED thermal on egress path = 0.002

2 min    10 sec
         (130 sec)                    Room 1    Outside

         Layer (m)                    1.953
         Upper Temp (C)               61.8
         Lower Temp (C)               26.0
         HRR (kW)                     124.1
         Visibility (m) at 2m         20+
         FED gases on egress path = 0.000
         FED thermal on egress path = 0.002
```

```
2 min    11 sec
         (131 sec)                    Room 1    Outside

         Layer (m)                    1.940
         Upper Temp (C)               62.0
         Lower Temp (C)               26.0
         HRR (kW)                     124.1
         Visibility (m) at 2m         20+
         FED gases on egress path = 0.000
         FED thermal on egress path = 0.003

2 min    12 sec
         (132 sec)                    Room 1    Outside

         Layer (m)                    1.928
         Upper Temp (C)               62.1
         Lower Temp (C)               26.0
         HRR (kW)                     124.1
         Visibility (m) at 2m         20+
         FED gases on egress path = 0.000
         FED thermal on egress path = 0.003

2 min    13 sec
         (133 sec)                    Room 1    Outside

         Layer (m)                    1.915
         Upper Temp (C)               62.2
         Lower Temp (C)               26.1
         HRR (kW)                     124.1
         Visibility (m) at 2m         20+
         FED gases on egress path = 0.000
         FED thermal on egress path = 0.004

2 min    14 sec
         (134 sec)                    Room 1    Outside

         Layer (m)                    1.902
         Upper Temp (C)               62.4
         Lower Temp (C)               26.1
         HRR (kW)                     124.1
         Visibility (m) at 2m         20+
         FED gases on egress path = 0.000
         FED thermal on egress path = 0.004

2 min    15 sec
         (135 sec)                    Room 1    Outside

         Layer (m)                    1.890
         Upper Temp (C)               62.5
         Lower Temp (C)               26.1
         HRR (kW)                     124.1
         Visibility (m) at 2m         20+
         FED gases on egress path = 0.000
         FED thermal on egress path = 0.004

2 min    16 sec
         (136 sec)                    Room 1    Outside

         Layer (m)                    1.877
         Upper Temp (C)               62.6
         Lower Temp (C)               26.2
         HRR (kW)                     124.1
         Visibility (m) at 2m         20+
         FED gases on egress path = 0.000
         FED thermal on egress path = 0.005

2 min    17 sec
         (137 sec)                    Room 1    Outside

         Layer (m)                    1.865
         Upper Temp (C)               62.8
         Lower Temp (C)               26.2
         HRR (kW)                     124.1
```

```
         Visibility (m) at 2m          20+
         FED gases on egress path = 0.000
         FED thermal on egress path = 0.005

2 min    18 sec
         (138 sec)                     Room 1    Outside

         Layer (m)                     1.852
         Upper Temp (C)                62.9
         Lower Temp (C)                26.2
         HRR (kW)                      124.1
         Visibility (m) at 2m          20+
         FED gases on egress path = 0.000
         FED thermal on egress path = 0.006

2 min    19 sec
         (139 sec)                     Room 1    Outside

         Layer (m)                     1.840
         Upper Temp (C)                63.1
         Lower Temp (C)                26.3
         HRR (kW)                      124.1
         Visibility (m) at 2m          20+
         FED gases on egress path = 0.001
         FED thermal on egress path = 0.006

2 min    20 sec
         (140 sec)                     Room 1    Outside

         Layer (m)                     1.828
         Upper Temp (C)                63.2
         Lower Temp (C)                26.3
         HRR (kW)                      124.1
         Visibility (m) at 2m          20+
         FED gases on egress path = 0.001
         FED thermal on egress path = 0.007

2 min    21 sec
         (141 sec)                     Room 1    Outside

         Layer (m)                     1.816
         Upper Temp (C)                63.3
         Lower Temp (C)                26.3
         HRR (kW)                      124.1
         Visibility (m) at 2m          20+
         FED gases on egress path = 0.001
         FED thermal on egress path = 0.007

2 min    22 sec
         (142 sec)                     Room 1    Outside

         Layer (m)                     1.804
         Upper Temp (C)                63.5
         Lower Temp (C)                26.4
         HRR (kW)                      124.1
         Visibility (m) at 2m          20+
         FED gases on egress path = 0.001
         FED thermal on egress path = 0.007

2 min    23 sec
         (143 sec)                     Room 1    Outside

         Layer (m)                     1.792
         Upper Temp (C)                63.6
         Lower Temp (C)                26.4
         HRR (kW)                      124.1
         Visibility (m) at 2m          20+
         FED gases on egress path = 0.001
         FED thermal on egress path = 0.008

2 min    24 sec
         (144 sec)                     Room 1    Outside
```

```
         Layer (m)                    1.780
         Upper Temp (C)               63.7
         Lower Temp (C)               26.5
         HRR (kW)                     124.1
         Visibility (m) at 2m         20+
         FED gases on egress path = 0.001
         FED thermal on egress path = 0.008

2 min    25 sec
         (145 sec)                    Room 1    Outside

         Layer (m)                    1.768
         Upper Temp (C)               63.9
         Lower Temp (C)               26.5
         HRR (kW)                     124.1
         Visibility (m) at 2m         20+
         FED gases on egress path = 0.001
         FED thermal on egress path = 0.009

2 min    26 sec
         (146 sec)                    Room 1    Outside

         Layer (m)                    1.756
         Upper Temp (C)               64.0
         Lower Temp (C)               26.5
         HRR (kW)                     124.1
         Visibility (m) at 2m         20+
         FED gases on egress path = 0.001
         FED thermal on egress path = 0.009

2 min    27 sec
         (147 sec)                    Room 1    Outside

         Layer (m)                    1.745
         Upper Temp (C)               64.2
         Lower Temp (C)               26.6
         HRR (kW)                     124.1
         Visibility (m) at 2m         20+
         FED gases on egress path = 0.001
         FED thermal on egress path = 0.010

2 min    28 sec
         (148 sec)                    Room 1    Outside

         Layer (m)                    1.733
         Upper Temp (C)               64.3
         Lower Temp (C)               26.6
         HRR (kW)                     124.1
         Visibility (m) at 2m         20+
         FED gases on egress path = 0.001
         FED thermal on egress path = 0.010

2 min    29 sec
         (149 sec)                    Room 1    Outside

         Layer (m)                    1.722
         Upper Temp (C)               64.4
         Lower Temp (C)               26.6
         HRR (kW)                     124.1
         Visibility (m) at 2m         20+
         FED gases on egress path = 0.001
         FED thermal on egress path = 0.011

2 min    30 sec
         (150 sec)                    Room 1    Outside

         Layer (m)                    1.710
         Upper Temp (C)               64.6
         Lower Temp (C)               26.7
         HRR (kW)                     124.1
         Visibility (m) at 2m         20+
         FED gases on egress path = 0.001
         FED thermal on egress path = 0.011
```

2 min 31 sec
(151 sec) Room 1 Outside

Layer (m) 1.699
Upper Temp (C) 64.7
Lower Temp (C) 26.7
HRR (kW) 124.1
Visibility (m) at 2m 20+
FED gases on egress path = 0.001
FED thermal on egress path = 0.012

2 min 32 sec
(152 sec) Room 1 Outside

Layer (m) 1.688
Upper Temp (C) 64.8
Lower Temp (C) 26.8
HRR (kW) 124.1
Visibility (m) at 2m 20+
FED gases on egress path = 0.001
FED thermal on egress path = 0.012

2 min 33 sec
(153 sec) Room 1 Outside

Layer (m) 1.676
Upper Temp (C) 65.0
Lower Temp (C) 26.8
HRR (kW) 124.1
Visibility (m) at 2m 20+
FED gases on egress path = 0.001
FED thermal on egress path = 0.013

2 min 34 sec
(154 sec) Room 1 Outside

Layer (m) 1.665
Upper Temp (C) 65.1
Lower Temp (C) 26.8
HRR (kW) 124.1
Visibility (m) at 2m 20+
FED gases on egress path = 0.001
FED thermal on egress path = 0.013

2 min 35 sec
(155 sec) Room 1 Outside

Layer (m) 1.654
Upper Temp (C) 65.3
Lower Temp (C) 26.9
HRR (kW) 124.1
Visibility (m) at 2m 20+
FED gases on egress path = 0.001
FED thermal on egress path = 0.014

2 min 36 sec
(156 sec) Room 1 Outside

Layer (m) 1.643
Upper Temp (C) 65.4
Lower Temp (C) 26.9
HRR (kW) 124.1
Visibility (m) at 2m 20+
FED gases on egress path = 0.001
FED thermal on egress path = 0.014

2 min 37 sec
(157 sec) Room 1 Outside

Layer (m) 1.632
Upper Temp (C) 65.5
Lower Temp (C) 27.0

```
        HRR (kW)                      124.1
        Visibility (m) at 2m          20+
        FED gases on egress path = 0.001
        FED thermal on egress path = 0.015

2 min   38 sec
        (158 sec)                     Room 1    Outside

        Layer (m)                     1.621
        Upper Temp (C)                65.7
        Lower Temp (C)                27.0
        HRR (kW)                      124.1
        Visibility (m) at 2m          20+
        FED gases on egress path = 0.001
        FED thermal on egress path = 0.015

2 min   39 sec
        (159 sec)                     Room 1    Outside

        Layer (m)                     1.610
        Upper Temp (C)                65.8
        Lower Temp (C)                27.0
        HRR (kW)                      124.1
        Visibility (m) at 2m          20+
        FED gases on egress path = 0.001
        FED thermal on egress path = 0.016

2 min   40 sec
        (160 sec)                     Room 1    Outside

        Layer (m)                     1.600
        Upper Temp (C)                65.9
        Lower Temp (C)                27.1
        HRR (kW)                      124.1
        Visibility (m) at 2m          20+
        FED gases on egress path = 0.001
        FED thermal on egress path = 0.016

2 min   41 sec
        (161 sec)                     Room 1    Outside

        Layer (m)                     1.589
        Upper Temp (C)                66.1
        Lower Temp (C)                27.1
        HRR (kW)                      124.1
        Visibility (m) at 2m          20+
        FED gases on egress path = 0.001
        FED thermal on egress path = 0.017

2 min   42 sec
        (162 sec)                     Room 1    Outside

        Layer (m)                     1.578
        Upper Temp (C)                66.2
        Lower Temp (C)                27.2
        HRR (kW)                      124.1
        Visibility (m) at 2m          20+
        FED gases on egress path = 0.002
        FED thermal on egress path = 0.017

2 min   43 sec
        (163 sec)                     Room 1    Outside

        Layer (m)                     1.568
        Upper Temp (C)                66.4
        Lower Temp (C)                27.2
        HRR (kW)                      124.1
        Visibility (m) at 2m          20+
        FED gases on egress path = 0.002
        FED thermal on egress path = 0.018

2 min   44 sec
        (164 sec)                     Room 1    Outside
```

```
         Layer (m)                    1.557
         Upper Temp (C)               66.5
         Lower Temp (C)               27.3
         HRR (kW)                     124.1
         Visibility (m) at 2m         20+
         FED gases on egress path = 0.002
         FED thermal on egress path = 0.018

2 min    45 sec
         (165 sec)                    Room 1    Outside

         Layer (m)                    1.547
         Upper Temp (C)               66.6
         Lower Temp (C)               27.3
         HRR (kW)                     124.1
         Visibility (m) at 2m         20+
         FED gases on egress path = 0.002
         FED thermal on egress path = 0.019

2 min    46 sec
         (166 sec)                    Room 1    Outside

         Layer (m)                    1.537
         Upper Temp (C)               66.8
         Lower Temp (C)               27.4
         HRR (kW)                     124.1
         Visibility (m) at 2m         20+
         FED gases on egress path = 0.002
         FED thermal on egress path = 0.019

2 min    47 sec
         (167 sec)                    Room 1    Outside

         Layer (m)                    1.526
         Upper Temp (C)               66.9
         Lower Temp (C)               27.4
         HRR (kW)                     124.1
         Visibility (m) at 2m         20+
         FED gases on egress path = 0.002
         FED thermal on egress path = 0.020

2 min    48 sec
         (168 sec)                    Room 1    Outside

         Layer (m)                    1.516
         Upper Temp (C)               67.1
         Lower Temp (C)               27.4
         HRR (kW)                     124.1
         Visibility (m) at 2m         20+
         FED gases on egress path = 0.002
         FED thermal on egress path = 0.020

2 min    49 sec
         (169 sec)                    Room 1    Outside

         Layer (m)                    1.506
         Upper Temp (C)               67.2
         Lower Temp (C)               27.5
         HRR (kW)                     124.1
         Visibility (m) at 2m         20+
         FED gases on egress path = 0.002
         FED thermal on egress path = 0.021

2 min    50 sec
         (170 sec)                    Room 1    Outside

         Layer (m)                    1.496
         Upper Temp (C)               67.3
         Lower Temp (C)               27.5
         HRR (kW)                     124.1
         Visibility (m) at 2m         20+
         FED gases on egress path = 0.002
```

```
        FED thermal on egress path = 0.021

2 min   51 sec
        (171 sec)                   Room 1    Outside

        Layer (m)                   1.486
        Upper Temp (C)              67.5
        Lower Temp (C)              27.6
        HRR (kW)                    124.1
        Visibility (m) at 2m        20+
        FED gases on egress path = 0.002
        FED thermal on egress path = 0.022

2 min   52 sec
        (172 sec)                   Room 1    Outside

        Layer (m)                   1.476
        Upper Temp (C)              67.6
        Lower Temp (C)              27.6
        HRR (kW)                    124.1
        Visibility (m) at 2m        20+
        FED gases on egress path = 0.002
        FED thermal on egress path = 0.022

2 min   53 sec
        (173 sec)                   Room 1    Outside

        Layer (m)                   1.466
        Upper Temp (C)              67.8
        Lower Temp (C)              27.7
        HRR (kW)                    124.1
        Visibility (m) at 2m        20+
        FED gases on egress path = 0.002
        FED thermal on egress path = 0.023

2 min   54 sec
        (174 sec)                   Room 1    Outside

        Layer (m)                   1.456
        Upper Temp (C)              67.9
        Lower Temp (C)              27.7
        HRR (kW)                    124.1
        Visibility (m) at 2m        20+
        FED gases on egress path = 0.002
        FED thermal on egress path = 0.024

2 min   55 sec
        (175 sec)                   Room 1    Outside

        Layer (m)                   1.446
        Upper Temp (C)              68.0
        Lower Temp (C)              27.8
        HRR (kW)                    124.1
        Visibility (m) at 2m        20+
        FED gases on egress path = 0.002
        FED thermal on egress path = 0.024

2 min   56 sec
        (176 sec)                   Room 1    Outside

        Layer (m)                   1.436
        Upper Temp (C)              68.2
        Lower Temp (C)              27.8
        HRR (kW)                    124.1
        Visibility (m) at 2m        20+
        FED gases on egress path = 0.002
        FED thermal on egress path = 0.025

2 min   57 sec
        (177 sec)                   Room 1    Outside

        Layer (m)                   1.427
        Upper Temp (C)              68.3
```

```
         Lower Temp (C)               27.9
         HRR (kW)                     124.1
         Visibility (m) at 2m         20+
         FED gases on egress path = 0.002
         FED thermal on egress path = 0.025

2 min    58 sec
         (178 sec)                    Room 1    Outside

         Layer (m)                    1.417
         Upper Temp (C)               68.5
         Lower Temp (C)               27.9
         HRR (kW)                     124.1
         Visibility (m) at 2m         20+
         FED gases on egress path = 0.002
         FED thermal on egress path = 0.026

2 min    59 sec
         (179 sec)                    Room 1    Outside

         Layer (m)                    1.407
         Upper Temp (C)               68.6
         Lower Temp (C)               28.0
         HRR (kW)                     124.1
         Visibility (m) at 2m         20+
         FED gases on egress path = 0.002
         FED thermal on egress path = 0.026

3 min    00 sec
         (180 sec)                    Room 1    Outside

         Layer (m)                    1.398
         Upper Temp (C)               68.7
         Lower Temp (C)               28.0
         HRR (kW)                     124.1
         Visibility (m) at 2m         20+
         FED gases on egress path = 0.002
         FED thermal on egress path = 0.027


================================================================
Event Log
================================================================
0 sec. Item 1 description ignited.
Iteration 1


================================================================
Computer Run-Time = 0.3 seconds.
================================================================
```